Fan-Shaped Hole Film Cooling on Turbine Blade and Vane in a Transonic Cascade with High Freestream Turbulence: Experimental and CFD Studies

Song Xue

Dissertation submitted to the faculty of the Virginia Polytechnic Institute and State University in partial fulfillment of the requirements for the degree of

Doctor of Philosophy
In
Mechanical Engineering

Wing F. Ng, Committee Chair
Srinath V. Ekkad
Danesh K. Tafti
Tom E. Diller
William J. Devenport
Clinton L. Dancey

June 28, 2012
Blacksburg, VA

Keywords: Gas Turbines, Film Cooling, Heat Transfer, Transonic Cascade, CFD, Shock effect, curvature effect

Fan-Shaped Hole Film Cooling on Turbine Blade and Vane in a Transonic Cascade with High Freestream Turbulence: Experimental and CFD Studies

Song Xue

ABSTRACT

The contribution of present research work is to experimentally investigate the effects of blowing ratio and mainstream Mach number/Reynolds number (from 0.6/8.5X10^5 to 1.0/1.4X10^6) on the performance of the fan-shaped hole injected turbine blade and vane. The study was operated with high freestream turbulence intensity (12% at the inlet) and large turbulence length scales (0.26 for blade, 0.28 for vane, normalized by the cascade pitch of 58.4mm and 83.3mm respectively). Both convective heat transfer coefficient, in terms of Nusselt number, and adiabatic effectiveness are provided in the results. Present research work also numerically investigates the shock/film cooling interaction. A detailed analysis on the physics of the shock/film cooling interaction in the blade cascade is provided.

The results of present research suggests the following major conclusions. Compared to the showerhead only vane, the addition of fan-shaped hole injection on the turbine Nozzle Guide Vane (NGV) increases the Net Heat Flux Reduction (NHFR) 2.6 times while consuming 1.6 times more coolant. For the blade, combined with the surface curvature effect, the increase of Mach number/Reynolds number results in an improved film cooling effectiveness on the blade suction side, but a compromised cooling performance on the blade pressure side. A quick drop of cooling effectiveness occurs at the shock impingement on the blade suction side near the trailing edge. The CFD results indicate that this adiabatic effectiveness drop was caused by the strong secondary flow after shock impingement, which lifts coolant away from the SS surface, and increases the mixing. This secondary flow is related to the spanwise non-uniform of the shock impingement.

RECOGNITION OF CO-AUTHORS

Wing F. Ng is the Chris Kraft Endowed Professor in the Mechanical Engineering Department at Virginia Tech. Ng's research interest focuses on the experimental studies of aerodynamics and heat transfer in gas turbine engine components. He has received several teaching awards from the Virginia Tech. In the present research, Ng was the primary advisor and mentor throughout the duration of the film cooling projects. He coordinated the research expenditures and the experimental facilities.

Srinath Ekkad is the Professor in Mechanical Engineering Department at Virginia Tech. Ekkad's research interest focuses on experimental and numerical studies of film cooling the gas turbine engine components. In the present research, Ekkad was the co-advisor. He provides technical guidance in the present research.

Andrew Newman was a Master's candidate with the Transonic Wind Tunnel Lab at the Virginia Tech during the film cooled vane project. He received his Master's degree in May 2010. Newman's contributions to the film cooled vane study include the initial design of the experiment, the wind tunnel test section setup, the experiment operation, and data post-process.

Hee-Koo Moon and Luzeng Zhang are engineers in Solar Turbines Inc. The experimental research on film cooled vane and blade was financially sponsored by the Solar Turbines Inc. Moon and Zhang coordinated the research goals and provided technique supports for the present research.

ACKNOWLEDGEMENT

The experimental studies in this dissertation were sponsored by Solar Turbines Inc. and conducted under the direction of Dr. Hee-Koo Moon and Dr. Luzeng Zhang. I would like to thank them for their support of the projects.

I would like to express my deepest sense of gratitude to my advisor Dr. Wing Ng for giving me the opportunity, and continually supporting me to study and work as a PhD candidate in the Transonic Wind Tunnel Lab at Virginia Tech. Dr. Ng has been a great mentor as well as a great manager. He made a perfect balance on giving student proper guidance and adequate trust and responsibility. Most of the things I have learned from him substantially helped the research process, and will be valuable in my future life. I also want to thank my co-advisor Dr. Srinath Ekkad for his patient guidance and inspiration throughout the research in this dissertation. I would like to express my feeling of gratitude to the members of my committee, Dr. Diller, Dr. Tafti, Dr. Dancey, and Dr. Devenport for their help and advice during the course of my research. Special thanks should be extended to Dr. Diller and Dr. Tafti for their helpful discussion on the experimental data analysis and suggestions on the CFD study.

Thanks to all the members of the research team in the Transonic Wind Tunnel Lab. It was very nice to work with Santosh Abraham, Kapil Pancal, Andrew Newman, and Anto Karu. Special thanks to Colin Reagle and Jacob Delimont for their inspiring discussions and help on my language improvement. I am also grateful to the graduate students in other groups, such as Ramesh and Arnab; the ladies in ME office, such as Diana, Brandy and Cathy; the members of ME Machine Shop, such as Johnny and Bill; and the IT technicians Ben and James. Their excellent contributions to our department made a great environment for my research, without which the studies could not have been achieved in such a short duration.

Finally, I would like to thank my parents, Yuanxing Xue and Shaorong Wang, and my girlfriend, Sha Wang. Their unconditional love is invaluable support to me, which

provides me the strength and enthusiasm to overcome the difficulties in my research. Any achievement in my life owes its existence to them.

PREFACE

This dissertation is organized in a manuscript format that mainly includes three individual research papers that document present studies on fan-shaped hole film cooling. The author was responsible for most aspects of experimental studies, which includes designing the test section, instrumentation, conducting tests, processing and analyzing data. The author was also responsible for all aspects of the 3-D CFD study of the shock/film cooling interaction, which includes, geometry generating, meshing, boundary condition setting, and post-processing and analysis of the data.

In the first paper, experiments on a fan-shaped hole film cooled blade was performed in a 2-D linear turbine blade cascade at transonic Mach number and high inlet freestream turbulence intensity (12%) with a large length scale (0.26 normalized by cascade pitch). The convective heat transfer coefficient and the film cooling performance data were recorded at three different exit Mach/Reynolds numbers and two different blowing ratios. The data was reported in terms of Nusselt number and adiabatic film effectiveness. The data was presented at the 50th AIAA Aerospace Science Meeting.

The second paper is a 3-D CFD study of the shock/film cooling interaction. In the experimental study of the first paper, a quick drop of film cooling effectiveness has been observed at the location of the shock impingement on the blade suction side near the trailing edge. It is believed the film cooling effectiveness trend was influenced by the shock impingement. The objective of the study in the second paper is to use CFD tool to explore the flow physics of the shock/film cooling interaction, and to explain the trend of the film cooling effectiveness that is observed in the experiment. The centerline film cooling effectiveness is presented and compared with the experimental data. Detail flow structure plots and discussion on the shock/film cooling interaction are provided. This paper is being prepared to be presented at the Turbo Expo 2013 conference.

In the third paper, film cooling performance tests were conducted in a 2-D linear cascade of a turbine NGV profile. Data were recorded at three exit Mach number/Reynolds number combinations: 1.0/1,400,000; 0.85/1,150,000; and 0.60/850,000. At exit Mach numbers of 1.0 and 0.85, three blowing ratio conditions were tested: BR = 1.0, 1.5, and

2.0. All tests were performed at high freestream turbulence intensity (12%) with large length scale (0.28 normalized by the cascade pitch). Vane surface film cooling effectiveness and net heat flux reduction distributions were presented and compared with literature. The data was presented at the Turbo Expo 2011 conference, and the revised paper has been accepted by the ASME Journal of Turbomachinery.

After the main part of the dissertation, there are a series of appendices which provide additional information of the experimental and numerical studies. The appendices include extensive literature review of shock/film cooling interaction, experimental setup, uncertainty analysis, and the entire set of experimental data of the film cooled blade.

TABLE OF CONTENTS

PAPER 3: HEAT TRANSFER PERFORMANCE OF A SHOWERHEAD AND SHAPED HOLE FILM COOLED VANE AT TRANSONIC CONDITIONS

List of Figures

List of Tables

Preface paper 1

Paper 1 experimentally studied a fan-shaped hole film cooled blade in a 2-D linear turbine blade cascade at transonic Mach number and high inlet freestream turbulence intensity (12%) with large length scale (0.26 normalized by cascade pitch). The convective heat transfer coefficient and the film cooling performance data were recorded at three different exit Mach/Reynolds numbers and two different blowing ratios. The paper has been presented at the 50th AIAA Aerospace Science Meeting (AIAA-2012-0368), January 2012, in Nashville, Tennessee. It has also been edited and submitted to the AIAA Journal of Propulsion & Power.

FAN-SHAPED HOLE FILM COOLING ON A TURBINE BLADE IN A TRANSONIC CASCADE WITH HIGH FREESTREAM TURBULENCE

S. Xue, W. Ng, S. Ekkad
Mechanical Engineering
Virginia Polytechnic Institute and State University
Blacksburg, VA, USA

H. K. Moon and L. Zhang
Solar Turbines Incorporated
San Diego, CA, USA

AIAA-2012-0368

Submitted to the Journal of Propulsion and Power

Abstract

An experimental investigation was performed to study the cooling performance and convective heat transfer on a film cooled turbine blade surface. A 2-D linear cascade model of the first stage turbine rotor blade of a land-based gas turbine was employed in the study. The film cooling configuration on the blade comprises of 2 rows of fan-shaped holes on the pressure side (PS), and 1 row of fan-shaped holes on the suction side (SS). The tests were performed in the Virginia Tech transonic wind tunnel facility, which simulates engine representative conditions of high turbulence intensity at the inlet and transonic Mach numbers at the exit, with matching Reynolds number. All the tests were performed at inlet turbulence intensity of 12% with integral length scale of 0.26 normalized by cascade blade pitch. Exit Mach number of 0.67, 0.84, and 1.01 were chosen for the tests. Two combinations of blowing ratios at different rows of cooling holes were tested. (Nominal blowing ratio settings are: suction side injection BR=1.2 and 1.6; pressure side row 1 BR=2.8 and 3.8; pressure side row 2 BR=2.2, and 2.8.). The adiabatic effectiveness trend indicates that the combination of Mach number change and surface curvature has an important influence on the cooling film development on a blade surface. Compared with the solid blade data, the Nusselt number was augmented by the fan-shaped hole injection. The highest augmentation factor of 2.0 was observed in the near hole region. The Nusselt number increases on both SS and PS as the exit Mach/Reynolds number increases.

Nomenclature

BR	blowing ratio
C	chord
Cp	thermal capacity
D	cooling hole inlet diameter
LE	leading edge
M_{ex}	exit Mach number
Nu	Nusselt number
P	spanwise spacing of cooling holes
Pr	Prandtl number
PS	pressure surface
Re_C	exit Reynolds number based on true chord
SS	suction surface
St	Stanton number
T	temperature
TE	trailing edge
TFG	thin film gauge
Tu	streamwise freestream turbulence intensity
U	local velocity
X	blade surface distance from stagnation point (negative indicate pressure side)
h	heat transfer coefficient
k	thermal conductivity
q”	heat flux
t	time
y	surface depth

Greek

α	Thermal diffusivity
ρ	local density

η	adiabatic effectiveness

Subscripts

a	air
aw, w	adiabatic wall, wall
c	coolant
o	uncooled
r	recovery condition
x	surface local distance
∞	freestream

Introduction

As a result of pursuing high efficiency and high output in gas turbine engine design, the turbine inlet gas temperature is being pushed to a limit that no conventional material could sustain from melting without additional thermal protection. So far, film cooling technology has been developed as the most effective thermal protection scheme. In film cooling, cool air is injected from small holes in the blade walls, generating a thin, cool, insulating layer along the blade surface to separate the blade from the hot gas flow.

Kuepper [1] reported the first film cooling experiment on turbine blade profile in Germany and called it “Boundary-layer Cooling”. Han et al. [2] provide a detailed summary of film cooling technology in gas turbines of all work prior to year 2000. The effect of parameters such as Mach number, Reynolds number, turbulence intensity, blowing ratio, coolant-to-gas temperature ratio, coolant-to-gas density ratio, coolant-to-gas pressure ratio, and injection angle have been studied. A warm wind tunnel was employed to measure both heat-transfer coefficient and adiabatic effectiveness. However, most of these studies were focused on coolant injection from a cylindrical hole. Although, Goldstein et al. [3] had demonstrated the potential of shaped hole film cooling over that of cylindrical holes in 1974, in the early years, for the purpose of studying details of the injection flow structure, most of the fan shaped hole injection cooling studies were large scale simulations, which were performed on a flat plate in low speed wind

tunnels before 2000. Bunker [4] presented a detailed update on the effectiveness of shaped hole film cooling in modern gas turbines in the consideration of both cooling effectiveness and manufacturability. The basic idea of using a fan-shaped hole to replace a cylindrical hole is that, on one hand, the expanded cross-sectional area reduces the injection velocity, therefore restraining the coolant from penetrating the cross flow boundary layer; and on the other hand, the lateral expansion of a fan-shaped hole provides better spanwise coolant coverage.

Fan-shaped hole film cooling in cascade wind tunnel test has been the focus of studies in recent years. For example, Colban et al. [5-6] performed a series of experiments on film cooled NGV in a low speed linear cascade wind tunnel using a steady-state Infrared camera technique. Other studies have looked into high Mach number and high free stream turbulence intensity effects on film cooling. Zhang and Pudupatty [7] and Zhang and Moon [8] studied the shower-head and shaped hole film cooling effect on a NGV cascade at exit Mach number 0.6 with a free-stream turbulence intensity of 12%; Schnieder et al. [9] tested the film cooling effect on the PS of a NGV with shower-head and multiple rows of shaped hole cooling, at exit Mach number 0.6 with an inlet turbulence intensity of 15%; Newman et al. [10] reported both heat transfer coefficient and adiabatic effectiveness on an NGV surface with shower-head and shaped hole injection under high Mach number conditions with an inlet turbulence intensity of 12%.

In addition to the studies on NGVs, there are many other film cooling studies on cascades of turbine blades. However, most studies have been performed at low speed or low inlet turbulence intensity. Very few reported experimental studies on shaped hole film cooling on a turbine blade at high Mach number with high free stream turbulence. Zhang and Moon [11] reported their study on multiple rows of fan-shaped hole film cooling in a linear blade cascade, using the pressure sensitive paint (PSP) technique. In their paper, only the adiabatic effectiveness was reported. In open literature, there is no published experimental data on the heat transfer coefficient of a fan-shaped hole film cooled blade at transonic Mach number with high free-stream turbulence intensity.

The main objective of this paper is to explore the film cooling performance of fan-shaped holes in a turbine blade cascade under transonic Mach number conditions with high turbulence intensity. The adiabatic film cooling effectiveness at three exit Mach numbers and two different

blowing ratios will be presented. The heat transfer coefficient will be presented in terms of Nusselt number.

Experimental Facility and Method

The experiments were performed in the Transonic Cascade Wind Tunnel at Virginia Tech. The facility is shown in Figure 1. 1 schematically. It is a blow-down, transonic, transient wind tunnel, including a heating loop for heat transfer testing. The facility is capable of tests with cascade exit Mach numbers from 0.4 to 1.2. For the heat transfer tests, the mainstream flow temperature can be set as high as 115°C at the start of the blow-down. More details of the test facility and method can be found in the report by Carullo et al. [12].

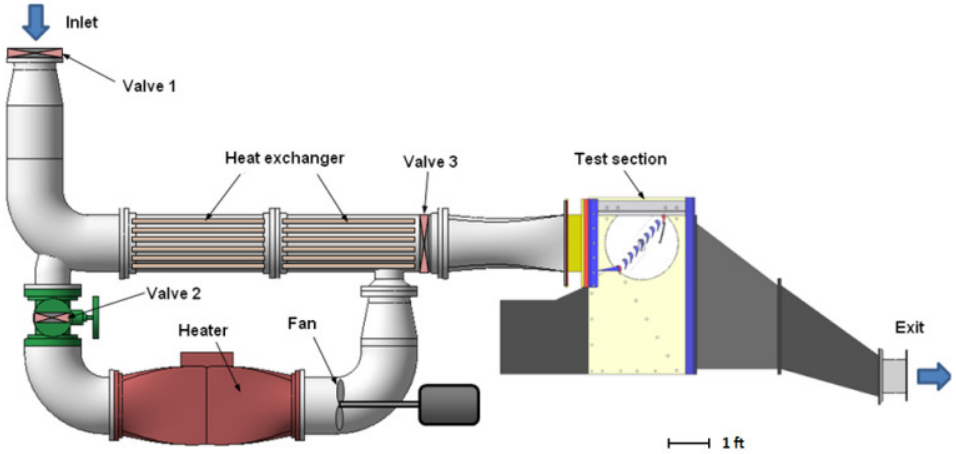

Figure 1. 1. Virginia Tech Transonic Cascade facility

In the present study, the free-stream turbulence was generated using a passive turbulence grid upstream of the test section, as shown in Figure 1. 2. The turbulence intensity at the cascade inlet, 0.5 axial chord upstream of the center blade leading edge, was measured to be 12% with an integral length scale of 0.26 normalized by the cascade pitch.

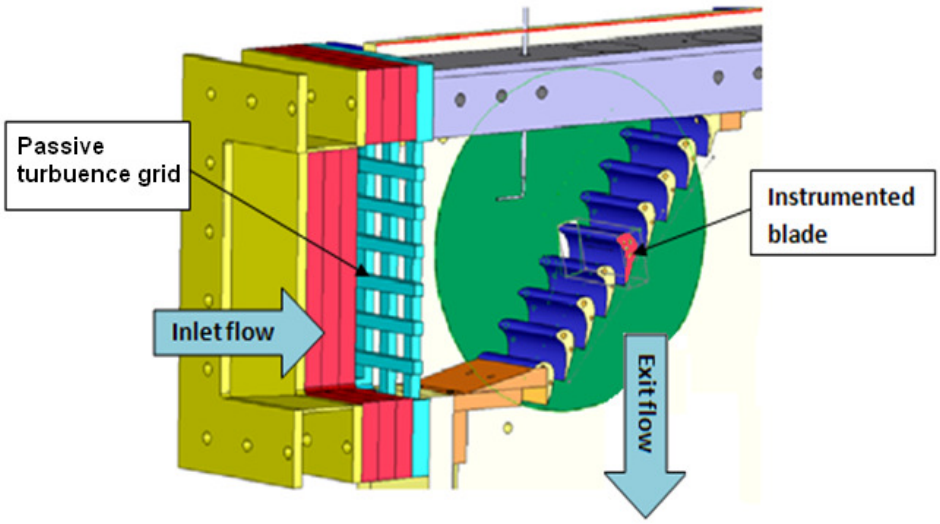

Figure 1. 2. Close-up blade cascade test section

The tested blade profile was provided by Solar Turbines Inc., and the basic parameters are shown in Table 1. 1. Only the instrumented blade in the center of the cascade has coolant injection. There are 3 rows of fan-shaped holes on the blade surface, with one row on the SS, and 2 rows on the PS. The SS cooling holes have a flow direction inclination angle of 40^{o}, with its exit located at X/C=0.304 from the leading edge. Both rows of the PS cooling holes have a flow direction inclination angle of 45^{o}, with their exits located at X/C=-0.299 and X/C=-0.470, from the physical leading edge respectively. The inlet diameter of the cooling holes is 0.79 mm. Each of the cooling holes has a 10^{o} lateral expansion angle and a 10^{o} laid-back angle at the exit, which makes the outlet/inlet area ratio to be 3.0. The fan-shaped holes do not have spanwise compound angle. Each row of cooling holes includes 15 holes, with the spanwise spacing between two holes (P/D) equal to 5.5 times of the hole inlet diameter. The three rows of cooling holes are supplied by three plenums separately, with a plenum diameter of 4.83 mm, as shown in Figure 1. 3.

Table 1. 1. Test blade parameters

True Chord	C	69.85 mm
Pitch	P	58.17 mm
Span	-	152.40 mm
Film-Cooled Span	-	63.50 mm
Inlet Angle	-	40.00 degree
Exit Angle	-	67.5 degree
Coolant Hole Diameter	D	0.79 mm

The blade surface temperature was measured using platinum Thin Film Gages (TFGs). The gages were manufactured by Air Force Research Lab using the method described by Joe [13], with a similar design as the Oxford gages of Doorly and Oldfield [14]. The gages were instrumented at the midspan of the blade, so that they all follow the centerline of one of the fan-shaped holes (Fig. 1. 3).

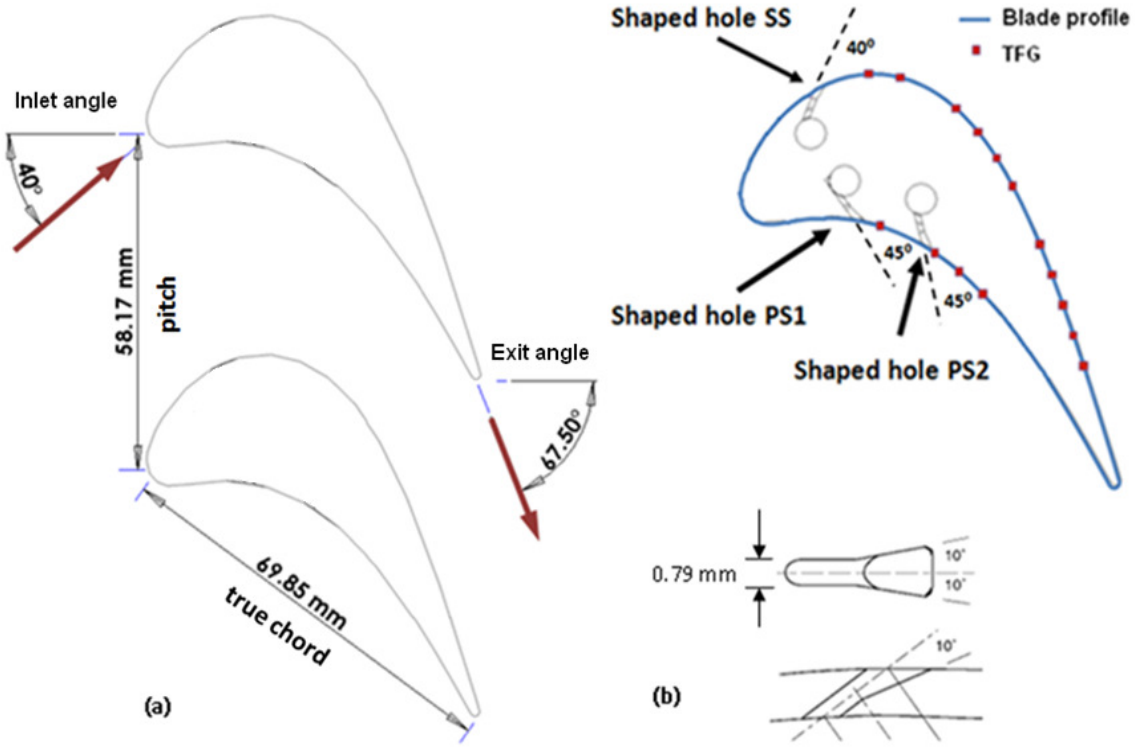

Figure 1. 3. a) blade cascade geometry; b) injection hole geometry and instrumentation

There are 15 valid gages instrumented on the test blade as is shown in Figure 1. 3. Downstream of the SS cooling holes, 11 gauges are instrumented in the region of

0.42<X/C<1.29. One gage was instrumented between the first and the second row of the holes on the PS at X/C=-0.363; 3 gages were instrumented downstream of the second row of holes on PS, at -0.701<X/C<-0.560. With the TFG technology, the present data are available only along the centerline of fan-shaped hole.

Data Reduction

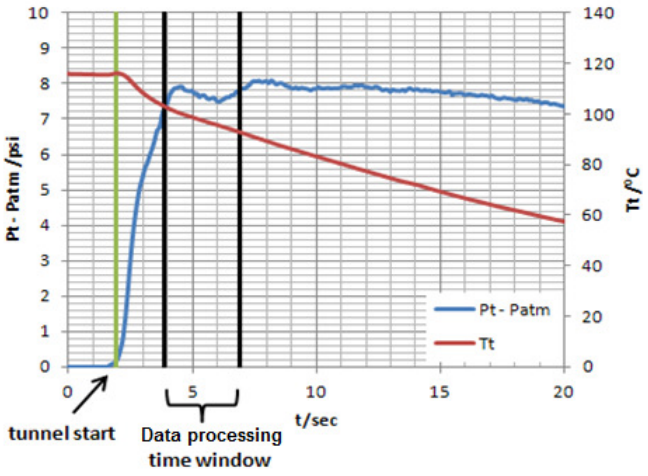

Figure 1. 4. Time history of upstream total pressure and total temperature

Figure 1. 4 shows the time history of upstream total temperature and total pressure. The data reduction time window for linear regression process begins 2 seconds after the tunnel starting, and lasts 3 seconds.

The test blade was made of a special ceramic glass, known as Macor ®, which has low thermal conductivity (k=1.46 W/mºC). A 1D assumption of surface heat flux (eq. 1.1) is valid on the test blade during the data acquisition time window. A finite difference code developed by Cress [15] was employed to calculate heat flux.

$$\frac{\partial^2 T}{\partial y^2} = \frac{1}{\alpha}\frac{\partial T}{\partial t} \qquad (1.1)$$

A linear regression method developed by Popp et al. [16] was used to determine the heat transfer coefficient and film cooling effectiveness. This method starts with the fundamental convective heat transfer equation

$$q" = h(T_{aw} - T_w) \qquad (1.2)$$

The adiabatic effectiveness (non-dimensionalized adiabatic wall temperature) is defined as

$$\eta = \frac{T_{aw} - T_r}{T_c - T_r} \qquad (1.3)$$

where Tr is the recovery temperature, which is determined by the assumed recovery factor ($\sqrt[3]{\text{Pr}}$) and the local Mach number.

Combining Equations 1.2 and 1.3 yields a linear expression of the relationship between heat flux and adiabatic effectiveness in the form of y = mx + b.

$$\frac{q"}{T_r - T_c} = h\left(\frac{T_r - T_w}{T_r - T_c}\right) - h \cdot \eta \qquad (1.4)$$

To reduce the uncertainty a dual-data-regression method was employed in data reduction. For this technique, two runs are performed at identical mainstream flow conditions and blowing ratio but with different coolant temperatures. This technique reduces uncertainty by increasing the number of data points used for regression and adding points closer to the x-axis, reducing the distance the line fit is extrapolated to calculate effectiveness. Figure 1. 5 shows the double linear regression technique performed on a sample data set, with heat transfer coefficient and film effectiveness highlighted.

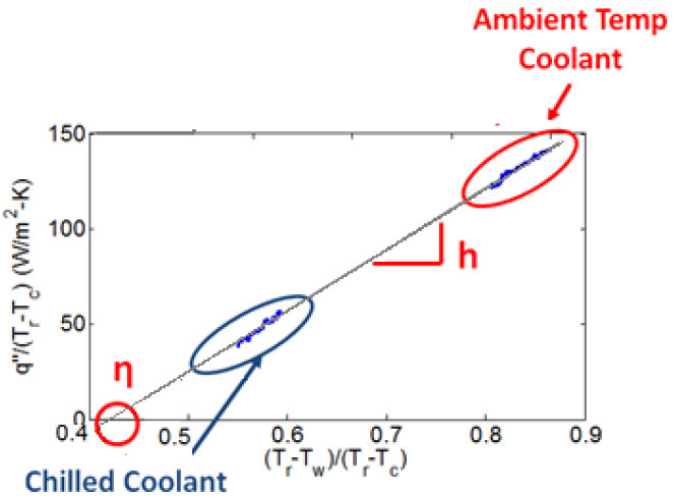

Figure 1. 5. Dual-data-regression line fit

Uncertainty was calculated based on errors present in measured data which were propagated first through the finite difference calculation of q" then through the linear regression of heat transfer coefficient and film effectiveness. Error in heat flux was calculated using Moffat's [17] perturbation method due to the finite difference code used to calculate heat transfer coefficient and adiabatic effectiveness. Brown and Coleman's [18] linear regression analysis was then used to calculate the uncertainty of heat transfer coefficient and film effectiveness based on the x and y-axis uncertainties. The average uncertainty in heat transfer coefficient is ± 8% of full scale, and an average uncertainty in film effectiveness is ± 0.08. More details on the data reduction method and uncertainty analysis can be found in the report by Newman et al. [10] and Newman [19].

When using chilled coolant, the coolant to mainstream density ratio changes from the room temperature case. In general, the density ratio of chilled coolant is about 7% ~ 15% higher than that of the room temperature coolant. Ekkad et al. [20] have shown, for higher blowing ratios (BR>1), increasing of coolant density within a certain range showed no appreciable effect on film effectiveness distributions. Based on this information, film effectiveness distributions from the present study should not be affected by using two coolant temperatures as all cases considered are at BR>1.

In the following discussion, the heat transfer coefficient will be non-dimensionalized as Nusselt number, defined in Equation 1.5.

$$Nu = \frac{h \cdot C}{k_a} \qquad (1.5)$$

Test Matrix

The tests were performed at multiple exit Mach/Reynolds numbers. Table 1. 2 shows the matrix of test conditions. The Reynolds numbers were based on the exit velocity (m/s) and blade true chord (m). In the current test facility the Mach number and Reynolds number are coupled and cannot be changed independently.

The coolant blowing ratio, as defined in Equation 1.6, of each row of the fan-shaped holes was calculated based on the plenum total pressure and the local static pressure at the cooling hole exit. The metering area for the holes is the inlet area.

$$BR = \frac{\rho_c U_c}{\rho_\infty U_\infty} \qquad (1.6)$$

Table 1. 2. Matrix of basic test conditions

Inlet Tu	Exit Ma	Exit Re	Nominal BR	Blowing Ratio			Density Ratio		
				SS	PS1	PS2	SS	PS1	PS2
12%	0.67	$8.1X10^5$	High BR	1.6	4.0	3.1	1.43	1.64	1.54
			Low BR	1.1	2.7	2.2	1.20	1.43	1.39
	0.84	$1.08X10^6$	High BR	1.6	3.7	2.8	1.62	1.60	1.49
			Low BR	1.3	3.0	2.2	1.20	1.44	1.38
	1.01	$1.42X10^6$	High BR	1.5	3.8	2.9	1.30	1.42	1.39
			Low BR	1.2	2.9	2.4	1.23	1.36	1.33

Result and Discussion

In the first part of this section, the isentropic Mach number distributions are given, and a comparison of Stanton number with the flat plate correlation is presented to provide fundamental insight on how the boundary layer is behaving on the blade surface. Then, the data recorded at different Mach numbers and blowing ratios was presented. The trends of Nusselt number and

adiabatic effectiveness were discussed. The film cooling effectiveness is highly dependent on the interaction between the coolant injection flow and the blade boundary layer flow.

Mach number distribution

Figure 1. 6 shows the local Mach number distributions, which was measured by Carullo et al. [12] on the solid blade surface. The flow accelerates over most of the pressure side except for a short deceleration region downstream of the stagnation point (x/c=-0.25). The flow on the suction side continually accelerates up to throat area (x/c=0.84). For the exit Mach 0.67 and 0.84 cases, the deceleration occurred immediately after the throat, whereas for exit Mach 1.01case the acceleration continued to supersonic until the shock occurred at x/c=1.05.

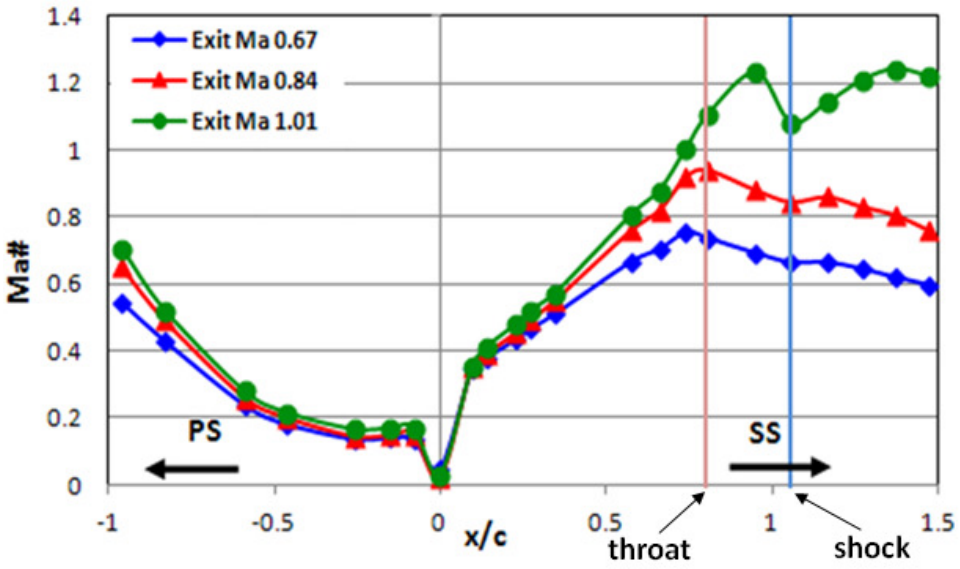

Figure 1. 6. Local Mach number distribution at different exit Mach numbers

Stanton number comparison with analytical solution

Stanton number is one of the most commonly used measures of convective heat transfer. It is defined as the ratio of heat transfer coefficient and the thermal capacity of the fluid. In Figures 1. 7 and 1. 8, Stanton number distributions on the blade with and without film cooling are compared with the computed analytical values of both laminar and turbulent boundary layers on a flat plate with zero pressure gradient, plotting against local Reynolds number (Rex). This comparison is useful to gain fundamental insight on how the boundary layer is behaving on the blade surface. The data on the blade without film cooling (solid blade) was reported by Carullo

et al. [12], which was measured on the same blade profile but without cooling holes. The analytical Stanton number on a flat plate was based on the correlation presented by Incropera and De Witt [21]. Equations 1.7 and 1.8 are the equations of laminar and turbulent boundary layers respectively.

$$St_x = \frac{0.332 Re_x^{1/2} Pr^{1/3} k_a}{x \rho_x U_x C_{p,\infty}} \qquad (1.7)$$

$$St_x = \frac{0.0296 Re_x^{4/5} Pr^{1/3} k_a}{x \rho_x U_x C_{p,\infty}} \qquad (1.8)$$

The experimental data with and without film cooling, in Figures 1. 7 and 1. 8, was recorded at ReC ≈ 8x10^5. The film cooled data was recorded at low blowing ratio.

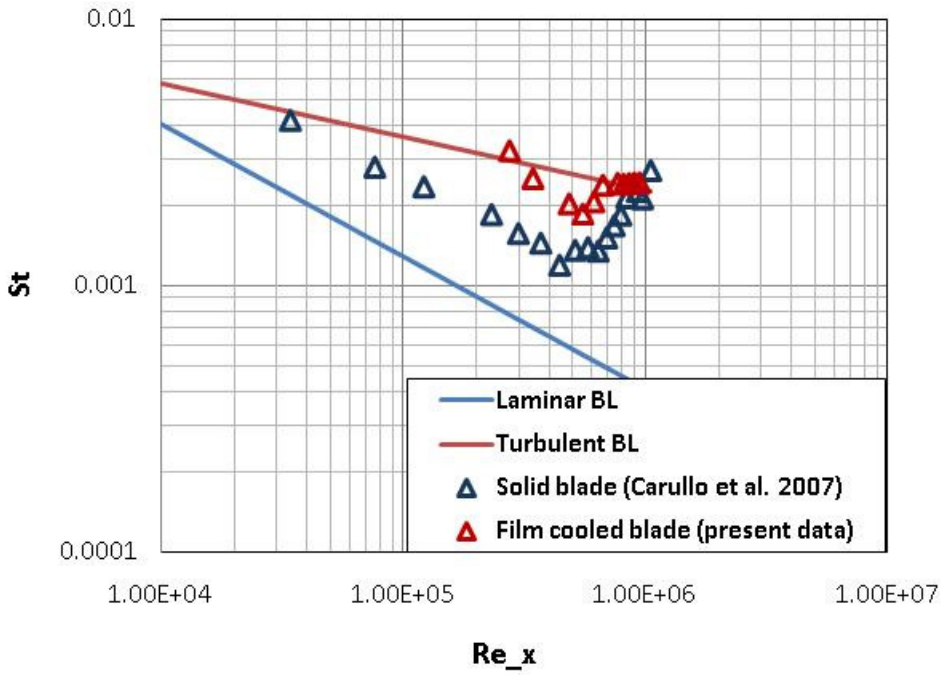

Figure 1. 7. SS Stanton number at exit ReC ≈ 8x10^5 comparison with analytical solution on flat plate with zero pressure gradient

Figure 1. 7 shows the comparison of Stanton number on the SS. The solid blade data first follows the trend of the laminar boundary layer solution, but is at a higher level due to the high freestream turbulence that enhances the convective heat transfer coefficient on the SS. As the flow develops downstream, a clear boundary layer transition can be identified by a quick rise of

the Stanton number to the level of the turbulent boundary layer correlation. On the film cooled blade SS, the Stanton number starts from a value higher than the turbulent analytical line. This may be due to the injection flow disrupting the boundary layer, causing vortices and mixing, which further elevates the heat transfer coefficient. After the near hole region the Stanton numbers decrease slightly. At almost the same location where the boundary layer transition starts on the solid blade, the Stanton number of film cooled blade also starts to increase and finally reaches the turbulent boundary level.

Figure 1. 8 shows the comparison of Stanton number with the correlations on the PS. The solid blade data follows the turbulent boundary layer correlation all the way to the trailing edge, which suggests the boundary layer on the PS is fully turbulent. Usually, the local acceleration on the PS is supposed to cause the reversed transition of the boundary layer, and has a stabilizing effect. However, in the present study, the PS is a concave surface with a high curvature. The surface curvature increase turbulence in the boundary layer on a concave surface in two ways. One is caused by the centrifugal force, which generates Taylor-Göertler vortex. Another is caused by the extra term in the Reynolds stress equation due to the existing of the curvature. Therefore the turbulence level is high on the PS; the Stanton numbers at the first 2 points of film cooled blade are significantly higher than the turbulent boundary layer line. As mentioned previously, this may be caused by the coolant injection disrupting the boundary layer. After the first 2 points the Stanton number decreases to the same level as the solid blade.

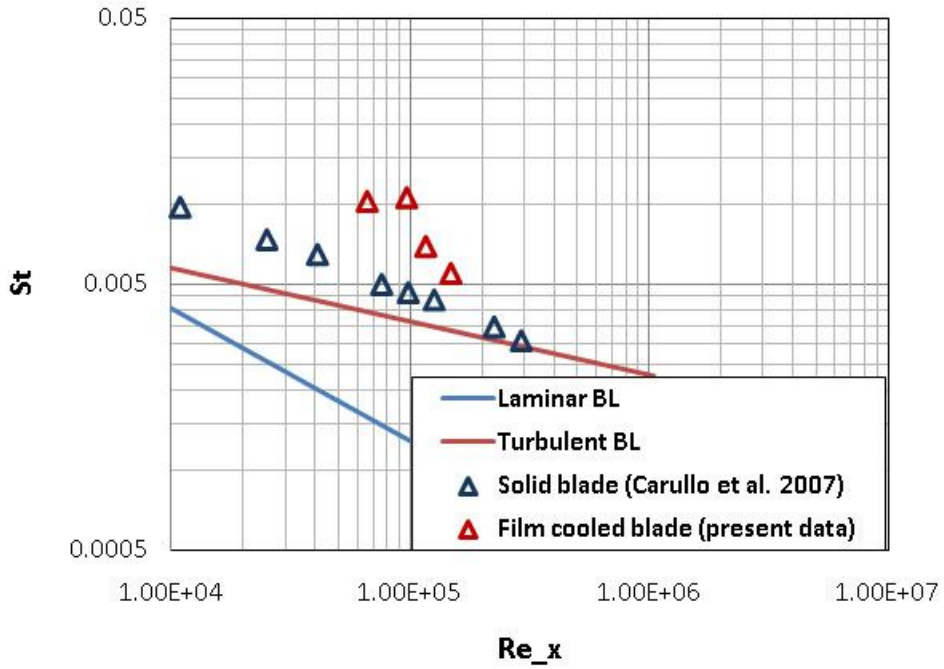

Figure 1. 8. PS Stanton number at exit ReC ≈ 8x10^5 comparison with analytical solution on flat plate with zero pressure gradient

Comparison between film cooled blade and solid blade

Figure 1. 9 shows the Nusselt number comparison between the solid blade and the film cooled blade. Both cases, with and without film cooling data, were recorded at exit ReC ≈ 8x10^5, and the film cooled blade was at low blowing ratio of the SS BR=1.1; PS row 1 BR=2.7; PS row 2 BR=2.2.

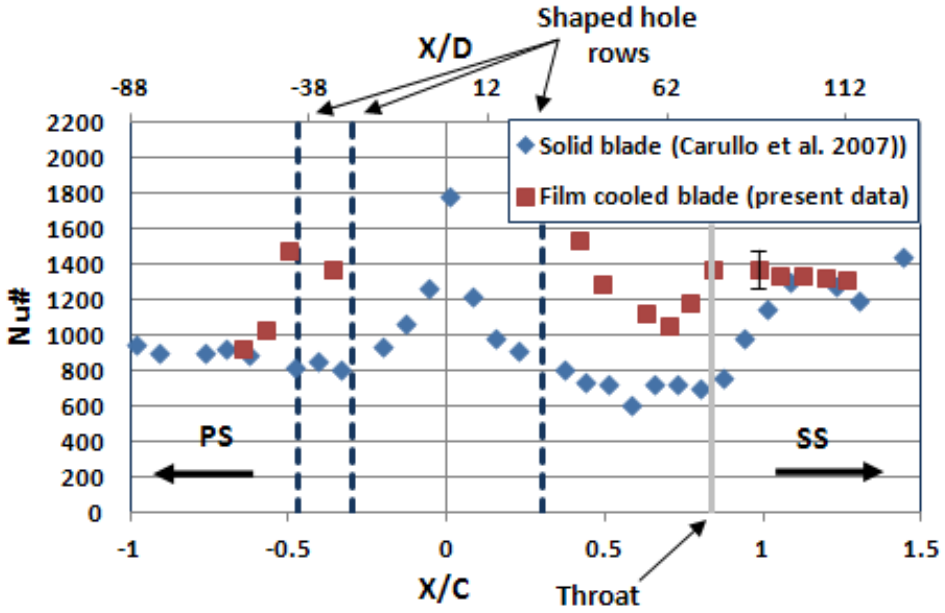

Figure 1. 9. Nusselt number comparison between solid blade and film cooled blade at $Re_C \approx 8\ X10^5$

For the solid blade, the highest Nusselt number is observed at the leading edge, which is expected as a result of the incoming flow impinging on the leading edge. Further downstream, as the boundary layer grows thicker, the Nusselt numbers decrease on both SS and PS. On the SS, it is conjectured that boundary layer transition starts at x/c=0.6. Due to the high acceleration flow on the SS surface (the acceleration parameter in this region is higher than 1.0). This transition lasts for a long distance, and it completes at x/c=1.15, where the Nusselt number reaches the level of a turbulent boundary layer, and thereafter, stays at the same level. On the PS, since the boundary layer develops on a concave surface, it is highly unstable. As a result, the boundary layer becomes turbulent very early (Fig. 1. 8). After the leading edge region, the Nusselt number decreases directly to the level of a turbulent boundary layer, and stays at that level all the way to the blade trailing edge.

From Figure 1. 9, the first noticeable feature for the film cooled blade is that on both SS and PS, in the near hole region, the Nusselt number is augmented by the coolant injection by approximately factor of 2.0. Nusselt number augmentation above 2.0 was reported by Lu et al. [22] on a flat plate and by Saumweber et al. [23] on a surface cooled by two rows injection. Further downstream, on the SS, it can be observed that the coolant injection causes higher Nusselt number, compared to the solid blade. The distance of the transition region on the film

cooled SS is much shorter than on the solid blade. The transition completed at X/C=0.84 on the film cooled blade, and at X/C=1.15 on the solid blade. This is due to the injection tripping the boundary layer, and accelerating the transition. On the PS, after the two rows of injection, the Nusselt number decreases quickly to the level of the solid blade.

Mach/Reynolds number effect

Figure 1. 10 shows the Nusselt number distributions for different exit Mach/Reynolds numbers at low blowing ratio. It can be observed that the exit Mach/Reynolds number has a considerable influence on Nusselt number. Increasing exit Mach/Reynolds number augments the Nusselt number on both SS and PS. The same effect of Mach/Reynolds number on Nusselt number was observed by many other studies on film cooled and non film cooled surface, such as Reiss and Bölcs [24] and Drost et al. [25]. From Figure 1. 10, it can be noticed that there is a dip in Nusselt number at X/C=1.05 for the Mex=1.01 case. This may be caused by the shock/boundary layer interaction.

Figure 1. 11 shows the effect of exit Mach/Reynolds number on adiabatic effectiveness distribution at a low nominal blowing ratio as the SS BR=1.2, PS row 1 BR=2.8, PS row 2 BR=2.2. On the SS, the adiabatic effectiveness for different exit Mach/Reynolds numbers start from the same value of 0.33 in the near hole region. Within 0.6<X/C<1.2, the effectiveness is improved by the increased exit Mach/Reynolds number. After X/C=1.2, the effectiveness of different exit Mach/Reynolds number merges together. Similar to the Nusselt number discussion above, the trend of the Mex=1.01 case is slightly different from the subsonic cases. There is a plateau of the effectiveness in the region of 0.8<X/C<1.05, and after X/C=1.05 the effectiveness drops quickly. This is believed to be caused by the shock/boundary layer interaction, which will be specifically discussed in another paper with CFD study. The same trend for the subsonic cases was observed by Newman et al. [10] on a NGV SS. On the PS, the adiabatic effectiveness is degraded by the increased exit Mach/Reynolds number. The effectiveness of Mex=0.67 is close to the effectiveness of Mex=0.84, because the PS blowing ratio of Mex=0.67 is slightly lower than the other two Mach numbers. This is due to a blowing ratio control issue inherent in the test setup.

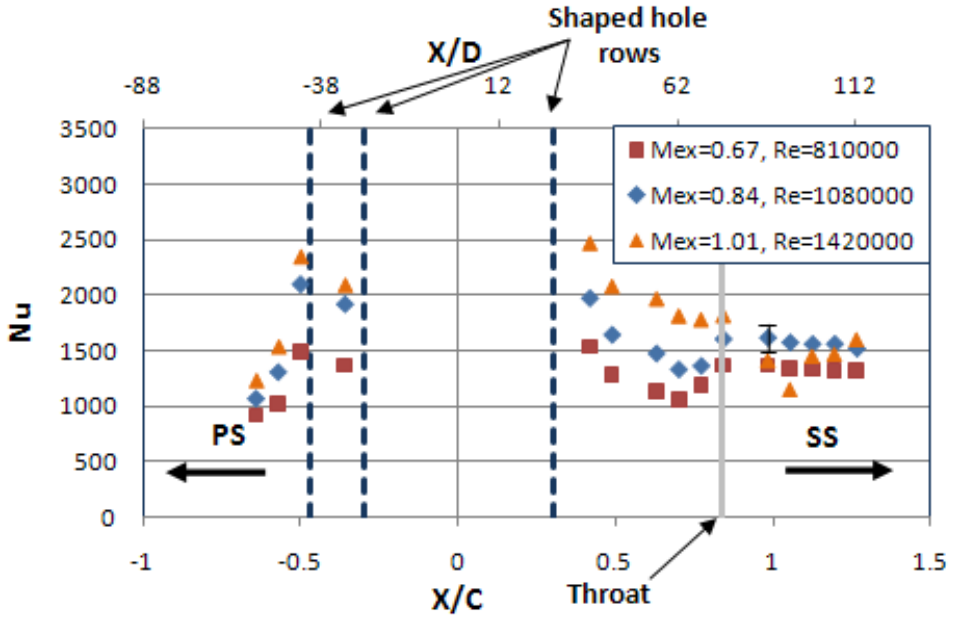

Figure 1. 10. Nusselt number for different exit Mach/Reynolds number at Low BR

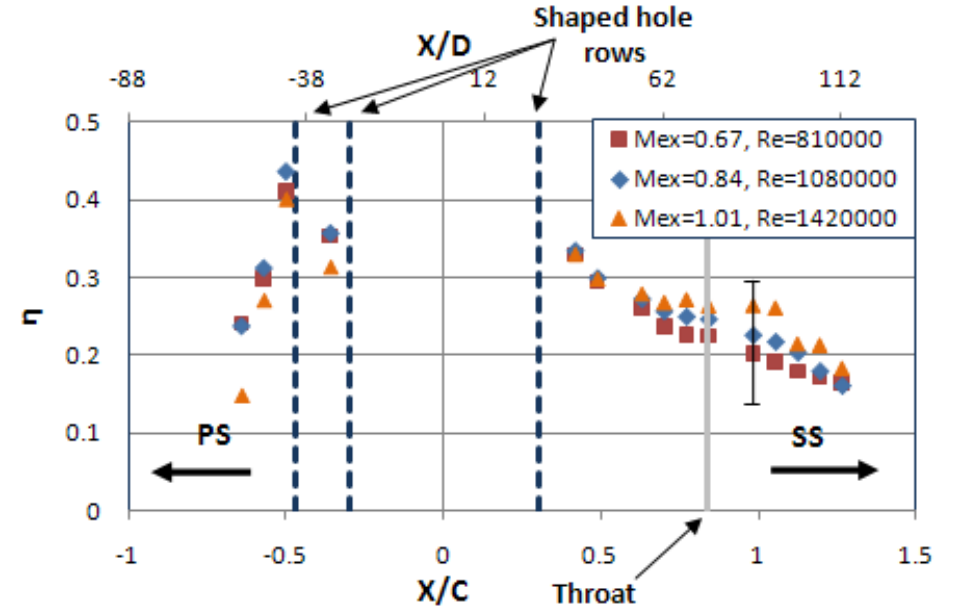

Figure 1. 11. Adiabatic effectiveness for different exit Mach/Reynolds number at Low BR

The decay of adiabatic effectiveness on the PS is much faster than on the SS. This trend was also observed by others such as Takeishi et al. [26]. It was pointed out by Schwarz and Goldstein [27] that the different effects of centrifugal force on convex and concave surface could be the main factor that caused the different effectiveness distributions on PS and SS.

When the fluid passes over a curved surface, the centrifugal force and the pressure gradient balance each other. At the near hole region, when the blowing ratio is not too high, usually the injection flow has a low streamwise velocity. The centrifugal force of the injection flow is too low to balance the pressure gradient. Thus, the pressure gradient pushes the cooling flow towards a convex surface, and lifts it away from a concave surface. For the extreme high blowing ratio injection, since the streamwise velocity of the injection flow is higher than the mainstream, the centrifugal force is larger than the pressure gradient force, and the curvature effect on injection flow will reverse. According to the detail studies on film injection using CFD, such as Hyams and Leylek [28], the mixing of coolant with the hot gas was mainly driven by the counter rotating vortices (kidney vortices). For low blowing ratio cases, the convex curvature reduces the kidney vortices, and the concave curvature intensifies it. The famous Taylor-Couette experiment showed that even without any injection on a concave surface the centrifugal force itself is able to generate vortices, known as the Taylor vortices, which mix the flow transversely between the upper and lower layers in the boundary layer.

In the present investigation, as the Mach/Reynolds number increases, the local velocity increases the centrifugal effect on the convex (SS) and concave (PS) surface. The effect of centrifugal force stabilizes the boundary layer flow on the film cooled SS and de-stabilizes the boundary layer flow on the film cooled PS. based on the discussion above, and the data in literature, it is suggested in the design of the film cooling system in a high turning gas turbine blade, less amount of coolant injection is needed on the SS, and the coolant film lasts far downstream. Thus, less rows of injection is needed on the SS. On the PS contrary, multiple rows of injection is needed, because the coolant mixed up with the hot main flow very fast.

Blowing ratio effect

Figure 1. 12 shows the blowing ratio effect on Nusselt number distribution at Mex = 0.84.

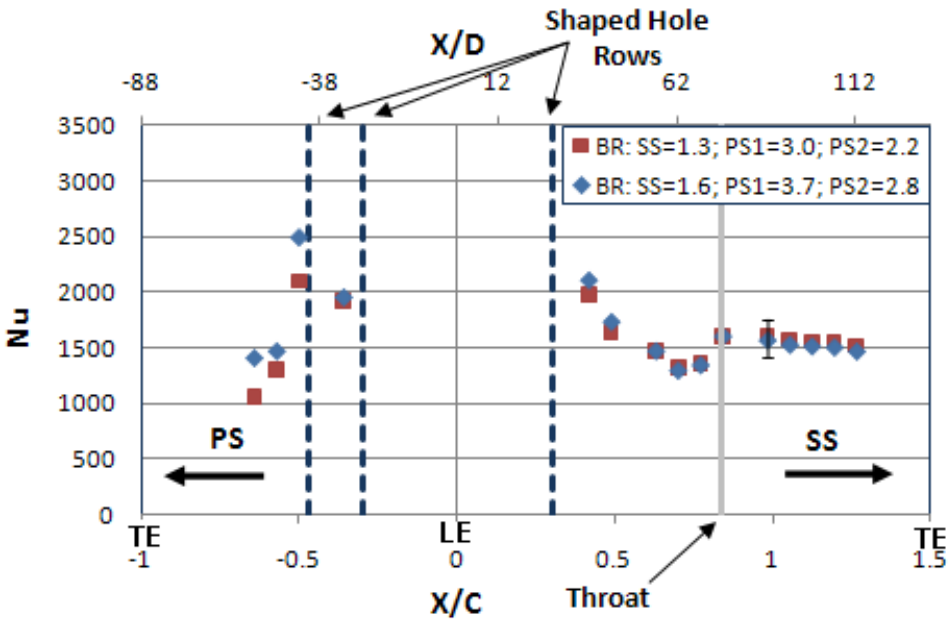

Figure 1. 12. Nusselt number of different BR at Mex=0.84

The Nusselt number seems insensitive to the change of blowing ratio on the SS. There is very little augmentation in the near hole region as the blowing ratio increase from 1.3 to 1.6, which is within the uncertainty. After the first two points, the Nusselt numbers of the two different blowing ratio cases are almost identical. On the PS, increasing the blowing ratio augments the Nusselt number slightly. It should be noticed that after the first row of injection on the PS, the Nusselt number of the two different blowing ratios are still very close.

In Figure 1. 13, the adiabatic effectiveness of two blowing ratios at Mex=0.84 are plotted together. Generally, the effectiveness is more sensitive to the blowing ratio change than the Nusselt number. Increasing blowing ratio augments the effectiveness by an average of 0.05 on both the SS and the PS.

The blowing ratio effect on Nusselt number and effectiveness on the SS suggests the boundary layer flow pattern on the SS of low and high blowing ratio are similar.

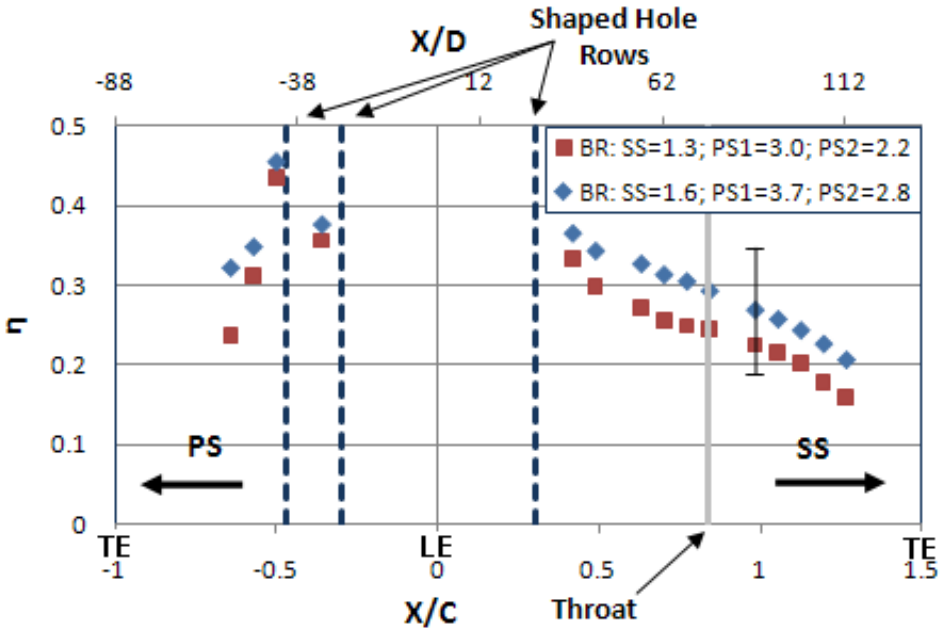

Figure 1. 13. Adiabatic effectiveness of different BR at Mex=0.84

Conclusion

Blowdown experiments on a fan-shaped hole film cooled blade was performed in a 2-D linear turbine blade cascade at transonic Mach number and high inlet freestream turbulence intensity with large length scale. The convective heat transfer coefficient and the film cooling performance data were recorded at three different exit Mach/Reynolds numbers and two different blowing ratios. The data was reported in terms of Nusselt number and adiabatic film effectiveness.

The data in the present study confirmed the results in literature on fan-shaped hole film cooling. Comparing with solid blade data, the Nusselt number was augmented by the fan-shaped hole injection. The highest augmentation factor of 2.0 was observed in the near hole region.

The Nusselt number increases on both SS and PS as the exit Mach/Reynolds number increases; the effectiveness was improved on the SS, and was compromised on the PS, by the increased exit Mach/Reynolds number. The different centrifugal effects on the convex and concave surface are believed to be the reason for the different trends in effectiveness on the SS and the PS of the blade.

The Nusselt number is less sensitive to the blowing ratio change than the effectiveness. Increased blowing ratio appears to enhance effectiveness on both the SS and the PS.

Acknowledgement

The authors are thankful to Solar Turbines incorporated for supporting this research and granting the permission to publish the result. Special thanks to Dr. Richard Anthony (AFRL) for providing the thin film gages used in this study. Particular appreciation goes to Dr. Diller for his helpful discussions. The authors are grateful to Andrew Newman and Adam Shoemaker for their assistant on the experiment. The authors also like to express their gratitude to The Connecticut Center for Advanced Technology, Inc. for their help in machining of the fan-shaped holes.

Reference

[1] Kuepper, K. H., 1944, "Temperature Measurements on Two Stationary Blade Profiles for Gas Turbines with Boundary-Layer Cooling", DVL-St-Report, No. 81 (in German); also 1946, *U. S. Air Force Air Material Command,* Translation No. F-TS-1543-RE.

[2] Han, J. C., Dutta, S., and Ekkad, S. V., 2000, "Gas Turbine Heat Transfer and Cooling Technology," *Taylor & Francis, 29 West 35th Street, New York,* NY 10001.

[3] Goldstein, R. J., Eckert, E. R. G., and Burggraf, F., 1974, ''Effects of Hole Geometry and Density on Three-Dimensional Film Cooling,'' *Int. J. Heat Mass Transfer*, Vol. 17, p. 595–607.

[4] Bunker, R. S., 2005, "A Review of Shaped Hole Turbine Film-Cooling Technology," *ASME Journal of Heat Transfer*, Vol. 127, p. 441-453.

[5] Colban, W., Gratton, A., Thole, K. A., and Haendler, M., 2005, "Heat Transfer and Film-Cooling Measurements on a Stator Vane with Fan-Shaped Cooling Holes". *IGTI Turbo Expo*, GT2005-68258.

[6] Colban, W., Thole, K. A., and Haendler, M., 2007, "Experimental and Computational Comparisons of Fan-Shaped Film Cooling on a Turbine Vane Surface". *ASME Journal of Turbomachinery*, Vol. 129, p. 23-31.

[7] Zhang, L., Pudupatty, R., 2000, "The Effects of Injection Angle and Hole Exit Shape on Turbine Nozzle Pressure Side Film Cooling". *IGTI Turbo Expo*, *Munich,* 2000-GT-247

[8] Zhang, L. and Moon, H. K., 2008, “The Effect of Wall Thickness on Nozzle Suction Side Film Cooling”. *IGTI Turbo Expro*, GT2008-50631.

[9] Schnieder, M., Parneix, S., and Wolfersdorf, J. V., 2003, “Effect of Showerhead Injection on Superposition of Multi-Row Pressure Side Film Cooling with Fan Shaped Holes”. *IGTI Turbo Expro*, GT2003-38693.

[10] Newman, A., Xue, S., Ng, W., Moon, H. K. and Zhang, L., 2011, "Performance of A Showerhead and Shaped Hole Film Cooled Vane at High Freestream Turbulence and Transonic Conditions," *ASME Turbo Expo*, GT2011- 45142.

[11] Zhang, L. and Moon, H. K., 2007, “Turbine Blade Film Cooling Study – the Effects of Film Hole Location on the Pressure Side”. *IGTI Turbo Expro*, GT2007-27546.

[12] Carullo, J. S., Nasir, S., Cress, R. D., Ng, W. F., Thole, K. A., Zhang, L., and Moon, H. K., 2007, "The Effects of Freestream Turbulence, Turbulence Length Scale, and Exit Reynolds Number on Turbine Blade Heat Transfer in a Transonic Cascade," *IGTI Turbo Expo*, *Montreal,* GT2007-27859.

[13] Joe, C. R., 1997, “Unsteady Heat Transfer on the Turbine Research Facility at Wright Laboratory,” *Ph.D. Dissertation, Syracuse University.*

[14] Doorly, J. E., Oldfield, M. L. G., 1987, “The Theory of Advanced Multi-Layer Thin Film Heat Transfer Gages,” *Int. J. Heat and Mass Transfer*, 30, p. 1159–1168.

[15] Cress, R. D., 2006, “Turbine Blade Heat Transfer Measurements in a Transonic Flow Using Thin film Gages,” *Master’s Thesis, Virginia Polytechnic Institute and State University.*

[16] Popp, O., Smith, D. E., Bubb, J. V., Grabowski, H. C., Diller, T. E. Schetz, J. A., Ng. W. F., 2000, “An Investigation of Heat Transfer in a Film Cooled Transonic Turbine Cascade, Part II: Unsteady Heat Transfer,” *IGTI Turbo Expo*, *Berlin,* GT-2000-203.

[17] Moffat, R. J., 1988, “Describing Uncertainties in Experimental Results,” *Exp. Thermal and Fluid Science,* 1, pp. 3-17.

[18] Coleman, H. W., Brown, K. H., and Steele, W. G., 1995, “Estimating Uncertainty Intervals for Linear Regression,” AIAA-1995-0796.

[19] Newman, A., 2010, "Performance of a Showerhead and Shaped Hole Film Cooled Vane at High Freestream Turbulence and Transonic Conditions," *Master’s Thesis, Virginia Polytechnic Institute and State University.*

[20] Ekkad, S. V., Han, J. C., Du, H., 1998, "Detailed Film Cooling Measurements on a Cylindrical Leading Edge Model: Effect of Free-Stream Turbulence and Coolant Density," *ASME J. Turbomachinery,* 120, pp. 799-807.

[21] Incropera, F. P. and DeWitt, D. P., 2002, "Fundamentals of Heat and Mass Transfer," *5th Ed., John Wiley and Sons, New York.*

[22] Lu, Y., Dhungel, A., Ekkad, S. V., Bunker, R. S., 2009, "Effect of Trench Width and Depth on Film Cooling from Cylindrical Holes Embedded in Trenches," *ASME J. Turbomachinery*, Vol. 131, p. 1-13.

[23] Saumweber, C., Schulz, A., 2004, "Interaction of Film Cooling Rows: Effects of Hole Geometry and Row Spacing on the Cooling Performance Downstream of the Second Row of Holes," *ASME J. Turbomachinery*, Vol. 126, p. 237-246.

[24] Reiss, H. and Bölcs, A., 2000, "The Influence of the Boundary Layer State and Reynolds Number on Film Cooling and Heat Transfer on a Cooled Nozzle Guide Vane", *IGTI Turbo Expo,* GT2000-205.

[25] Drost, U., Bölcs, A., 1999, "Investigation of Detailed Film Cooling Effectiveness and Heat Transfer Distributions on a Gas Turbine Airfoil", *ASME Journal of Turbomachinery*, Vol. 121, p. 233-242.

[26] Takeishi, K., Aoki, S., Sato, T., Tsukagoshi, K., 1992, "Film Cooling on a Gas Turbine Rotor Blade." *ASME Journal of Turhomachinery*, Vol. 114, p. 828-834.

[27] Schwarz, S. G., Goldstein, R. J., 1989, "The Two-Dimensional Behavior of Film Cooling Jets on Concave Surfaces." *ASME Journal of Turhomachinery*, Vol. 111, p. 124-130.

[28] Hyams, D. G. and Leylek, J. H., 2000, "A Detailed Analysis of Film Cooling Physics: Part III—Streamwise Injection With Shaped Holes," *ASME Journal of Turbomachinery*, vol. 122, p. 122-132.

Preface Paper 2

Paper 2 numerically investigated the shock/film cooling interaction. The objective of the study in paper 2 is to use CFD tool to explore the flow details of the shock/film cooling interaction, and to explain the trend of the film cooling effectiveness that was observed in the experiment. The centerline film cooling effectiveness was presented and compared with the experimental data. Detail flow structure plots and discussion on the shock/film cooling interaction were provided. The paper is in preparation for submission to the ASME TURBO EXPO 2013.

SHOCK EFFECT ON FAN-SHAPED FILM COOLED TRANSONIC GAS TURBINE BLADE: CFD AND COMPARISON WITH EXPERIMENT

S. Xue, W. Ng, S. Ekkad
Mechanical Engineering Department
Virginia Polytechnic Institute and State University
Blacksburg, VA, USA

In preparation for IGTI conference publication

Abstract

A CFD investigation of the shock effect on film cooling performance has been carried out on a fan-shaped hole injected blade model. The shock/ film cooing interaction on the blade suction side (SS) near the trailing edge was observed in the experimental study by Xue et al. [1]. The experimental data showed that the adiabatic effectiveness has a noticeable decrease (about 25%) at the location of shock impingement. The objective of the present CFD study is to explore the details of the shock/film cooling interaction, and try to explain the physics of the observations. The CFD results indicate that the adiabatic effectiveness drop was caused by the strong secondary flow, which sucks the hot air from sides and lifts the cooling flow away from the SS surface, and increases the mixing. This secondary flow is related to the non-uniformity of the shock in the cross stream plane.

Nomenclature

a	speed of sound
BR	blowing ratio
C	chord
d	cooling hole inlet diameter
Ma	Mach number
P	pressure
PR	pressure ratio (injection total pressure/main stream local static pressure)
PS	pressure surface
Re	Reynolds
R	curvature radius/individual gas constant

SS	suction surface
s	surface distance from blade leading edge or SS injection
T	temperature
Tu	streamwise freestream turbulence intensity
U	local velocity
Greek	
η	adiabatic effectiveness
γ	adiabatic index
θ	non-dimensional temperature ($\theta = T/\mathrm{T}_{0\_inlet}$)
δ	non-dimensional pressure ($\delta = P/P_{0\_inlet}$)
Subscripts	
1	status before the shock
2	status after the shock
aw	adiabatic wall
c	coolant
0	stagnation status
r	recovery condition

Introduction

Film cooling technology has been developed as the most effective thermal protection scheme in gas turbine engines ever since 1940s, and has been extensively studied in the past 30 years both experimentally and numerically. The major objectives for film cooling scheme design is to generate a thin, cool, insulating layer of injected air along the blade surface to separate the blade from the hot gas. The measure of this effect is defined by Equation 2.1, known as the adiabatic effectiveness.

$$\eta = (T_r - T_{aw})/(T_r - T_c) \qquad (2.1)$$

Where $\mathrm{T_r}$ is the local recovery temperature of the hot main flow, $\mathrm{T_{aw}}$ is the adiabatic surface temperature, and $\mathrm{T_c}$ is the coolant temperature of the injection. The adiabatic effectiveness is essentially a scalar which reflects the mixing between the coolant film and the

hot main flow. The experimental studies on film cooling prior to year 2000 has been summarized by Han et al. [2], and the early years (1971-1996) CFD study on film cooling was list in Kercher's bibliography [3].

As reported by Ito et al. [4] and Lutum et al. [5], on a gas turbine blade SS, when the film cooling blowing ratio is not too high, due to the convex surface curvature stabilizing the coolant film flow, a single row injection cooling effectiveness last far downstream. When the turbine blade operates at a supersonic exit condition, it is common that one leg of the fishtail shock from the adjacent upper blade trailing edge impinges the SS boundary layer of the lower blade, as shown in Figure 2. 1. As the cooling film flow passes through the shock impingement on SS, it interacts with the shock, and causes complicated aerodynamic and heat transfer interaction. The present study is dealing with this pattern of shock/film cooling interaction.

This pattern of shock/film cooling interaction has been experimentally investigated by Göttlich et al. [6]. In their experiment, the coolant was injected from a row of innovative geometry holes on the PS, and then wrap over the leading edge to the SS. They measured the adiabatic film effectiveness on the suction side of a blade trailing edge in a linear cascade, and they concluded that the oblique shock impingement does not significantly affect the film effectiveness. Ochs et al. [7] used a contoured plate and curved surface to simulate shock impingement at a turbine stage exit. According to their observation, the shock effect on the adiabatic film effectiveness is secondary, when the injection is far upstream (s/d=43). However, there is a 25% increase of heat transfer coefficient at the location of shock impingement.

In the present study, the coolant was injected at s/c=0.304 on the SS, with the local Mach number is 0.52 at the fan-shaped hole exit. The shock occurs near the trailing edge, at s/c=1.05 (s/d=66 from the SS injection). Unlike the result reported by Göttlich et al. [6] and Och et al. [7], some interesting trend was observed in the present experimental investigation, and the following CFD study provides detailed analysis of the shock effect on film cooling performance.

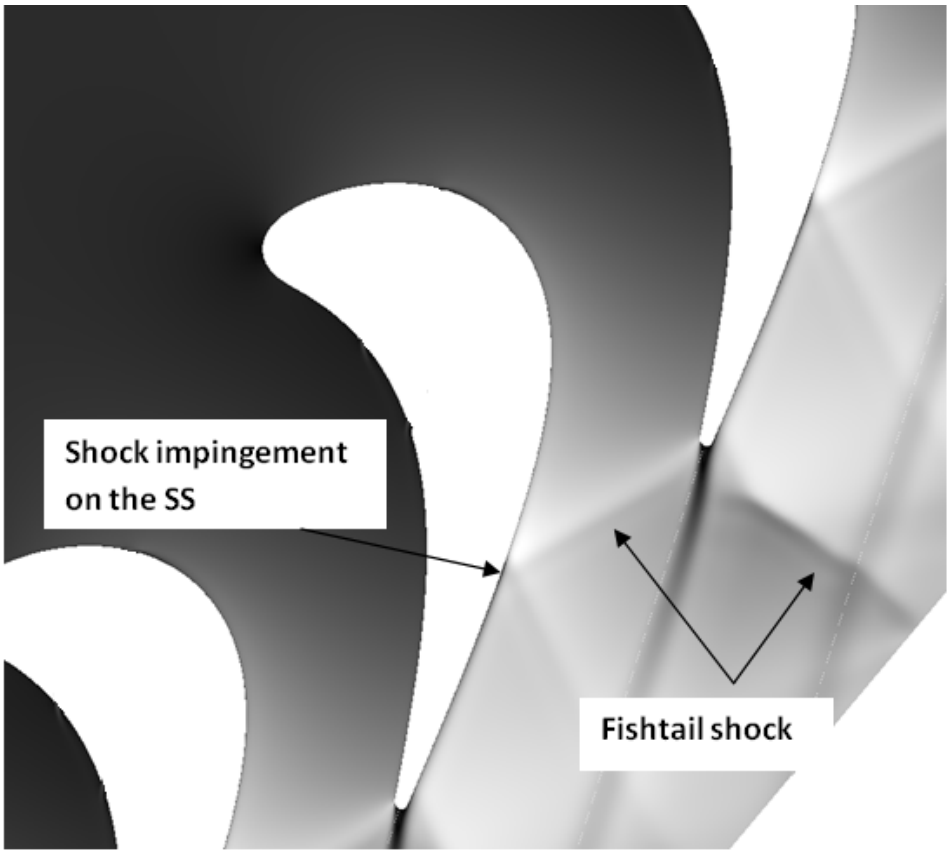

Figure 2. 2. The shock structure in a transonic blade cascade

Simulation Method Details

Geometry and boundary conditions

Figure 2. 2. shows the profile of the film cooled blade and the geometry of the fan-shaped hole that is employed in present study. The streamwise film injection angle is 40 degrees on the SS, and 45 degrees on the pressure side (PS). The injection hole inlet diameter is 0.79mm, and its fan-shaped exit has a 10 degree lateral expansion angle at both left and right side, it also has a 10 degree streamwise laid-back angle. The length of the hole is about 5d, with spanwise spacing ratio of 5.5d. More details of the experimental set up can be found in Ref. [1].

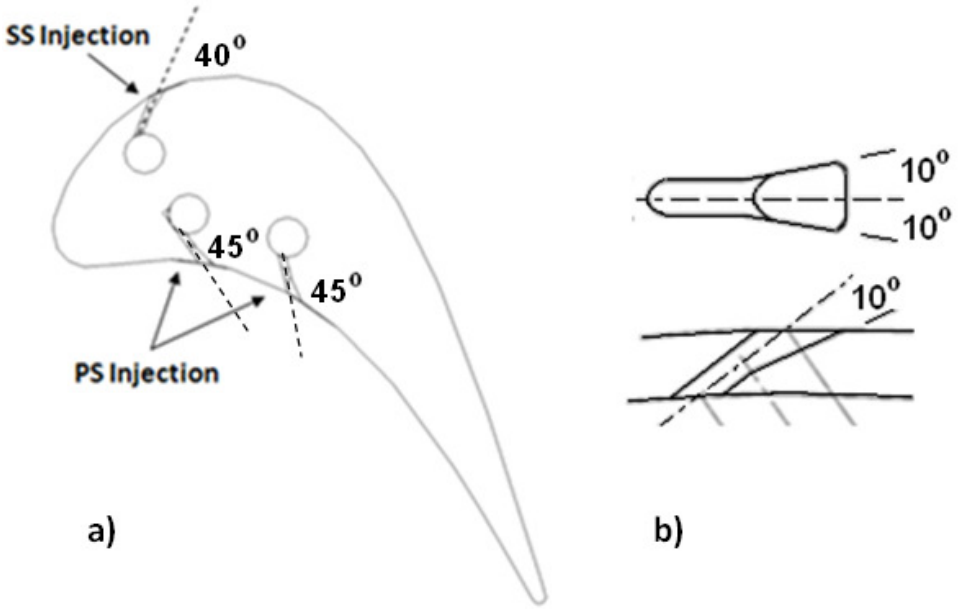

Figure 2. 2. a) Film cooled blade profile; b) Fan-shaped hole geometry

Figure 2. 3 shows the computational domain with the corresponding boundary conditions. To minimize the computational cost, in the pitchwise direction, only one passage was simulated from the turbine blade cascade, and a periodic boundary condition was imposed at both top and bottom. A thin slice, including 3 injection holes, was cut from the entire span of the test section, and symmetric boundary condition was imposed on both left and right side. In the experiment, there are two rows of injection on pressure side (PS), which were also included in the computational domain. However, the discussion in this paper focuses only on the shock/film cooling interaction occurring on the SS. A complete set of the boundary conditions and operating parameters is given in Table 2. 1.

Table 2. 1. Parameters of CFD boundary conditions

Inlet turbulence intensity	Tu_{inlet}	12%
Reynolds number (based on blade true chord & exit velocity)	Re_{exit}	$1.48X10^6$
Exit static pressure	δ_{exit}	0.49
coolant total temperature	θ_{0c}	0.77
SS injection blowing ratio	BR_{SS}	1.30
PS1 injection blowing ratio	BR_{PS1}	3.04
PS2 injection blowing ratio	BR_{PS2}	2.52
SS injection pressure ratio	PR_{SS}	1.16
PS1 injection pressure ratio	PR_{PS1}	1.12
PS2 injection pressure ratio	PR_{PS2}	1.10

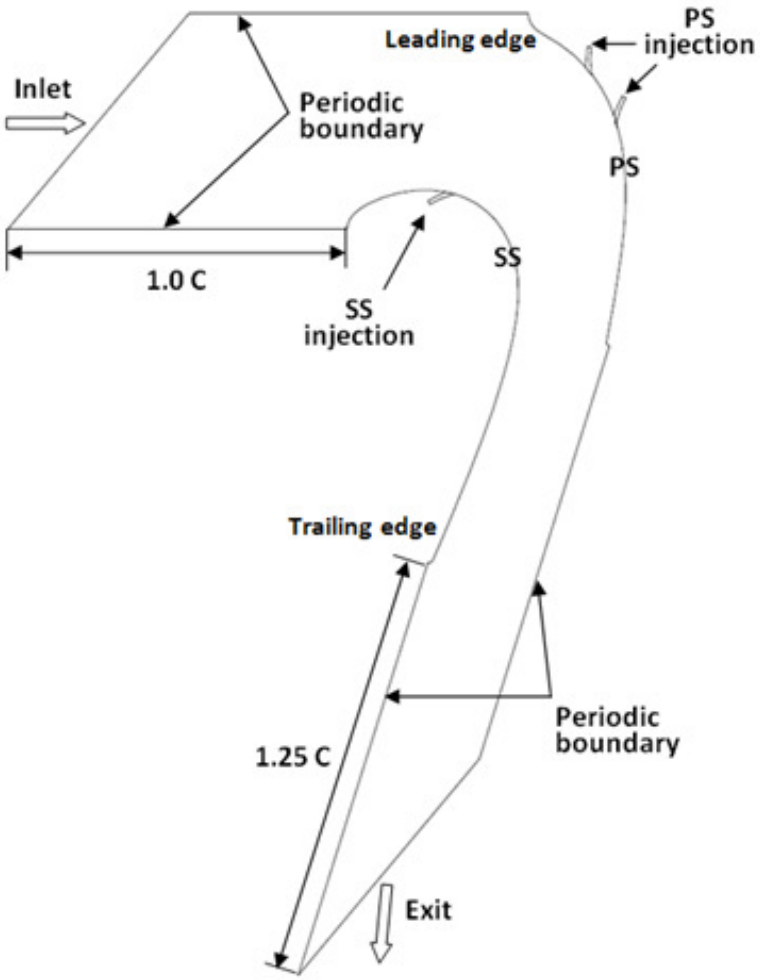

Figure 2. 3. Boundary condition setting of the CFD domain (side view)

CFD solver

Although CFD studies on film cooling have been intensively reported since 1990s, most of the current CFD tools are still having difficulty in obtaining film cooling results that quantitatively agree well with experimental data. However, commercial CFD codes are still being used for film cooling studies, and popular turbulence models are able to provide qualitatively reasonable predictions of film cooling performance. Habeeb et al. [8] made comparisons of different turbulence models on film cooling, and concluded k-ε model provides better result. K-ε model has been employed in film cooling study by many others, such as Zhang and Hassan [9] and Walters et al. [10]. There are also many CFD studies on film cooling performed with the k-ω model, such as Ledezma et al. [11] and Rigby and Heidman [12]. Present

study does not mean to compare different turbulence models on the prediction of film cooling performance. In present study, the Reynolds-Averaged Navier-Stokes equations were solved using commercial CFD solver CFX by ANSYS Inc. The k-ω model, developed by Wilcox [13], is selected to compute the Reynolds Stresses. The automatic wall treatment was used for k-ω model, with y+ $\leq$1.0 for the first layer grid. The k-ε model was also tried in present study. Comparing to the result of k-ω model, the k-ε model provides similar trend of adiabatic effectiveness, but the level does not match well with the experimental data. Thus, all the discussions in the rest of the paper are based on the CFD data computed with k-ω model.

Mesh of the CFD domain

Figure 2. 4 shows the mesh of the computational domain. The overview of the mesh with the local details at the SS injection was given. The local grid on the SS was refined, with minimum size of $5.35X10^{-2}$d, to capture the detail flow structure of shock boundary layer interaction. The grid was finalized with $2.41X10^{6}$ nodes and 74. $6X10^{6}$ elements. In the CFX code, the automatic wall treatment was used for the k-ω turbulence model. Refined unstructured grids, with the first cell thickness of 1.27 $X10^{-3}$d, was employed at the near surface region to give a better prediction of the boundary layer flow.

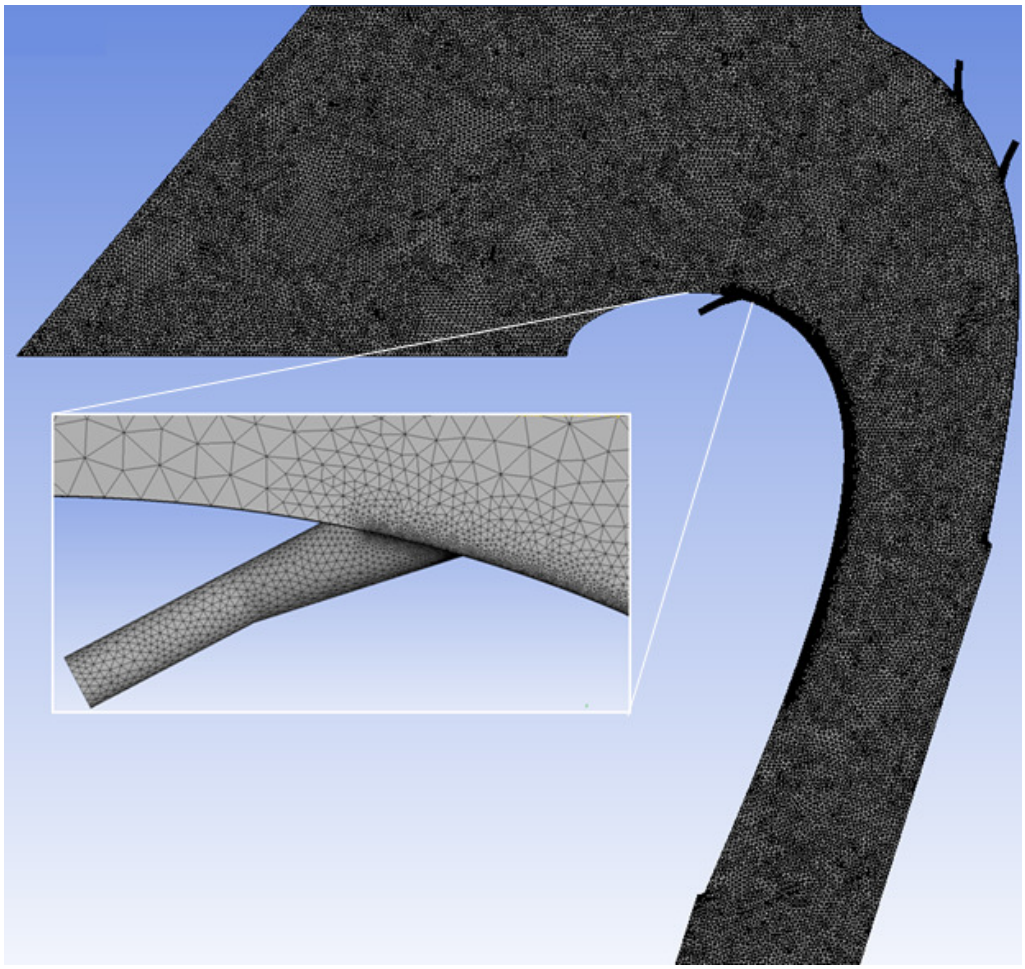

Figure 2. 4. Mesh of the computation domain

Result and Discussion

Comparison with experimental data

Figure 2. 5 compares the CFD and experiment data of the local Mach number distributions on the blade SS and PS. The experimental Mach number was recorded by Carullo et al. [14] on a solid blade without coolant injection, but having the same profile. It can be seen that CFD results match with the experimental data fairly well. The shock impingement location was predicted at s/c=1.05 from the blade leading edge (s/d=66 from the SS injection), which is indicated by the sudden drop of the local Mach number. compared to the experimental data, the CFD predicts a slightly stronger shock at further downstream. Figure 2. 6 shows the centerline film cooling effectiveness comparison between the experimental data and the CFD result. The

CFD result reasonably agrees with the trend of experimental data on the SS, the disagreement on the PS is probably due to the turbulence model failure to predict the flow on a concave surface. As it was pointed out by Undapalli and Leylek [15], improvements are needed on the current turbulence models to quantitatively predict the curvature effect on the Reynolds stress and turbulence heat flux. However, the present study focuses on the physics of the shock/film cooling interaction. As long as the CFD is successful in qualitatively predicting the trends of effectiveness drop at the shock impingement (at s/c=1.05), the CFD result is adequate for the detail analysis on the shock/film cooling interaction.

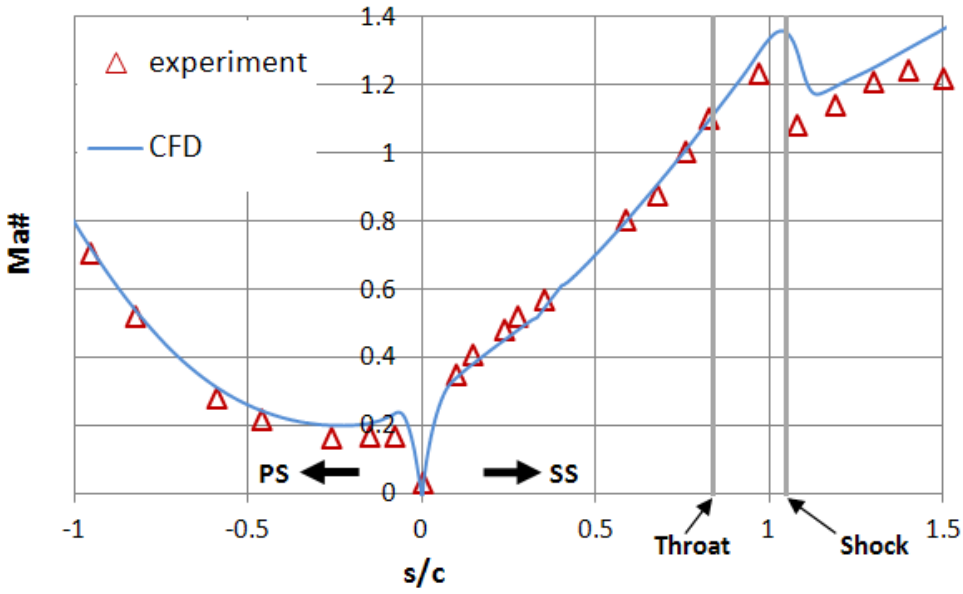

Figure 2. 5. Mach number distributions comparison of CFD and experimental data

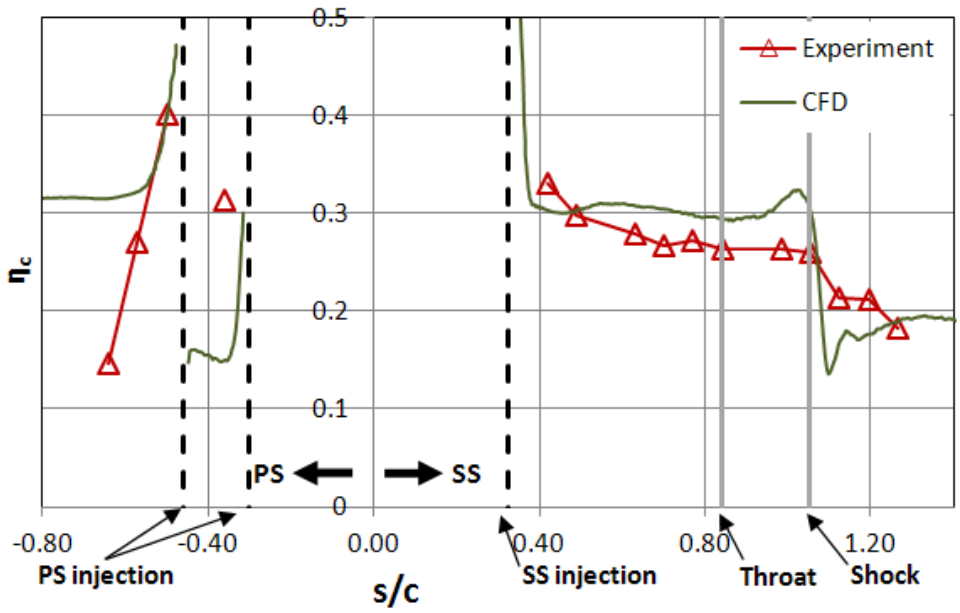

Figure 2. 6. Centerline adiabatic effectiveness comparison between different turbulence models and experimental data

Suction side film cooling performance before the shock impingement

As shown in Figure 2. 6, after the near hole region of the injection on the SS, the experimental adiabatic effectiveness decays slowly from a value of 0.33. This is mainly due to the high curvature of the convex surface on the SS, with smallest R/d=22 (where R is the surface curvature radius), keeps the cooling film attached to the SS surface. According to the detailed studies on film injection using CFD, such as Hyams and Leylek [16], the mixing of coolant with the hot gas was mainly driven by the counter rotating vortices (kidney vortices). However, the kidney vortices were suppressed after the near hole region by the curvature effect on the SS. Figure 2. 7 shows the velocity vector on the cross stream planes at different distances from the injection. It can be seen, as the cooling flow develops downstream, the kidney vortices were reduced, and almost eliminated at s/d=10 (Figure 2. 7 b and c). Similar observation was reported by Berhe and Patankar [17] [18] in their CFD study. After s/d=10, the curvature effect generates a pair of vortices, which rotate in the reversed direction of the kidney vortices (Figure 2. 7 d). This pair of reverse kidney vortices pushes the coolant towards the SS surface, and slightly spread it laterally. When the flow develops further downstream, As the SS surface become flat, this pair of reverse kidney vortex reduced, and disappeared gradually. The surface curvature effect on film cooling has been summarized by Lutum et al. [5]. They suggested that when the

blowing ratio is not too high, a convex surface will improve cooling performance, and slowdown the decay of cooling effectiveness.

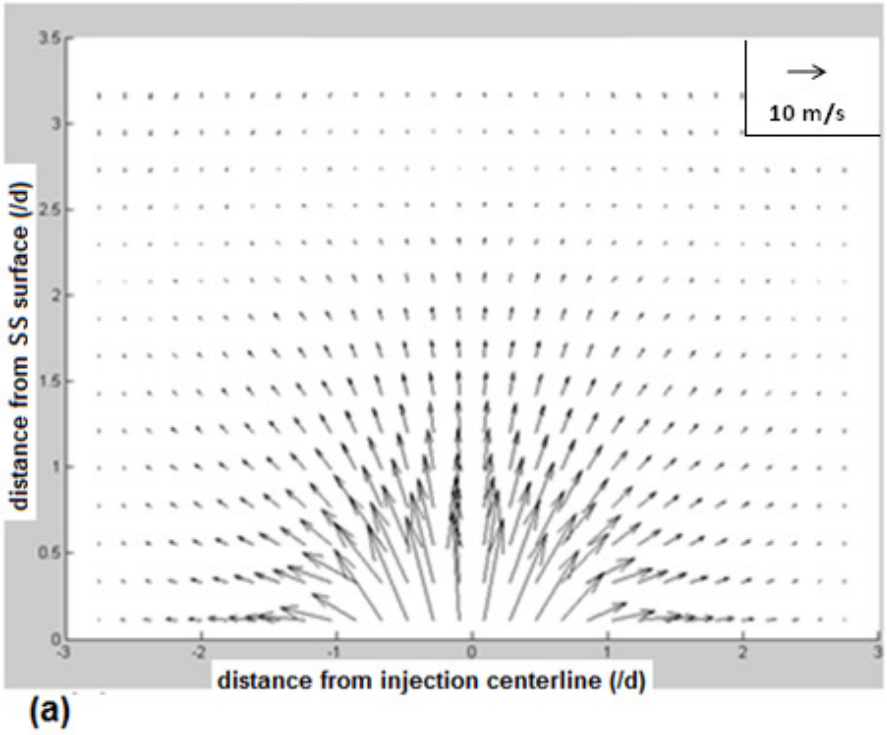

(a)

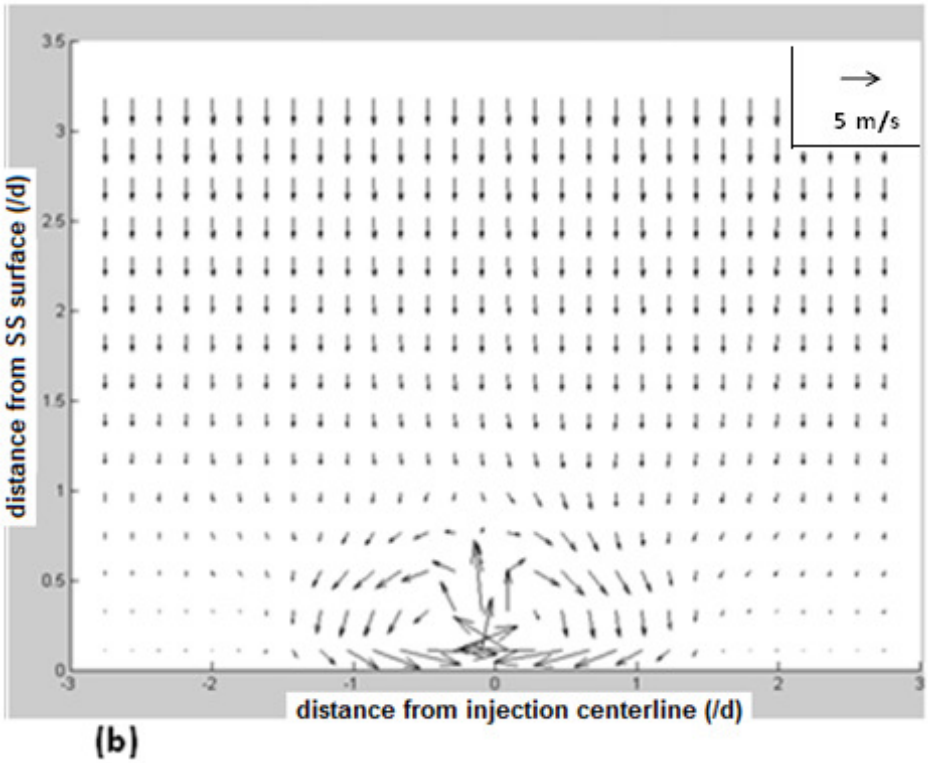

(b)

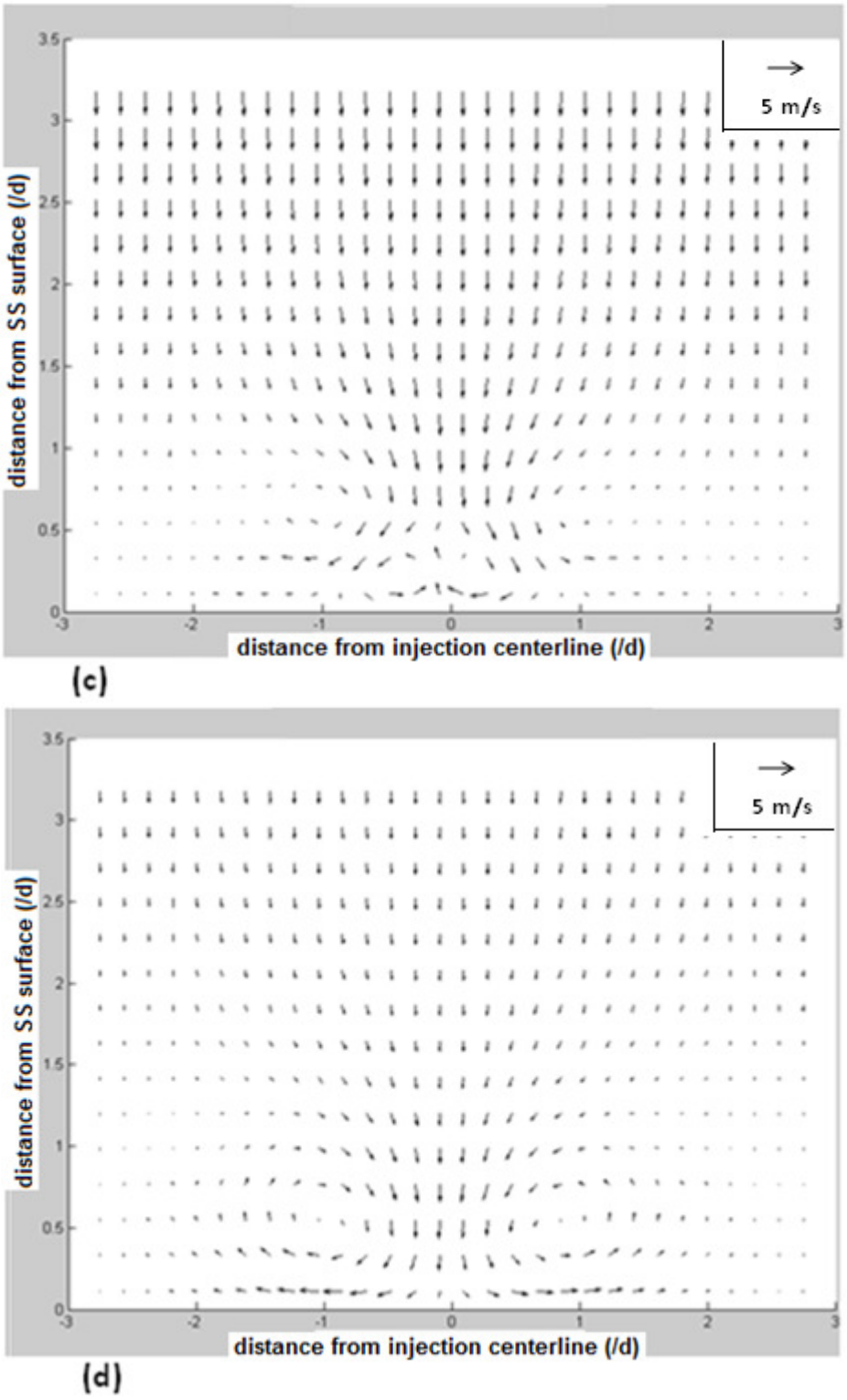

Figure 2. 7. Cross stream velocity vector at different distance from SS injection. (a) s/d=0; (b) s/d=5.0; (c) s/d=10.0; (d) s/d=20.0.

Shock/film cooling interaction

The unique observation in the present study is the quick drop of the film cooling effectiveness within a very short distance after the shock impingement. The flow structure in the CFD results indicate that one of the major factors which cause the drop of film cooling effectiveness are the strong secondary flows related to the shock impingement. Figure 2. 8-10 shows the pressure contours and velocity vectors at different distances downstream from the shock impingement. A local high pressure spot can be observed at the centerline above the SS surface. As the flow develops downstream, the high pressure spot moves quickly away from the SS surface. Accompanying the motion of the high pressure spot is the dramatic change of the secondary flow structure. As shown in Figure 2. 8, at 1.0d downstream of the shock impingement, there is a strong motion of secondary flow moving away from the SS surface. Near the SS surface, this lifting motion sucks the hot air from sides towards the centerline. The CFD results indicate this secondary flow from the sides towards the centerline begins before the shock impingement. This is probably due to the propagation of the spanwise non-uniform shock effect through the compression pressure waves in the low Mach number region near the surface causes the lateral pressure gradient in region immediately upstream of the shock impingement. As shown in Figure 2. 9, at 2.0d downstream of the shock, the lifting flow continues. It can be observed in Figure 2. 10, at 3.0d downstream of the shock impingement, a pair of vortices forms at the centerline, but the main trend of the secondary flow is still lifting. Because of this secondary flow, the cooling flow is lifted away from the SS surface in a very short streamwise distance. Figure 2. 11 compares the temperature plot before and after the shock impingement. It can be observed, the core of the cooling flow after the shock impingement is further away from the SS surface than it is before the shock. The secondary flow also significantly accelerates the mixing of cooling flow with the hot main flow.

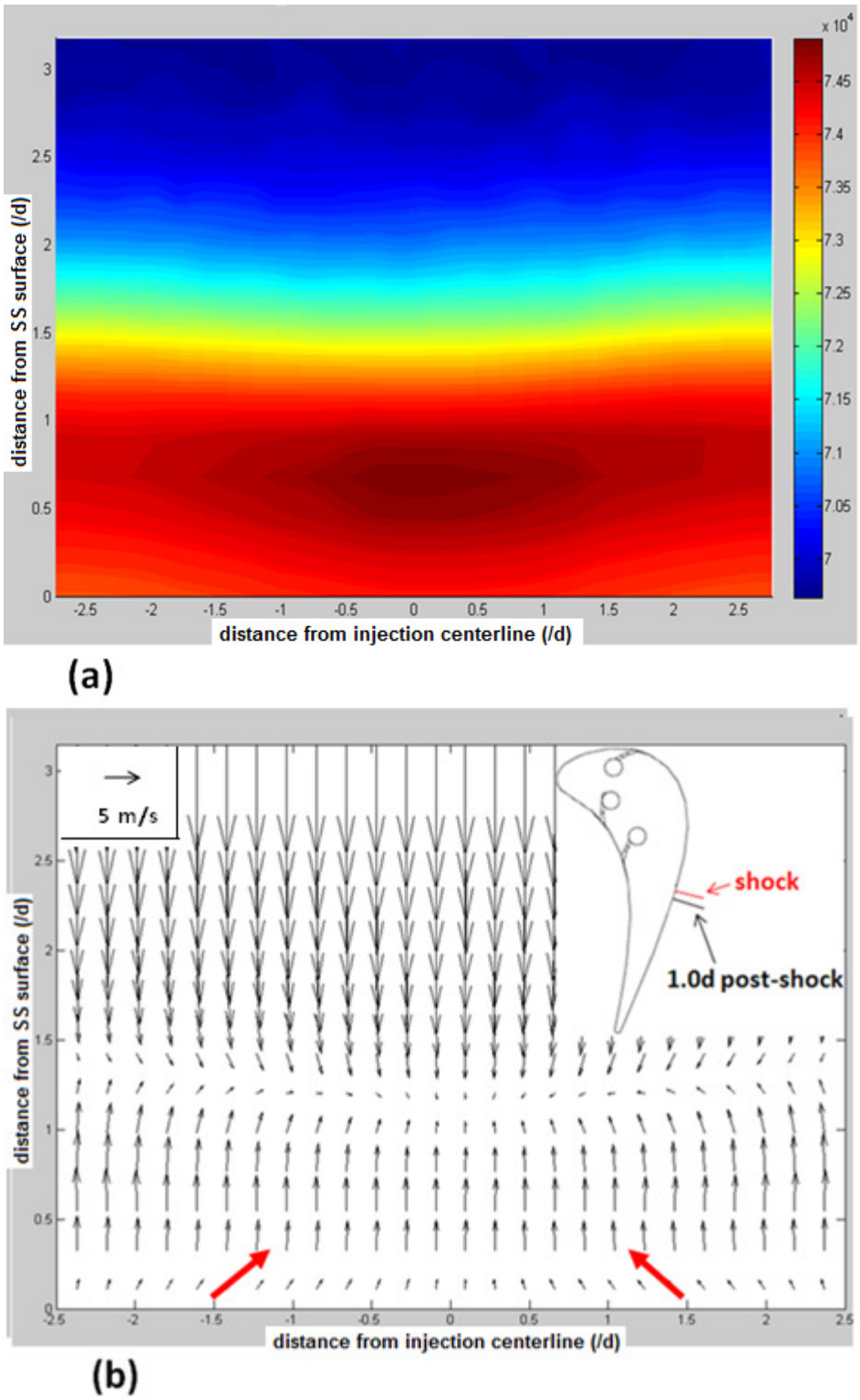

Figure 2. 8. Cross stream plots at 1.0d after shock: (a) pressure contour; (b) velocity vector.

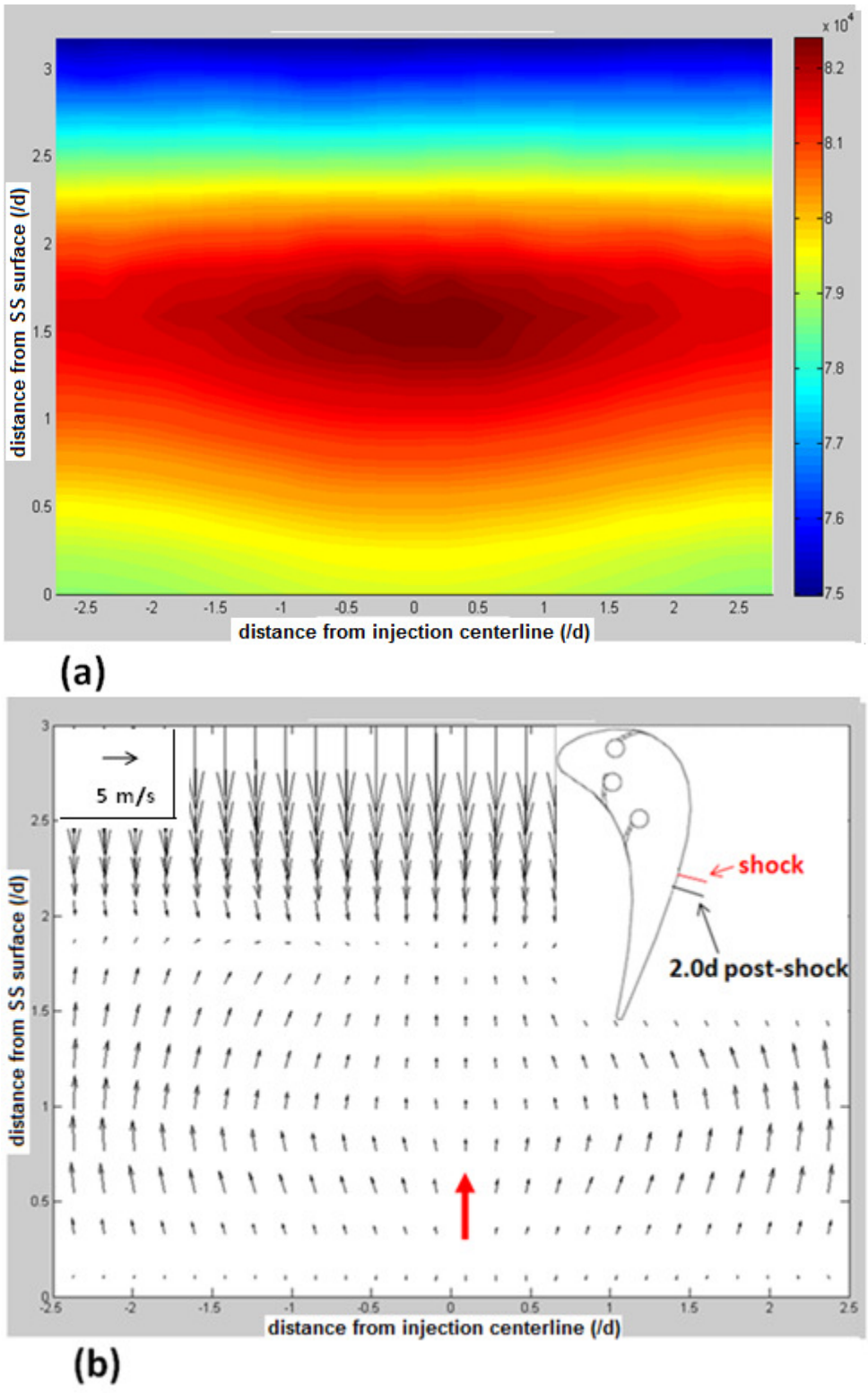

Figure 2. 9. Cross stream plots at 2.0d after shock: (a) pressure contour; (b) velocity vector.

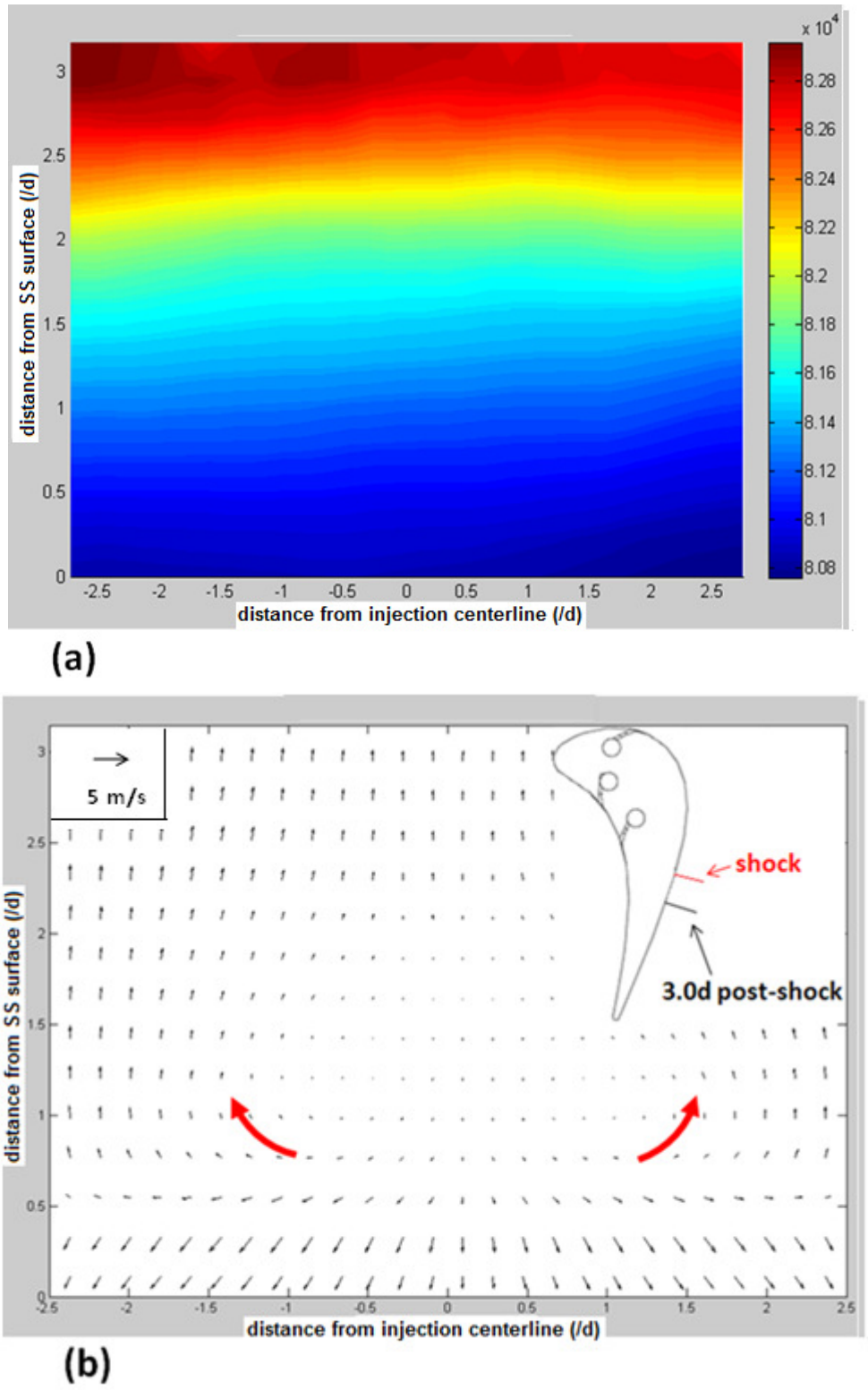

Figure 2. 10. Cross stream plots at 3.0d after shock: (a) pressure contour; (b) velocity vector.

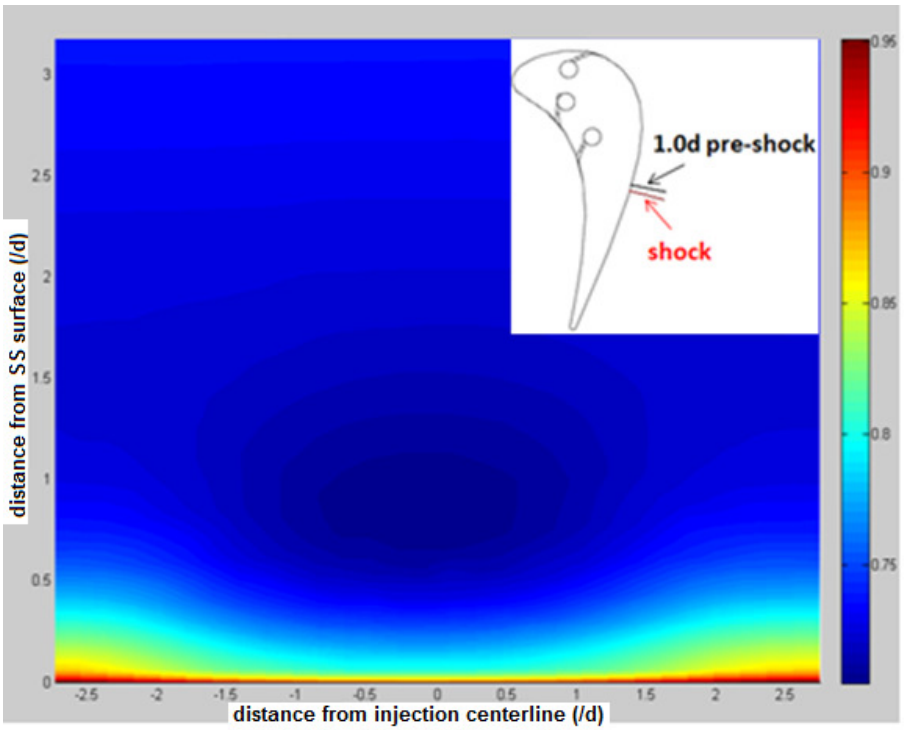

(a)

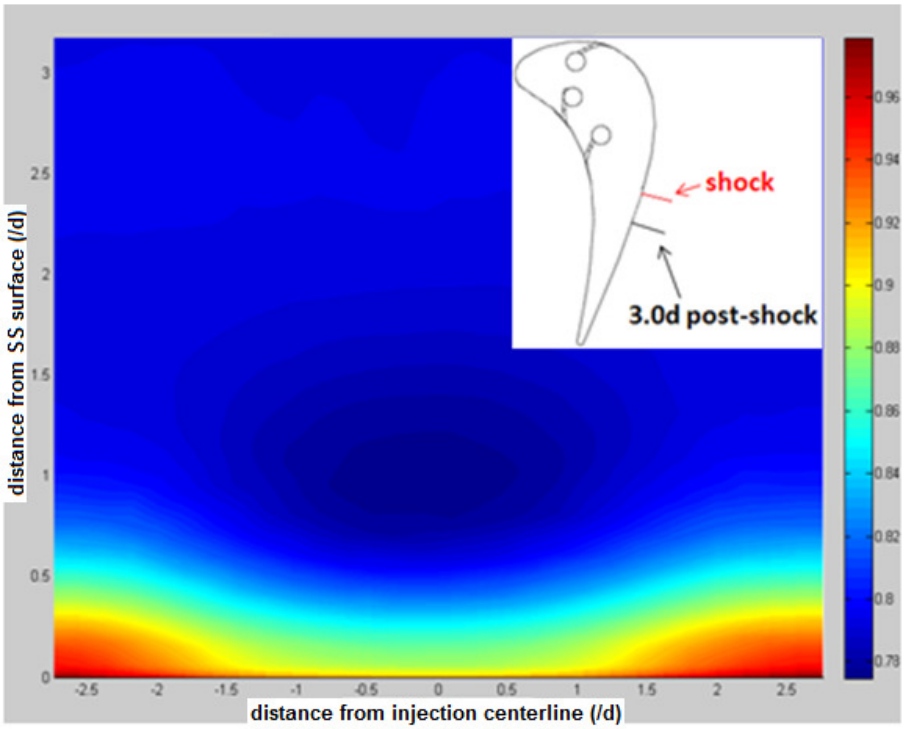

(b)

Figure 2. 11. Non-dimensional temperature θ contour: (a) 1.0d before shock; (b) 3.0d after shock.

The local high pressure spot downstream of the shock impingement is generated by the non-uniformity of the shock strength. Figure 2. 12 shows the Mach number contour at 1.0d upstream of the shock impingement. A high Mach number spot was observed at the centerline near the SS surface in front of the shock (about 3% higher than the adjacent area in spanwise direction). As Hollyer and Laporte [19] pointed out, the shock strength depends on the upstream Mach number, and a higher Mach number causes a stronger shock. According to the Rankine-Hugoniot's relations, the pressure ratio before and after an oblique shock can be determined by Equation 2.2.

$$\frac{P_2}{P_1} = \frac{7(Ma_1 \sin\ \alpha)^2 - 1}{6} \qquad (2.\ 2)$$

Where P1 is the pressure before the shock, P2 is the pressure after the shock; Ma1 is the Mach number before the shock; α is the impingement angle of the oblique shock. The pressure distribution before the shock impingement is almost uniform in spanwise direction. From Equation 2.2, with the Mach number distribution, it is easy to predict the high Mach number spot will cause a high pressure spot after the shock impingement. This was confirmed with the result observed in Figure 2. 8 (a). The Mach number gradient in the direction normal to the SS surface is due to the velocity gradient from the SS to the PS in the cascade channel. The Mach number gradient in the spanwise direction is mainly caused by the local low temperature at the core of the cooling flow.

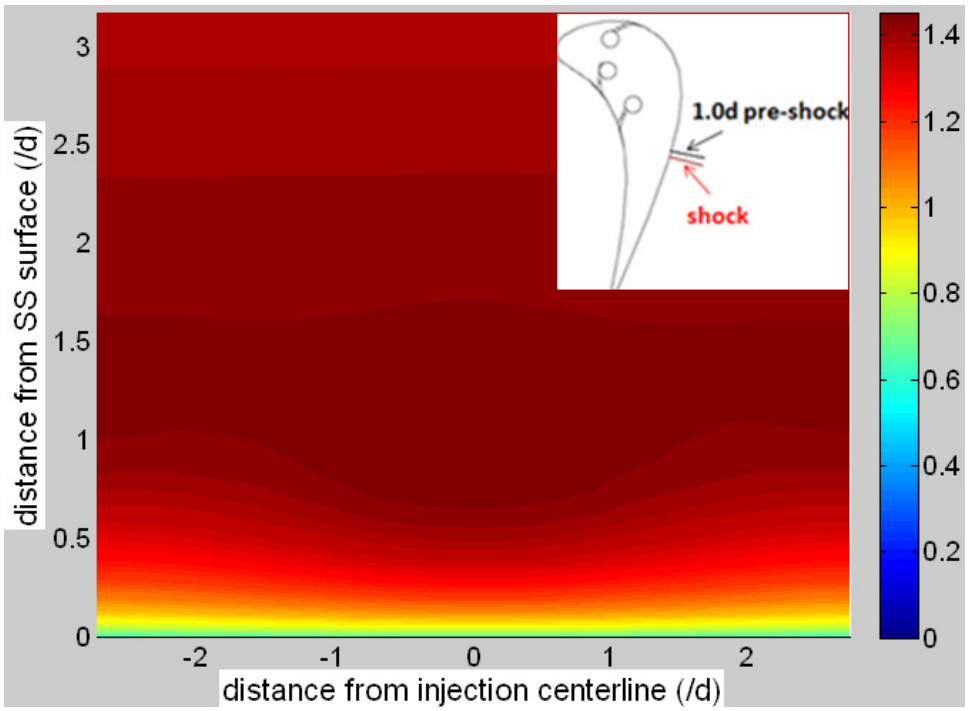

Figure 2. 12. Cross stream plot of Mach number contour at 1.0d before shock

As discussed above, it is believed the lifting motion of cooling flow driven by the secondary flow major reason that causes the film cooling effectiveness to drop after the shock impingement. The drop of effectiveness after the shock impingement is not apparent in the reports by Göttlich et al. [6], Ochs et al. [7]. One of the reasons may be that the surface curvature in their models is not as high as that in the present study. Their coolant may be diffused in spanwise direction before the flow approaches the shock impingement. Thus their shock is uniform in the spanwise direction. However, In Ochs's report [7], a fast decay of effectiveness after the shock impingement is still observable when the shock impingement occurs closer to the injection holes (s/d=8). It has to be pointed out, comparing with the experimental data, the present CFD study over predicts the shock effect on the film cooling effectiveness. Similar over prediction on the shock/film cooling interaction was also observed in the study reported by Luchi et al. [20], when they tried to match their CFD data with the experimental data reported by Ochs et al. [7]. The over prediction on shock/film cooling interaction is probably due to the turbulence model used in the present study under predicted the diffusion and mixing of the cooling flow. Thus, the non-uniformity of the shock impingement in CFD is much stronger than that in the experiment.

Conclusion

A CFD study on the shock/film cooling interaction was performed using popular turbulence models with the ANSYS-CFX codes. An oblique shock forms at the trailing edge of a turbine blade, and impinges on the SS of the adjacent blade. The cooling film was injected in the subsonic region upstream of the SS. The comparison with experimental data shows a reasonable agreement on the trend of the centerline adiabatic effectiveness.

A drop of the film cooling effectiveness was observed after the shock impingement in the experimental data. The details of flow structure were explored with the CFD results. The CFD data indicates that the drop of cooling effectiveness was caused by the secondary flow, which is related to the non-uniformity of the shock impingement. The discussion and comparison of present study and the observations in literature suggests the shock/film cooling interaction may vary, according to the flow structure upstream of the shock. In a highly turned gas turbine blade, the shock impingement may compromise the film cooling performance substantially. Therefore, it may be necessary to add some extra cooling after the shock impingement on the SS.

Acknowledgement

The authors are thankful to Drs Hee-Koo Moon and Luzeng Zhang from Solar Turbine Inc for supporting this study. The authors also appreciate Dr. Tafti for his helpful advice on the CFD operation.

Reference

[1] Xue, S., Ng, W., Zhang, L., Moon, H., 2012, “Fan-Shaped Hole Film Cooling on Turbine Blade in a Transonic Cascade with High Freestream Turbulence”. 50th AIAA Aerospace Sciences Meeting, Nashville Tennessee, AIAA-2012-0368.

[2] Han, J. C., Dutta, S., and Ekkad, S. V., 2000, “Gas Turbine Heat Transfer and Cooling Technology”. Taylor & Francis, 29 West 35th Street, New York, NY 10001.

[3] Kercher, D. M., 1998, “A Film-Cooling CFD Bibliography: 1971-1996”. International Journal of Rotating Machinery, 1998, Vol. 4, No. 1, pp. 61-72.

[4] Ito, S., Goldstein, R. J., Eckert, E. R. G., 1978, “Film Cooling of Gas Turbine Blade”. Journal of Engine for Power, 1978, Vol. 100, pp. 476-481.

[5] Lutum, E., Wolfersdorf, J. V, Semmler, K., Naik, S., Weigand, B., 2001, “Film Cooling on a Convex Surface: Influence of External Pressure Gradient and Mach Number on Film Cooling Performance”. Heat and Mass Transfer, 2001, Vol. 38, pp. 7-16.

[6] Göttlich, E., Lang, H., Sanz, W., Woisetschläger, J., 2002, "Experimental Investigation of an Innovative Cooling System (ICS) for High Temperature Transonic Turbine Stages". Proceeding of ASME TURBO EXPO 2002, Amsterdam, The Netherlands, GT-2002-30341.

[7] Ochs, M., Schulz, A., Bauer, H.-J., 2007, "Investigation of The Influence of Trailing Edge Shock Waves on Film Cooling Performance of Gas Turbine Airfoils". Proceedings of ASME Turbo Expo 2007, Montreal, Canada, GT-2007-27482.

[8] Oguntade, H. I., Andrews, G. E., Burns, A., Ingham, D., Pourkashanian, M., 2010, “CFD Predictions of Single Row Film Cooling with Inclined Holes: Influence of Hole Outlet Geometry”. Proceedings of ASME Turbo Expo 2010, Glasgow, UK, GT2010-22308.

[9] Zhang, C. X., Hassan, I., 2009, “Computational Study of the Effects of Shock Waves on Film Cooling Effectiveness”. ASME Journal of Engine for Gas Turbine and Power, 2009, Vol. 131, No. 031901.

[10] Walters, D. K., Leylek, J. H., Buck, F. A., 2002, “Film Cooling on a Modern HP Turbine Blade Part II: Compound-Angle Round Holes”. Proceedings of ASME Turbo Expo 2002, Amsterdam, Netherlands, GT-2002-30613.

[11] Ledezma, G. A., Laskowski, G. M., Dees, J. E., Bogard, D. G., 2011, “Overall and Adiabatic Effectiveness Values on a Scaled up Simulated Gas Turbine Vane: Part II – Numerical Simulations”. Proceedings of ASME Turbo Expo 2011, Vancouver, Canada, GT2011-46616.

[12] Rigby, D. L., Heidman, J. D., 2008, “Improved Film Cooling Effectiveness by Placing a Vortex Generator Downstream of Each Hole”. Proceedings of ASME Turbo Expo 2008, Berlin, Germany, GT2008-51361.

[13] Wilcox, D.C. (1988), "Re-assessment of the scale-determining equation for advanced turbulence models". *AIAA Journal*, vol. 26, no. 11, pp. 1299-1310.

[14] Carullo, J. S., Nasir, S., Cress, R. D., Ng, W. F., Thole, K. A., Zhang, L. J., and Moon, H. K., 2007, "The Effects of Freestream Turbulence, Turbulence Length Scale, and Exit

Reynolds Number on Turbine Blade Heat Transfer in a Transonic Cascade," IGTI Turbo Expo 2007, Montreal, GT2007-27859.

[15] Undapalli S., Leylek J. H., 2003, “Ability of a Popular Turbulence Model to Capture Curvature Effects: a Film Cooling Test Case”. Proceedings of ASME Turbo Expo 2003, Atlanta, Georgia, GT2003-38638.

[16] Hyams D. G. and Leylek J. H., 2000, “A Detailed Analysis of Film Cooling Physics: Part III—Streamwise Injection With Shaped Holes,” ASME Journal of Turbomachinery, vol. 122, p. 122-132.

[17] Berhe, M. K., Patankar, S. V., 1999a, “Curvature Effects on Discrete Hole Film Cooling”. ASME Journal of Turbomachinery, 1999, Vol. 121, pp. 781-791.

[18] Berhe, M. K., Patankar, S. V., 1999b, “Investigation of Discrete-Hole Film Cooling Parameters Using Curved-Plate Models”. ASME Journal of Turbomachinery, 1999, Vol. 121, pp. 792-803.

[19] Hollyer R. N. and Laporte O, 1953, “Parameters Characterizing the Strength of a Shockwave”. American Journal of Physics, 1953, Vol. 21(8), pp. 610.

[20] Luchi, R., Salvadori, S., Martelli, F., 2008, “Heat Transfer Prediction of Film Cooling in Supersonic Flow”. Numerical Analysis and Applied Mathematics, International Conference 2008.

Preface Paper 3

In paper 3, experimental investigation was performed on film cooling performance in a 2-D linear cascade of a turbine NGV profile. Data were recorded at three exit Mach number/Reynolds number and multiple sets of blowing ratio. All tests were performed at high freestream turbulence intensity (12%) with large length scale (0.28 normalized by the cascade pitch). Vane surface film cooling effectiveness and net heat flux reduction distributions were presented and compared with literature. The paper has been accepted to *ASME journal of Turbomachinery* (TURBO-11-1250).

HEAT TRANSFER PERFORMANCE OF A SHOWERHEAD AND SHAPED HOLE FILM COOLED VANE AT TRANSONIC CONDITIONS

S. Xue, A. Newman, W. Ng
Mechanical Engineering
Virginia Polytechnic Institute and State University
Blacksburg, VA, USA
xuesong@vt.edu, newman.ands@gmail.com, wng@vt.edu

H.K. Moon and L. Zhang
Solar Turbines Incorporated
San Diego, CA, USA
Moon_Hee_Koo_X@solarturbines.com, ZHANG_LUZENG_J@solarturbines.com

ASME TURBO EXPO GT2011- 45142

Accepted to the Journal of Turbomachinery

Abstract

An experimental study was performed to measure surface Nusselt number and film cooling effectiveness on a film cooled first stage nozzle guide vane (NGV), at high freestream turbulence, using a transient thin film gauge (TFG) technique. The information presented attempts to further characterize the performance of shaped hole film cooling by taking measurements on a row of shaped holes downstream of leading edge showerhead injection on both the pressure and suction surfaces (hereafter PS and SS) of a 1st stage NGV. Tests were performed at engine representative Mach and Reynolds numbers and high inlet turbulence intensity and large length scale at the Virginia Tech 2D Linear Transonic Cascade facility. Three exit Mach/Reynolds number conditions were tested: 1.0/1,400,000; 0.85/1,150,000; and 0.60/850,000 where Reynolds number is based on exit conditions and vane chord. At Mach/Reynolds numbers of 1.0/1,450,000 and 0.85/1,150,000 three blowing ratio conditions were tested: BR = 1.0, 1.5, and 2.0. At a Mach/Reynolds number of 0.60/850,000, two blowing ratio conditions were tested: BR = 1.5 and 2.0. All tests were performed at inlet turbulence intensity of 12% and length scale normalized by the cascade pitch of 0.28. Film cooling effectiveness and heat transfer results compared well with previously published data, showing a

marked effectiveness improvement (up to 2.5x) over the showerhead only NGV and also agreement with published showerhead-shaped hole data. Net heat flux reduction (NHFR) was shown to increase substantially (average 2.6x) with the addition of shaped holes, with an increase (average 1.6x) in required coolant mass flow. Based on the heat flux data, the boundary layer transition location was shown to be within a consistent region on the suction side regardless of blowing ratio and exit Mach number.

Introduction

As gas turbine manufacturers ever strive for higher efficiency and increased output from their products, turbine inlet temperatures have been increasing as a way to meet this end. The industry is already to a point where turbine inlet temperatures have reached greater values than blade and vane materials can withstand. In response to this problem, techniques such as complex internal and film cooling schemes and thermal barrier coatings have been employed to help increase engine component life and performance. This study attempts to further characterize the performance of shaped hole film cooling by taking measurements on a row of shaped holes downstream of leading edge showerhead injection on both the pressure and suction surfaces (hereafter PS and SS) of a 1st stage NGV. Data is not readily available in literature for the performance of a single row of shaped holes with showerhead interaction at high freestream turbulence intensity, large length scale, and engine-realistic Mach and Reynolds numbers.

The freestream turbulence level has a substantial effect on vane surface heat transfer. Goldstein et al. [1] and Koutmos and McGuirk [2] determined the turbulence intensity of 15% to 30% at the combustor exit, using can-type model with swirlers and dilution jets. Inlet freestream turbulence greater than 10% is usually employed by researchers in the cascade tunnel tests. For example Reiss and Bölcs [3] did their tests at Tu=10%; Ames [4] operated the experiment at Tu=12%; Guo et al. [5] ran their tests with Tu=13%, to list a few. The highest levels seen in the literature is about 20%, but those tests are operated at a very low speed, such as Cutbirth and Bogard [6] with an inlet velocity of 5.8m/s and Ou et al.[7] with an inlet velocity of 10m/s. In this paper all the tests were operated with an inlet freestream turbulence intensity level of 12%, and at transonic exit condition.

Initial research performed by Goldstein et al. [8] demonstrated the potential of shaped hole film cooling above and beyond that of cylindrical holes in simplified-geometry flat plate experiments. Since that time, many others have explored the effects of injection angle, row spacing, row interaction, hole shaping, and many other parameters that have a bearing on film cooling performance. Many have looked into the effect of hole shaping by way of low speed flat plate studies such as Schmidt et al. [9], Gritsch et al. [9], and Yu et al. [11]. Studies such as these explore different expansion angles in the span and streamwise directions, often comparing back to rows of cylindrical holes to emphasize shaped hole performance benefits. Studies such as Bell et al.[12], Dittmar et al. [13], and Yuen et al. [14] have expanded on Goldstein et al. [8] to include comparisons of single and multiple rows of fan shaped holes to multiple rows of cylindrical holes with compound injection and rows of slot-type holes. As it has proved so beneficial to cylindrical holes, compound injection for shaped holes has also been a topic of interest in the previous three studies as well. Many other design factors have been explored by way of low speed flat or curved plate experiments such as: hole trenching and tabs (Lu et al. [15], Dhungel et al. [16]), shaped hole channel and surface flowfields (Wittig et al. [17], Thole et al. [18], Saumweber and Schulz [19]), effect of mainstream turbulence (Saumweber et al. [20]) and row spacing (Saumweber and Schulz [19]) to name a few.

Shaped hole research has also been performed on NGVs in low-speed linear cascades. These studies tend to approximate engine Reynolds numbers by way of scaling, however they do not accurately represent engine-realistic Mach number. Colban et al. [21] performed heat transfer and film effectiveness measurements in a low-speed cascade using a steady state infrared imaging technique. Their study looked at the effect of upstream blowing, and showed that the presence of upstream blowing reduced the incidence of jet-liftoff at higher blowing ratios. Colban et al. [22] also performed a comparison of experimental shaped hole data with CFD using different turbulence models, showing that the RNG k-ε turbulence model better predicted effectiveness levels. Chappell et al. [23] performed a comparison of hole types and angles in a low speed cascade, concluding that compound angle had more effect on film cooling performance than hole shape.

In addition to low speed cascade studies, others have performed curved or flat plate studies at transonic Mach numbers to evaluate shaped hole performance. Wittig et al. [17] explored

internal and external flowfield on a transonic flat plate rig. Furukawa et al. [24] explored the effects of hole shape and angle on a suction side airfoil model finding that fan shaped holes at compound angles show a significant effectiveness benefit over shaped holes and cylindrical holes without compound injection.

There are many studies exploring fan shaped holes at low Mach numbers and/or with simplified geometry, however there are comparatively fewer with engine representative Mach numbers. Fewer still are fan shaped hole cascade studies performed on vanes at high turbulence and engine representative Mach and Reynolds numbers. Zhang and Pudupatty [25] and Zhang et al. [26] look at PS and SS film effectiveness (respectively) on a first stage NGV with showerhead and shaped hole film cooling. Tests were performed at transonic exit Mach numbers (0.74 and 0.61) and high inlet turbulence intensity (12%). Their findings in both cases were that upstream injection reduced the tendency of jet liftoff at high blowing ratios, and that little effectiveness benefit was seen from shaped holes at blowing ratios above 2. Zhang and Pudupatty [25] also found that at higher blowing ratios, showerhead injection augmented the effectiveness of downstream film cooling rows on the PS. Schnieder et al. [27] performed a study to investigate the effects of showerhead and PS row interaction at high inlet turbulence and high exit Mach number. Their findings indicated that the increased turbulence created by showerhead injection caused more rapid film diffusion of downstream rows of shaped holes. Other studies such as Thurman et al. [28] have looked at heat transfer due to shaped hole film cooling, showing local increases in injection regions.

In addition to linear cascade studies others have explored rows of shaped holes in annular cascades. Guo et al. [29] looked at the effect of using foreign gasses for coolant to achieve engine-representative density ratios in a transonic annular cascade. Sargison et al. [30] compared a converging-slot hole geometry to fan shape holes in the same facility as Guo et al. [29].

This paper will present the results of heat transfer and effectiveness measurements on a film cooled NGV with five rows of showerhead film cooling and one row of fan shaped holes on both the pressure and suction sides. These results are measured at three engine-representative exit Mach/Reynolds numbers and high inlet turbulence. The main objectives of this paper are to: investigate the effect of Mach number and blowing ratio on showerhead and downstream shaped

hole film cooling, to compare showerhead only with combined showerhead and shaped hole film cooling at multiple blowing ratios and Mach numbers, and to perform a NHFR comparison to illustrate the overall effect of adding shape hole cooling rows.

Experimental Facility and Instrumentation

Tests were performed in the Virginia Tech Transonic Cascade tunnel. This is a transient blowdown facility, a schematic of which can be seen in Figure 3.. The facility is also equipped with a heat exchanger capable of heating the mainstream flow to 150˚C (423˚K) for heat transfer testing. For heat transfer testing, there is a 10-15 second window of steady tunnel response in which data is taken.

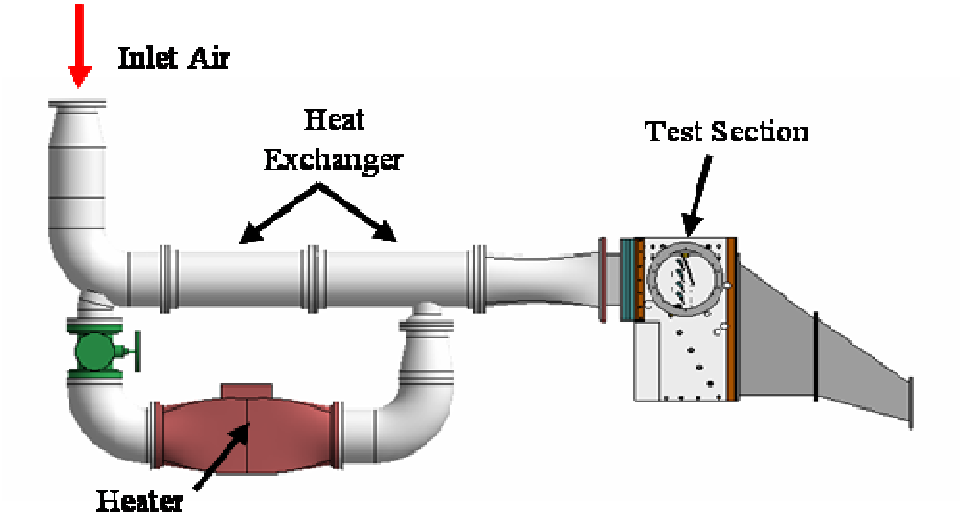

Figure 3. 1. Virginia Tech Transonic Cascade facility

Inlet turbulence is generated directly upstream of the test section by way of a passive mesh grid. The turbulence grid and its relation to the cascade can be seen in Figure 3. for these experiments this grid generates a turbulence intensity of 12% and turbulence length scale nondimensionalized by the cascade pitch of 0.28. This facility has been used by Reagle et al. [31], Bolchoz et al. [32], and Nasir et al. [33], [34] for vane and blade aerodynamic and heat transfer testing.

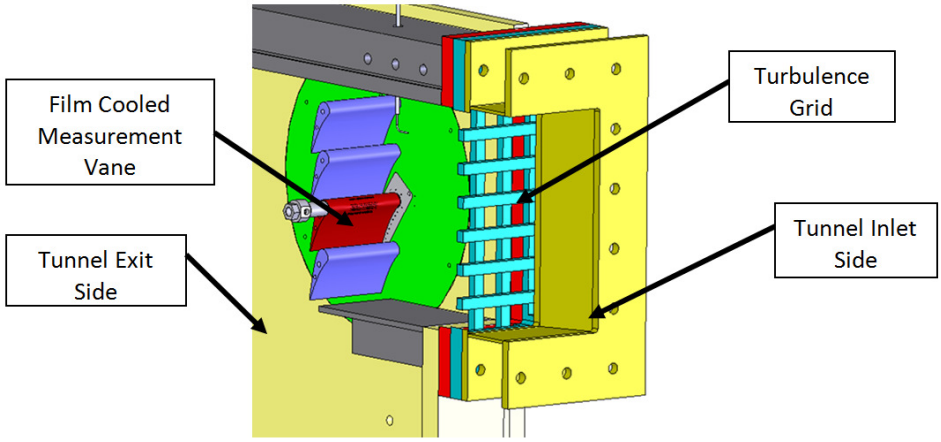

Figure 3. 2. Close-up of vane test section

The vane profile is that of a first stage NGV provide by Solar Turbines, Inc., and is scaled 1.5x to match engine Reynolds numbers. Detailed aerodynamic performance of this vane cascade has been previously published by Nasir et al. [33]. Details on the vane geometry can be found in Table 3. 1.

Table 3. 1. Showerhead-shaped hole vane parameters

Chord	**C**	**91.19 mm**
Pitch	**P**	**83.06 mm**
Span	**-**	**152.40 mm**
Film-Cooled Span	**-**	**59.18 mm**
Inlet Angle	**-**	**0 degree**
Exit Angle	**-**	**73.5 degree**
Coolant Metering Hole Diameter	**d**	**0.79 mm**

Heat transfer measurements are taken on the center vane in the cascade. This vane is made of Corning Macor® machineable glass-ceramic. Macor® is chosen for its relatively low thermal diffusivity and conductivity, allowing for the use of a 1-D semi-infinite assumption in data reduction. The center vane has a total of seven rows of film cooling holes: Five rows of

showerhead cooling on the LE, one row of shaped holes on the SS and one row of shaped holes on the PS.

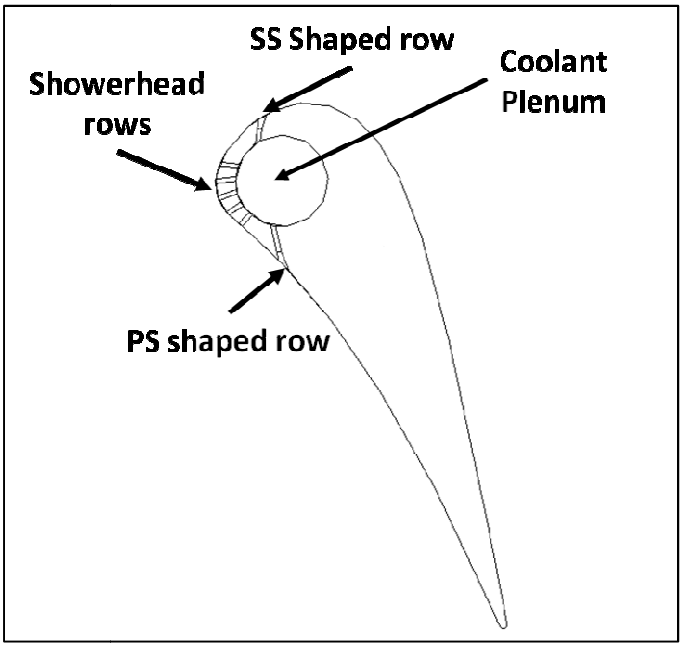

Figure 3. 3. Showerhead-shaped hole vane profile

The film cooled vane is instrumented with 25 thin-film type heat flux sensors (TFGs). The gages used in this study are designed similar to that of Doorly and Oldfield [35] and are manufactured by Air Force Research Lab using the method described in Joe [36]. The gages are applied to the measurement vane at 45% span, and are oriented such that the platinum sensing element is along a shaped hole centerline. Ten gages are instrumented on the PS of the vane, and 15 are instrumented on the SS.

Data Reduction

A finite difference code described by Nasir et al. [34] and developed by Cress [37] is used to calculate heat flux, q". This finite difference code solves the 1-D transient conduction equation for q" (eq. 3.1) based on the time response of the vane surface temperature and the thermal properties of the vane material.

$$\frac{\partial^2 T}{\partial x^2} = \frac{1}{\alpha}\frac{\partial T}{\partial t} \qquad (3.1)$$

Heat transfer coefficient and film cooling effectiveness are derived using a linear regression method developed by Popp et al. [38]. This method starts with the convective heat transfer equation

$$q" = h(T_{aw} - T_w) \qquad (3.2)$$

The equation for film cooling effectiveness (non-dimensionalized adiabatic wall temperature).

$$\eta = \frac{T_{aw} - T_r}{T_c - T_r} \qquad (3.3)$$

Where Tc is the coolant total temperature in the plenum. Equations 3.2 and 3.3 are then combined to yield an equation expressing heat transfer coefficient and film cooling effectiveness in the form of $y = mx + b$.

$$\frac{q"}{T_r - T_c} = h\left(\frac{T_r - T_w}{T_r - T_c}\right) - h \cdot \eta \qquad (3.4)$$

For this study heat transfer coefficient will be nondimensionalized by way of Nusselt number as defined in equation 3.5.

$$Nu = \frac{h \cdot C}{k_a} \qquad (3.5)$$

The average uncertainty in heat transfer coefficient of ± 7% and an average uncertainty in film effectiveness of ± 0.05. In addition to this analysis, tunnel repeatability was established for each Mach number case. More details on the experiment setup, data reduction and uncertainty analysis can be found in Newman's thesis [39].

Surface Measurement Results

Measurement results will first be compared with past studies performed by this group on a showerhead-only film cooled NGV using the same transient TFG technique. Results will also be compared to other available literature with similar Mach/Reynolds numbers, film cooling configurations, and turbulence levels. Following the comparison, most of the test conditions listed in table 3. 2 will be presented, and the comprehensive result is given in Newman's thesis [39]. Results will be presented in terms of Nusselt number distributions and film cooling effectiveness distributions.

Table 3. 2. Test matrix of surface measurements

Film Cooled Test Matrix			
Ma	**Re**	**Tu**	**BR, MFR %**
0.60	850,000	12%	1.5, 1.04
			2.0 , 1.15
0.85	1,150,000		1.0, 0.85
			1.5, 1.04
			2.0 , 1.15
1.00	1,400,000		1.0, 0.85
			1.5, 1.04
			2.0 , 1.15

Three blowing/mass flow ratios were tested at two exit Mach numbers (Mex = 1.0 and 0.85) with only two blowing/mass flow ratios tested at the low exit Mach number case of Mex = 0.60. The low coolant flow rates required for BR = 1.0 at the low exit Mach number case of Mex = 0.60 exceeded the lower physical limitations of the film cooling loop, resulting in non-repeatability. Results will be reported in terms of exit Mach number and blowing ratio, where blowing ratio is defined as the ratio of coolant density times velocity to freestream density times velocity. Equation 3.6 shows this relationship.

$$BR = \frac{\rho_c U_c}{\rho_\infty U_\infty} \qquad (3.6)$$

Mass flow ratio is the relationship of total coolant mass flow for all film cooling rows to passage mass flow as defined below in equation 3.7.

$$MFR\% = \frac{\dot{m}_c}{\dot{m}_p} \qquad (3.7)$$

All seven rows of film cooling holes (five LE showerhead, one SS shaped, and one PS shaped) are fed from a common plenum. The local blowing ratios of showerhead, SS shaped holes, and PS shaped holes were determined by the plenum total pressure and the surface static pressures at exit of each cooling row respectively. As a result of local velocity difference the local blowing ratios differ remarkably between SS shaped holes and PS shaped holes. Table 3. 3 shows the relationship between showerhead blowing ratio and shaped hole blowing ratio for each of the three blowing ratio cases tested. It can be observed that when showerhead blowing ratio changed from 1.0 to 2.0 the PS shaped hole blowing ratio changed from 1.7 to 3.0 (76% increase), but SS shaped hole blowing ratio only changed from 1.1 to 1.4 (27% increase). The uneven changing of PS and SS blowing ratio caused different trend of cooling effectiveness and Nusselt number on PS and SS, and this will be discussed later in the result section.

Table 3. 3. Relationship between showerhead and shaped hole BR

BR Showerhead	BR PS Shaped	BR SS Shaped
2.0	3.0	1.4
1.5	2.2	1.2
1.0	1.7	1.1

Literature Comparisons

Figures 3. 4 and 3. 5 show comparisons of the present study with Zhang et al. [25], [26] and Schnieder et al. [27]. Zhang et al [25], [26] were performed on an NGV of the same profile with similar hole shapes, but different injection locations. Schnieder et al. [27] is a showerhead-

shaped hole interaction study performed on the PS only. Both studies report only film cooling effectiveness and do not measure Nusselt number.

Figure 3. 4 is a pressure side results comparison where the origin of the axis is the shaped holes injection location and streamwise distance on the PS increases to the right of the plot. Figure 3. 5 is a comparison of SS effectiveness where the origin of axis is the shaped hole injection location, and streamwise distance down the SS increases to the right of the plot.

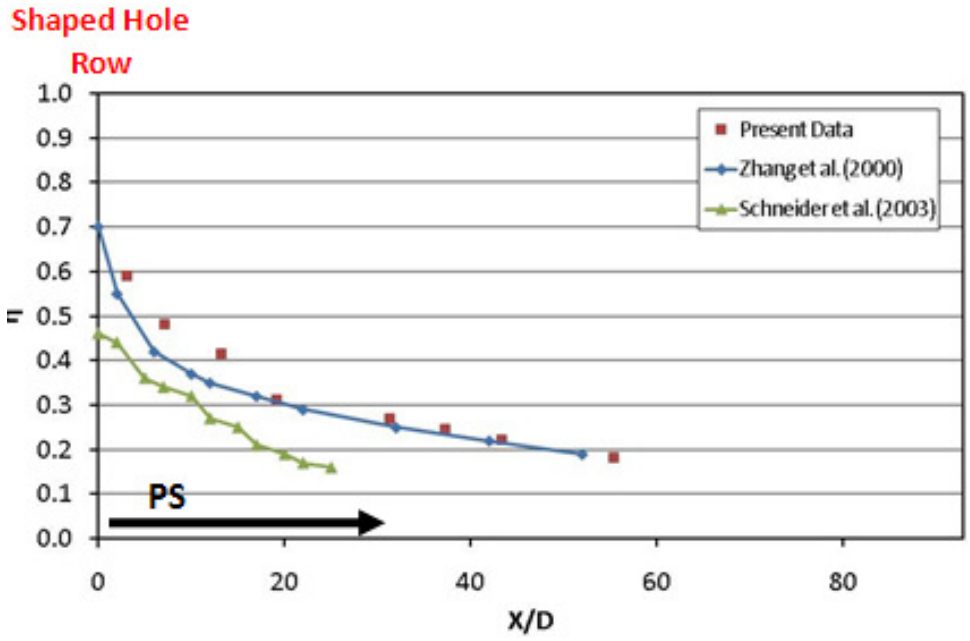

Figure 3. 4. PS effectiveness literature comparison

The present study shows very good agreement with Zhang et al. [25] on the PS of the vane (Fig. 3. 4). Since the data of current study is based on single point measurement by TFG, and the data from Zhang et al. [25] and Schnieder et al. [27] are the spanwise average values, the slight disagreement on the effectiveness trend is expected. Compare to current study and data from Zhang et al. [25], the data of Schnieder et al. [27] shows a faster decay of effectiveness. This may be due to their larger spanwise spacing. In their study p/D=6.0, and in both current study and study by Zhang et al. [25] p/D=3.5. Therefore in study by Schnieder et al. [27] the blade has a relatively poorer spanwise coverage.

On the SS, the present study again shows very good agreement with Zhang et al. [26] (Fig. 3. 5). Slight differences in trend and level may be due to different test methods as mentioned above.

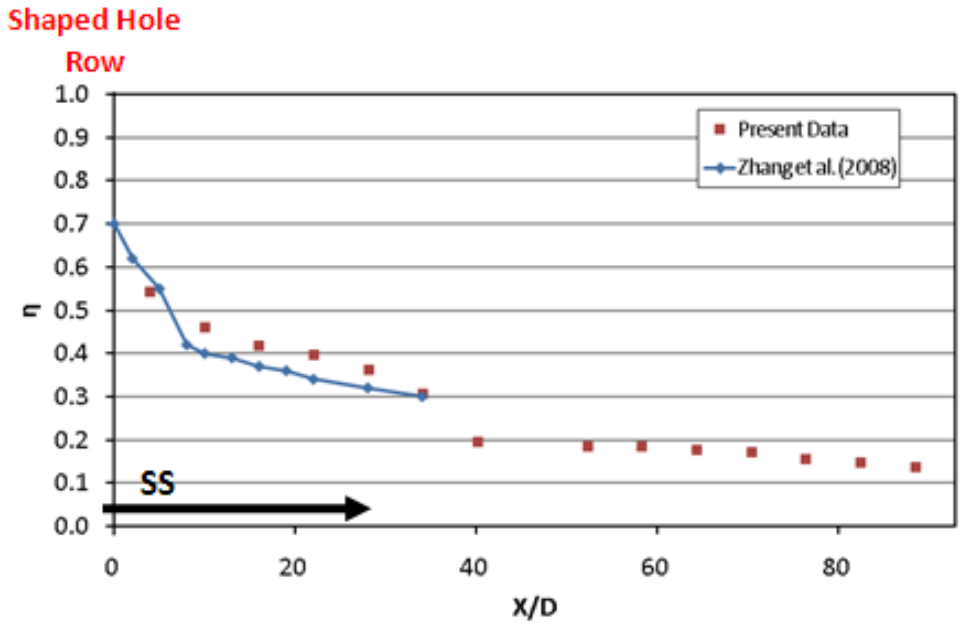

Figure 3. 5. SS effectiveness literature comparison

Laminar and Turbulent Flat Plate Correlation

Figures 3. 6 and 3. 7 show experimental Stanton number distributions from the present study compared with laminar and turbulent flat plate Stanton number predictions. This comparison is useful for gaining fundamental insight into how the boundary layer is behaving on the surface of the vane. It also serves to show whether or not the data falls within an acceptable range of values. For this comparison, the analytical solutions for laminar and turbulent flat plate Nusselt number as presented in Incorpera and De Witt [40] are used. Equation 3.8 is the laminar boundary layer equation and equation 3.9 is the turbulent boundary layer equation.

$$Nu_x = 0.332 {Re_x}^{1/2} Pr^{1/3} \qquad (3.8)$$

$$Nu_x = 0.0296 {Re_x}^{4/5} Pr^{1/3} \qquad (3.9)$$

Both of these equations use vane surface distance from the leading edge as the characteristic length parameter in the calculation of Nusselt number and Reynolds number.

Results are then converted from Nusselt number to Stanton number using equations 3.10 and 3.11 below.

$$h_x = \frac{Nu_x \cdot k_a}{x} \qquad (3.10)$$

$$St = \frac{h_x}{\rho_x U_x C_{p,\infty}} \qquad (3.11)$$

Figures 3. 6 and 3. 7 show experimental data at Mex = 0.85 and BR = 2.0 normalized in terms of Stanton number. Also plotted are the analytical Stanton number solutions for flat plate laminar and turbulent boundary layer cases calculated using equations 3.8 and 3.9.

Figure 3. 6 shows the comparison of PS data to the flat plate correlations. Experimental data shows a fairly good match with the turbulent boundary layer solution for most of the PS. The level of the data suggests that the boundary layer is turbulent for the entire length of the PS, and may be a result of high inlet turbulence intensity (12%). This type of heat transfer augmentation resulting from high turbulence intensity has also been shown experimentally by Blair [41]. The presence of film cooling may also be effecting the experimental Stanton number distribution, creating the large heat transfer augmentation (1.8x the turbulent flat plate solution) seen at lower Reynolds numbers which correspond to the near shaped hole region.

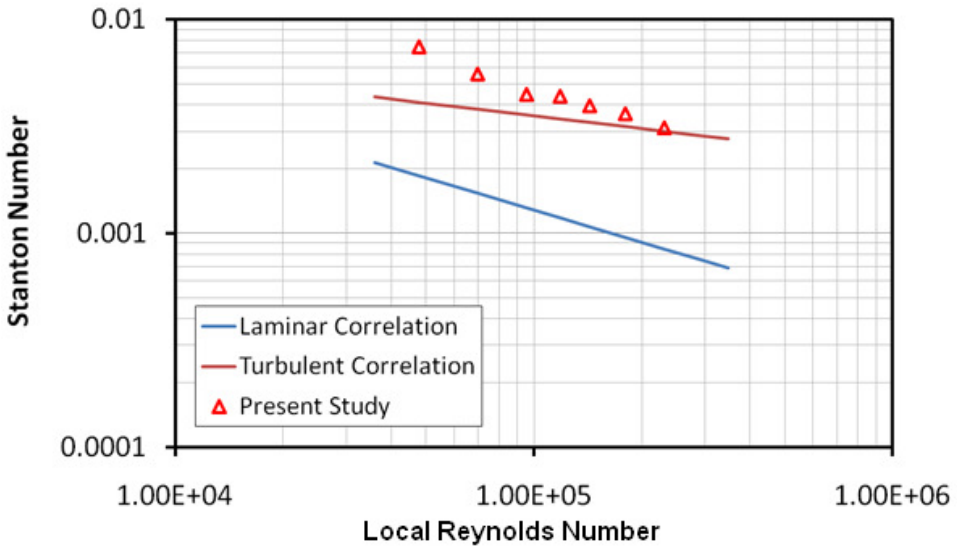

Figure 3. 6. PS M_{ex} = 0.85 BR = 2.0 data compared with flat plate correlations

Figure 3. 7 shows the comparison on the SS, and boundary layer transition is clearly evident on the plot. Most of the data falls between the laminar and turbulent correlation lines up to the transition point, where data shifts to more closely follow the turbulent correlation. The effect of heat transfer augmentation due to film cooling and inlet turbulence can also be seen before transition in the level and slope difference between the correlations and experimental data.

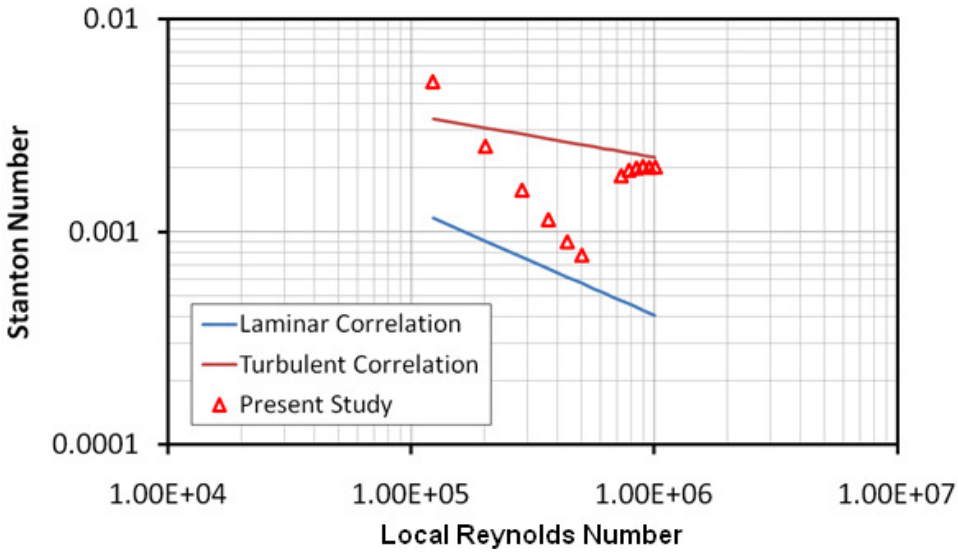

Figure 3. 7. SS M_{ex} = 0.85 BR = 2.0 data compared with flat plate correlations

Comparison with Showerhead-Only Vane

Figure 3. 8 shows a film cooling effectiveness comparison at M = 0.85, BR = 2.0 of data from the present study with that of Nasir et al. [34]. Nasir et al. [34] presents data taken on a vane of the same profile as the present study with only LE showerhead film cooling. The comparison shows that the addition of shaped hole rows on the PS and SS has increased film effectiveness across the board. Shaped holes show a 2-2.5x improvement in effectiveness over showerhead only film cooling across the measurement range with only a 1.6x increase in coolant usage. It should also be noted that the shaped holes hold higher effectiveness values farther downstream than the showerhead rows. This is to be expected with shaped holes as they have been shown to diffuse less rapidly with streamwise distance than cylindrical hole cooling. One particular area of interest for both studies has been $0.3<X/C<0.50$. In this region the showerhead only data shows an effectiveness plateau, while the showerhead and shaped hole vane shows a sharp effectiveness decrease. Nasir et al. [34] attributed the effectiveness plateau to high values of acceleration in this region. High acceleration could have a laminarizing effect on the boundary layer, resulting in delayed film diffusion and the effectiveness plateau seen in the figure. However, the Nusselt number trend (Fig 3. 9) suggests the boundary layer transition starts at X/C =0.3 for the showerhead only vane, so the film diffusion could not be delayed in this region. A more reasonable explanation is stated as following. The coolant from showerhead injection could be partially lift-off. Since the acceleration flow near the leading edge keeps the boundary layer laminar, the coolant diffuses slowly, before X/C=0.3, and forms a high concentration trace. For the showerhead only vane, the boundary layer transition starts from X/C=0.3, which is implied by the increase of Nusselt number (Fig 3. 9). In the boundary layer transition region, the increased turbulence makes high concentration trace of coolant diffuses faster. Part of the coolant spreads back towards the surface, which shortly delays the adiabatic effectiveness decay, and creates the plateau trend as shown on figure 3. 8. This plateau then decays quickly after the throat where the boundary layer turns into full turbulent. The plateau or even ramp-up trend of effectiveness at downstream of a cylindrical hole injection had been observed in other reports such as the CFD study by Gustavo et al. [42], experimental study by Rigby et al. [43], and Teng et al. [44]. The plateau trend did not happen on showerhead plus shaped hole vane, because the shaped hole injection dominant the effectiveness in this region.

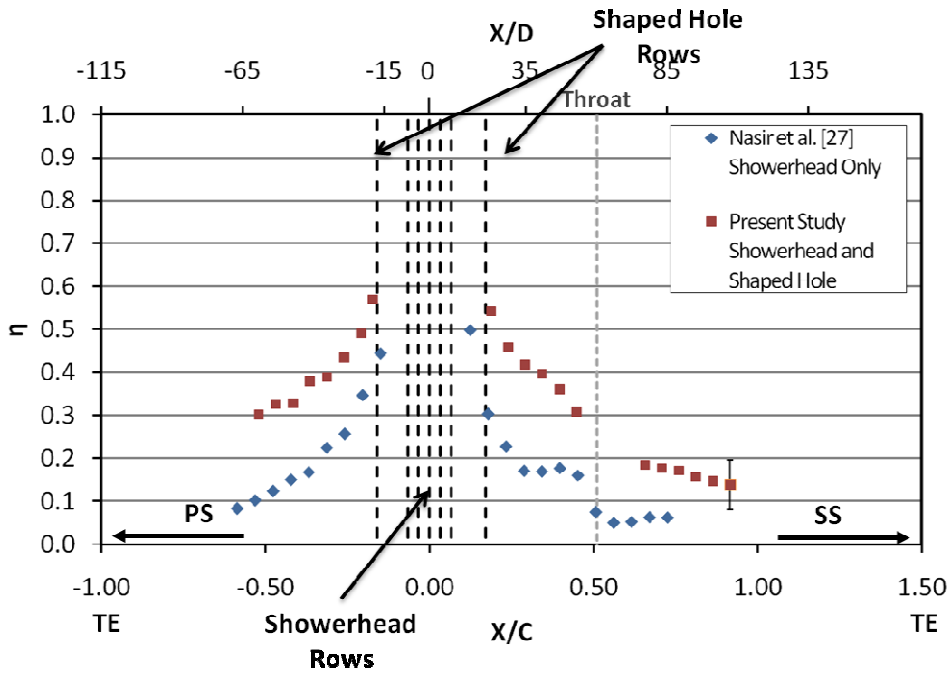

Figure 3. 8. Film cooling effectiveness comparison at M = 0.85, BR = 2.0

Figure 3. 9 shows a comparison of Nusselt number between data from Nasir et al. [34] at Mex = 0.76, BR = 2.0 and the present study at Mex = 0.85 and BR = 2.0. Nasir et al. [34] presents data taken on a vane of the same profile as the present study with only LE showerhead film cooling. The first noticeable feature of this plot is considerably higher heat transfer in the near shaped hole region. This is probably due to the injection flow disrupting the boundary layer. On the PS as the flow goes downstream, the near hole region effect reduces, and the Nusselt number of shaped hole injected vane decreases to the same level as the showerhead only vane; on the SS the decreasing of Nusselt number may be due to the boundary layer relaminarization, which is driven by the high favorable pressure gradient. The decreasing trend of the Nusselt number on the showerhead only vane lasts to X/C=0.3, and then, the Nusselt number increases, which indicates the boundary layer relaminarization ends, and the transition occurs. This is because, after X/C=0.3, the acceleration parameter drops to be lower than 3X10-6, the critical value of boundary layer relaminarization, which was suggested by Mayle [45]. (The distribution of acceleration parameter on the solid vane without film injection was reported by Nasir et al. [33].) However, for the shaped hole injected vane, after X/C=0.3, the Nusselt number keeps decreasing. On the shaped hole injected vane, Nusselt number starts increasing at the throat, where X/C=0.5. Comparing to the showerhead only vane, the trend of Nusselt number on shaped

hole injected vane suggests a delayed boundary layer transition. One of the possible explanations for this trend is that, in the favorable pressure gradient flow on the SS, besides disrupting the boundary layer and causing mixing, the shaped hole injection also adds streamwise momentum into the boundary layer, which accelerates the low speed sublayer, and makes the local acceleration parameter higher than the critical value to relaminarize the boundary layer. Therefore, by addition of the shaped hole injection, the boundary layer transition point on the SS was pushed from X/C=0.3 to X/C=0.5.

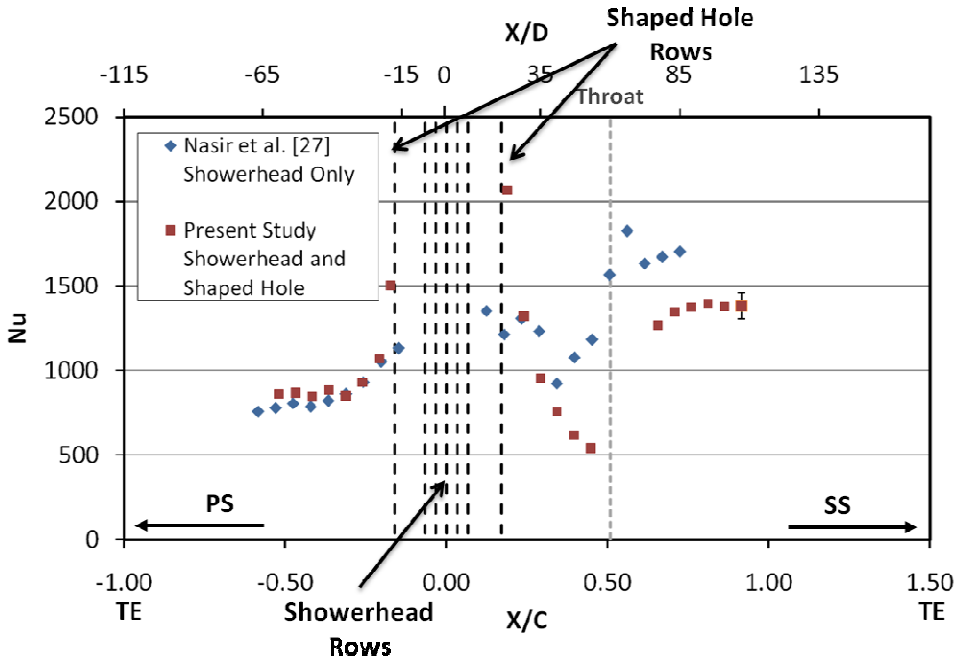

Figure 3. 9. Film cooling Nusselt number comparison, M = 0.85, BR = 2.0

Effect of Exit Mach/Reynolds Number on Film Effectiveness

Figure 3. 10 highlights the effect of increasing exit Mach/Reynolds number on film effectiveness distributions at a given blowing ratio of BR=2.0. The effectiveness of three different Mach numbers start at the same value at the near hole region. As the flow develops downstream, it seems higher Mach number results in slower decay of the effectiveness. This trend has been shown previously in literature by Mehendale and Han [47] for showerhead injection, and by E. Lutum et al. [48] on a convex surface for shaped hole injection. In their report, E. Lutum et al. suggested the increased freestream Mach number improves the cooling effectiveness by slightly changing the boundary layer thickness and suppressing the boundary

layer turbulence production. It was first suggested by Liess [49] that the interaction between coolant injection and boundary layer has a significant influence on the film effectiveness, when the boundary layer displacement thickness and the injection hole diameter ratio is close to 0.2. However, in present study, the accurate displacement thickness is unavailable. The physics of Mach number/Reynolds number effect on film effectiveness in current study is still not very clear.

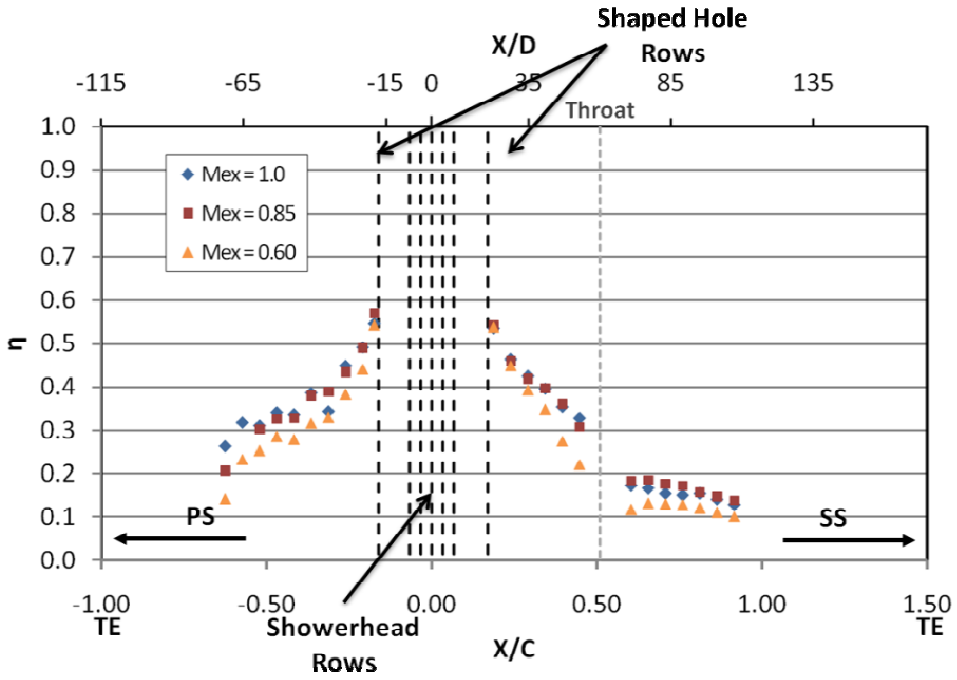

Figure 3. 10. Effect of exit Mach number on film effectiveness distribution, BR = 2.0

Effect of Blowing Ratio on Film Effectiveness

Figure 3. 11 highlights the effect of increasing blowing ratio on film effectiveness distributions. The general trend is that increases in blowing ratio increases film effectiveness. However, as compared with the PS, the effectiveness on SS is less sensitive to the blowing ratio change. This may be due to (in part) the different blowing ratios at the PS and SS shaped hole rows as a result of the vane's single plenum design. As it was shown in Table 3. 3, when the showerhead blowing ratio changed from 1.0 to 2.0, the PS blowing ratio increased from 1.7 to 3.0, whereas, the SS blowing ratio only increased from 1.1 to 1.4. Less change of effectiveness on the SS compare to the PS was also observed by Mhetras et al. [50]. In their test the same

plenum was shared by SS and PS cooling holes, and they attribute the minor increase of effectiveness on SS to the smaller increase of SS blowing ratio.

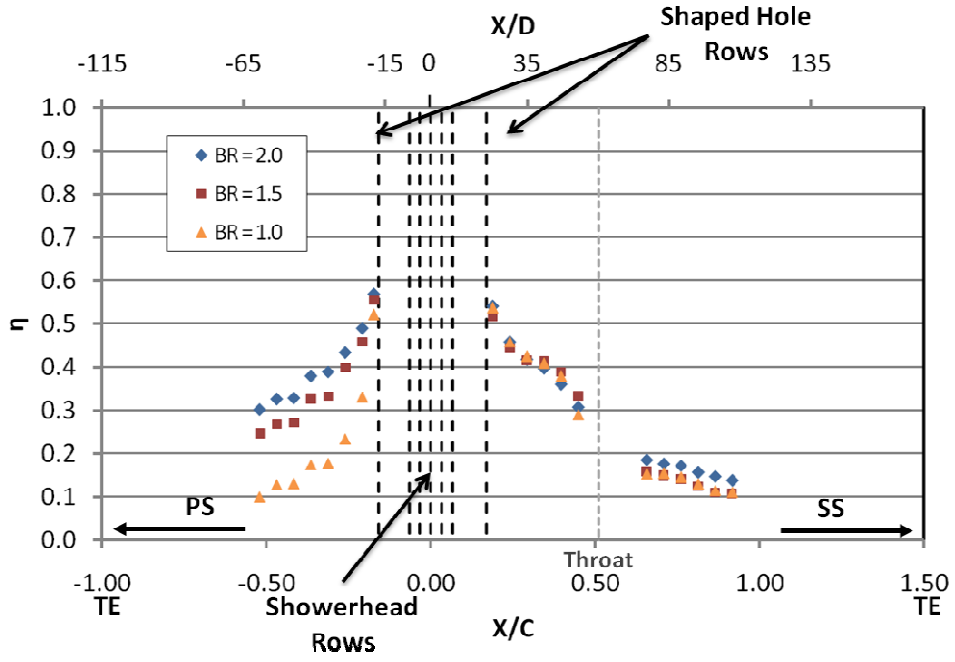

Figure 3. 11. Effect of blowing ratio on film effectiveness, M_{ex} = 0.85

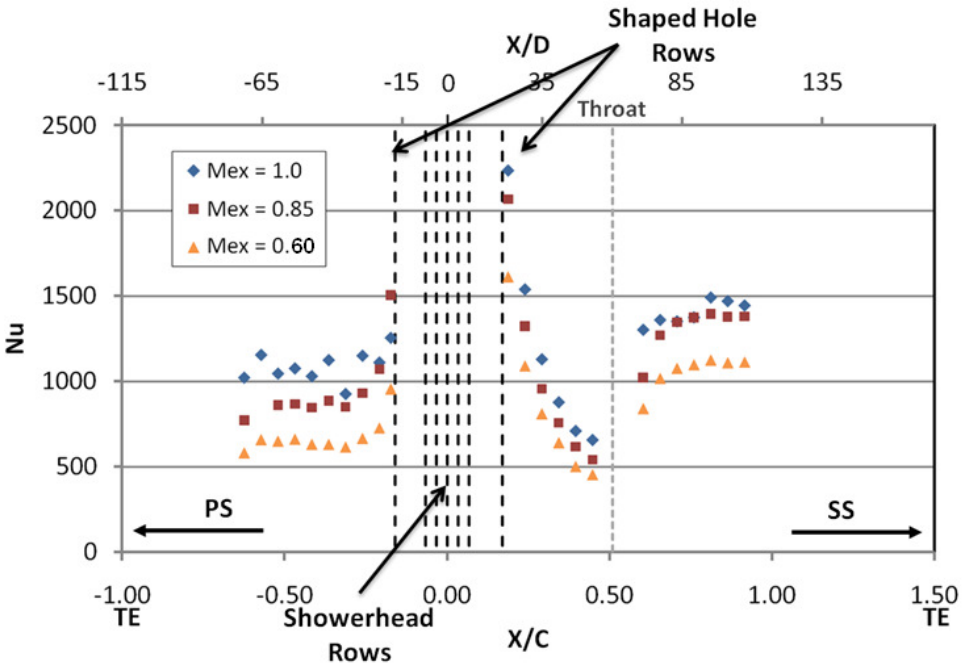

Figure 3. 12. Effect of exit Mach number on Nusselt number distribution, BR = 2.0

Effect of Exit Mach/Reynolds Number on Nusselt Number

Figure 3. 12 shows the effect of increasing exit Mach number on Nusselt number for the blowing ratio of BR=2.0. Increasing exit Mach number has the apparent effect of augmenting Nusselt number on both the PS and SS of the measurement vane. A trend of increasing Nusselt number with increasing Mach number has been shown by Nasir et al. [34] as well as others such as Reiss and Bölcs [3] and Abuaf et al. [51]. The region where transition occurs does not appear to be effected by change in Mach/Reynolds number. It is occurring in approximately the same region just upstream of the throat, and is identified by the sharp jump in Nusselt number seen on the SS. A lack of change in transition region with changing exit Mach number is consistent with the findings of Nasir et al. [34] on the showerhead-only vane.

Effect of Blowing Ratio on Nusselt Number

Figure 3. 13 shows the effect of blowing ratio on Nusselt number for Mex = 0.85. In general, as blowing ratio increases, Nusselt number increases on the PS; the SS also shows little change for all three blowing ratio cases. This may be a result of lower blowing ratio changes from the SS shaped holes due to the single-plenum coolant feed design, as mentioned before. On the PS, a trend of increasing Nusselt number with increasing blowing ratio is observed. Nusselt number augmentation as a result of higher blowing ratios is generally a result of increased local turbulence due to coolant injection and mixing. This trend has been seen elsewhere in literature such as Arts et al. [52] and Ekkad et al. [53] to name two. As was the case with varied exit Mach number, the location of boundary layer transition does not appear to change with blowing ratio.

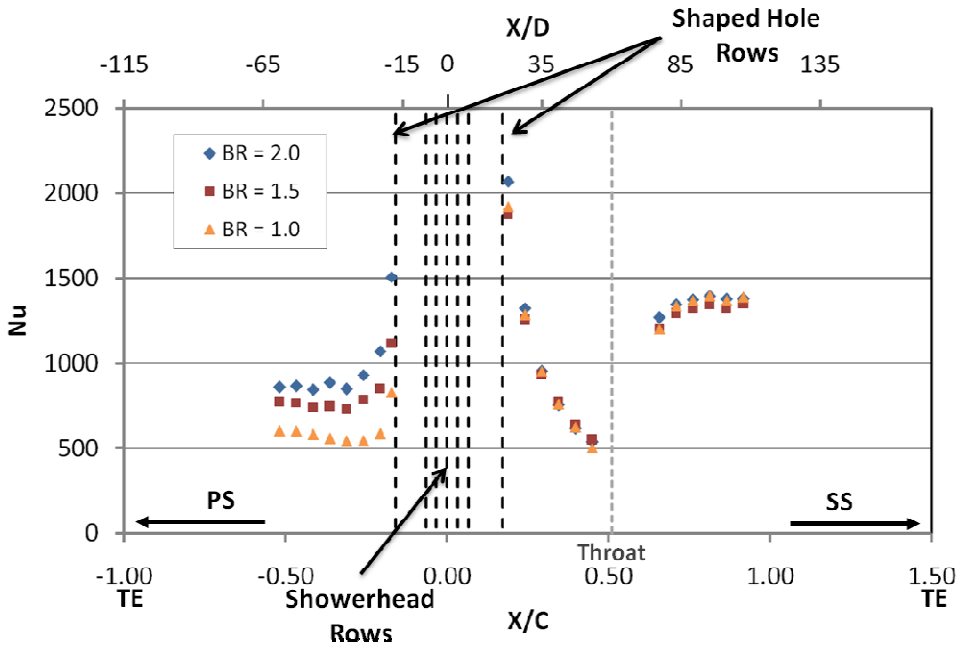

Figure 3. 13. Effect of blowing ratio on Nusselt number distribution, M_{ex} = 0.85

NHFR Comparison

Net heat flux reduction is a measure to evaluate the overall film cooling performance of coolant injection. Net heat flux reduction is defined below in equation 3.12.

$$NHFR = 1 - \frac{q''}{q_0''} = 1 - \frac{h}{h_0}\left(1 - \frac{\eta}{\phi}\right) \qquad (3.12)$$

In this equation ϕ refers to the overall film cooling effectiveness defined as in equation 3.13.

$$\phi = \frac{T_w - T_r}{T_c - T_r} \qquad (3.13)$$

This value is assumed to be between 0.5 and 0.7 according to Mehendale and Han[47]. A value in the middle of this range (0.6) will be used for NHFR analysis. This value has been used by Mehendale and Han [47], Drost et al. [53], and Nasir et al. [34] for high speed cascade studies. Heat transfer coefficient is normalized by heat transfer coefficient data taken by Nasir et

al. [34] on a solid, uncooled vane without cooling holes in the same facility. This method was also used by Mehendale and Han [47] to normalize heat transfer coefficient.

Figure 3. 14 compares NHFR data recorded by Nasir et al. [34] on a showerhead-only film cooled vane using the same transient TFG technique as the present study. As was the case with film effectiveness, the showerhead and shaped hole film cooled vane shows higher film cooling performance across the entire measurement surface with NHFR values an average of 2.6x higher across the measurement surface. Similar Nusselt number values combined with film effectiveness values 2-2.5x that of Nasir et al. [34] result in very large NHFR increases on the PS. On the SS, lower heat transfer augmentation from shaped hole film cooling results in slightly smaller gains over the showerhead-only case. However, the comparison supports the findings of the film effectiveness comparison: that film cooling performance is greatly improved downstream of the leading edge by adding shaped holes on the PS and SS. Again, this average 2.6x NHFR increase occurs with only a 1.6x increase in the required coolant mass flow.

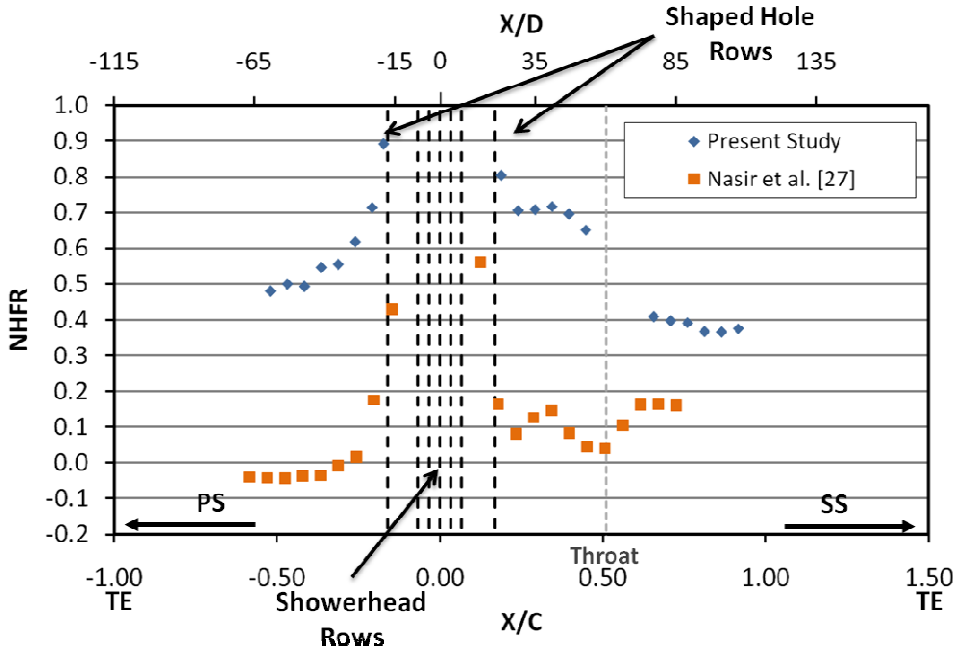

Figure 3. 14. Comparison of NHFR from Nasir *et al.* [34] with the present study at M_{ex} = 0.85, BR = 2.0

Conclusions

Film cooling performance tests were conducted for three exit Mach number/Reynolds number combinations: 1.0/1,400,000; 0.85/1,150,000; and 0.60/850,000. At exit Mach numbers of 1.0 and 0.85, three blowing ratio conditions were tested: BR = 1.0, 1.5, and 2.0. All tests were performed at high freestream turbulence levels with inlet turbulence intensity of 12% and turbulence length scale normalized by the cascade pitch of 0.28. Vane surface film cooling effectiveness and net heat flux reduction distributions were presented and compared with literature. The chief conclusions of the study are as follows:

Film cooling effectiveness data compared well in both level and trend with existing shaped hole literature at similar conditions. Stanton number compared favorably with analytical laminar and turbulent flat plate boundary layer solutions, with expected trends reported on the PS and SS.

The addition of shaped hole rows downstream of showerhead injection on both the PS and SS of the vane resulted in film effectiveness levels averaging 2-2.5x those of a showerhead only film cooled vane. Comparison of the Nusselt number between the showerhead only vane and the showerhead plus shaped hole vane suggested the interaction between the shaped holes injection and pressure gradient delays the boundary layer transition on the SS, and caused a lower heat flux in the region of $0.3<X/C<0.5$.

For constant blowing ratio, the increased exit Mach number caused slower decay of effectiveness and higher level of Nusselt number.

For constant Mach/Reynolds number, increasing blowing ratio showed increase in film effectiveness and heat transfer augmentation on the PS. Little significant increase in film effectiveness or heat transfer augmentation in SS data may be due to the small change on SS shaped hole blowing ratio.

A comparison of NHFR between a showerhead only and combined showerhead and shaped hole film cooled vane showed that the addition of a single row of shaped holes to both the PS and SS of the vane resulted in considerably increased NHFR (2.6x the value of showerhead-

only NHFR) downstream of the holes. This analysis showed that the addition of shaped holes reduced the amount of heat absorbed by the PS and SS over showerhead-only injection, with only 1.6x increase in coolant mass flow required.

Aknowledgement

The authors are thankful to Solar Turbines for supporting this research and granting the permission to publish the results. Special thanks to Eli Razinsky for his encouragement. Dr. Richard Anthony (AFRL) provided the thin film gages used in this study. The authors highly appreciate Dr. Ekkad's for his helpful discussions and Colin Reagle's for his assistance on the tests. The authors are also grateful to The Connecticut Center for Advanced Technology, Inc. for their help on the machining of the shaped holes.

Nomenclature

h	heat transfer coefficient
k	thermal conductivity
M	Mach number
Re	Reynolds number
Nu	Nusselt number
PS	pressure surface
q"	heat flux
r	recovery factor
SS	suction surface
T	temperature
t	time
TFG	thin film gauge
Tu	streamwise freestream turbulence intensity

U	local velocity
x	vane surface distance from stagnation point
C	true chord
y	surface depth
D	cooling hole diameter
A	area
BR	blowing ratio
LE	leading edge
NHFR	net heat flux reduction
$\dot{m}$	mass flow rate
MFR	mass flow ratio

Greek

γ	ratio of specific heats
ρ	local density
η	adiabatic effectiveness
φ	overall film cooling effectiveness

Subscripts

∞	freestream
aw, w	adiabatic wall, wall
ex	exit
i	initial, inlet

o	uncooled
r	recovery
s	surface
c	coolant
x	vane surface distance from stagnation point

References

[1] Goldstein, R. J., Lau, K. Y., and Leung, C. C., 1983, "Velocity and Turbulence Measurements in Combustion Systems," *Experiments in Fluids*, Vol. 1, pp. 93-99.

[2] Koutmos, P. and McGuirk, J. J., 1989, "Isothermal Flow in a Gas Turbine Combustor A Benchmark Experimental Study," *Experiment in Fluids*, Vol. 7, pp. 344-354.

[3] Reiss, H., Bölcs, A., 2000, "The Influence of the Boundary Layer State and Reynolds Number on Film Cooling and Heat Transfer on a Cooled Nozzle Guide Vane," *IGTI Turbo Expo,* Berlin, GT-2000-205.

[4] Ames, F. E., 1998, "Aspects of Vane Film Cooling With High Turbulence: Part I— Heat Transfer," *Journal of Turbomachinery*, 1998, Vol. 120, pp. 768-775.

[5] Guo, S. M., Oldfield, M. L. G., and Rawlinson, A. J., 2002, "Influence of Discrete Pin Shaped Surface Roughness (P-Pins) on Heat Transfer and Aerodyanmics of Film Cooled Aerofoil," *Proceedings of ASME Turbo Expo* GT-2002-30179.

[6] Cutbirth, J. M. and Bogard, D. G., 2002, "Evaluation of Pressure Side Film Cooling With Flow and Thermal Field Measurement, Part II: Turbulence Effects," *Proceedings of ASME Turbo Expo* GT-2002-30175.

[7] Ou, S., Rivir, R., Meininger, M., Soechting, F., and Tabbita, M., 2000, "Transient Liquid Crystal Measurement of Leading Edge Film Cooling Effectiveness and Heat Transfer with High Free Stream Turbulence," *Proceedings of ASME Turbo Expo* GT-2000-245.

[8] Goldstein, R. J., Eckert, E. R. G., and Burggraf, F., 1974, ‘‘Effects of Hole Geometry and Density on Three-Dimensional Film Cooling,’’ Int. *J. Heat Mass Transfer*, 17, pp. 595–607.

[9] Schmidt, D., Sen, B., and Bogard, D., 1996, "Film Cooling with Compound Angle Holes: Adiabatic Effectiveness," *ASME J. Turbomachinery*, 118, pp. 807-813

[10] Gritsch, M., Schulz, A., and Wittig, S., 1998, ''Heat Transfer Coefficients Measurements of Film-Cooling Holes With Expanded Exits,'' *IGTI Conference*, Stockholm, Paper 98-GT-28.

[11] Yu, Y., Yen, C. H., Shih, T. I. P., Chyu, M. K. and Gogineni, S., 2002, "Film cooling effectiveness and heat transfer coefficient distributions around diffusion shaped holes," *ASME J. Heat Transfer,* 124, pp. 820–827.

[12] Bell, C. M., Hamakawa, H., Ligrani, P. M., 2000, "Film Cooling From Shaped Holes," *ASME J. Heat Transfer,* 122, pp. 224–232.

[13] Dittmar, J., Schulz, A., Wittig, S., 2003, "Assessment of Various Film-Cooling Configurations Including Shaped and Compound Angle Holes Based on Large-Scale Experiments," *ASME J. Turbomachinery*, 125, pp. 57-64

[14] Yuen, C. H. N., Martinez-Botas, R. F., and Whitelaw, J. H., 2001, ''Film Cooling Effectiveness Downstream of Compound and Fan-Shaped Holes,*" IGTI Turbo Expo*, New Orleans, Paper 2001-GT-0131.

[15] Lu, Y., Dhungel, A., Ekkad, S. V., Bunker, R. S., 2009, "Effect of Trench Width and Depth on Film Cooling from Cylindrical Holes Embedded in Trenches," *ASME J. Turbomachinery*, 131, No. 011003

[16] Dhungel, A., Lu, Y., Phillips, W., Ekkad, S. V., Heidmann, J., 2009, "Film Cooling From a Row of Holes Supplemented with Antivortex Holes," *ASME J. Turbomachinery*, 131, No. 021007

[17] Wittig, S., Schulz, A., Gritsch, M., Thole, K. A., 1996, ''Transonic Film-Cooling Investigations: Effects of Hole Shapes and Orientations,*" IGTI Turbo Expo*, Birmingham, UK, Paper 1996-GT-222.

[18] Thole, K. A., Gritsch, M., Schulz, A., Wittig, S., 1998, "Flowfield Measurements for Film-Cooling Holes With Expanded Exits," *ASME J. Turbomachinery*, 120, pp. 327-336

[19] Saumweber, C., Schulz, A., 2004, "Interaction of Film Cooling Rows: Effects of Hole Geometry and Row Spacing on the Cooling Performance Downstream of the Second Row of Holes," *ASME J. Turbomachinery*, 126, pp. 237-246

[20] Saumweber, C., and Schulz, A., 2003, ‘‘Interaction of Film Cooling Rows: Effects of Hole Geometry and Row Spacing on the Cooling Performance Downstream of the Second Row of Holes,’’ *IGTI Turbo Expo*, Atlanta, Paper GT2003-38195.

[21] Colban, W., Gratton, A., Thole, K. A., Haendler, M., 2005, “Heat Transfer and Film-Cooling Measurements on a Stator Vane with Fan-Shaped Cooling Holes,” *IGTI Turbo Expo*, Reno-Tahoe, Paper GT2005-68258.

[22] Colban, W., Thole, K. A., Haendler, M., 2007, “Experimental and Computational Comparisons of Fan-Shaped Film Cooling on a Turbine Vane Surface,” *ASME J. Turbomachinery*, 129, pp. 23-31

[23] Chappell, J., Ligrani, P., Sreekanth, S., Lucas, T., 2008, “Suction-Side Gill-Region Film Cooling: Effects of Hole Shape and Orientation on Adiabatic Effectiveness and Heat Transfer Coefficient,” *IGTI Turbo Expo*, Berlin, Paper GT2008-50798.

[24] Furukawa, T., Ligrani, P., 2002, “Transonic Film Cooling Effectiveness from Shaped Holes on a Simulated Turbine Airfoil,” *AIAA J. Thermophysics and Heat Transfer,* 16, pp. 228-237

[25] Zhang, L., Pudupatty, R., 2000, “The Effects of Injection Angle and Hole Exit Shape on Turbine Nozzle Pressure Side Film-Cooling,” *IGTI Turbo Expo,* Munich, Paper 2000-GT-247.

[26] Zhang, L., Moon, H. K., 2008, “The Effect of Wall Thickness on Nozzle Suction Side Film Cooling,” *IGTI Turbo Expo,* Berlin, Paper GT2008-50631.

[27] Schnieder, M., Parneix, S., von Wolfersdorf, J., 2003, “Effect of Showerhead Injection on Superposition of Multi-Row Pressure Side Film Cooling with Fan Shaped Holes,” *IGTI Turbo Expo,* Atlanta, Paper GT2003-38693.

[28] Thurman, D. R., Poinsatte, P. E., Heidmann, J. D., 2008, “Heat Transfer Measurements for a Film Cooled Turbine Vane Cascade,” *IGTI Turbo Expo,* Berlin, Paper GT2008-50651

[29] Guo, S. M., Lai, C. C., Jones, T. V., Oldfield, M. L. G., Lock, G. D., Rawlinson, A. J., 1998, “The application of thin-film technology to measure turbine-vane heat transfer and effectiveness in a film-cooled, engine-simulated environment,” *Int. J. Heat and Fluid Flow,* 19, pp. 594-600

[30] Sargison, J. E., Guo, S. M., Oldfield, M. L. G., Lock, G.. D., Rawlinson, A. J., 2002, "A Converging Slot-Hole Film-Cooling Geometry—Part 2: Transonic Nozzle Guide Vane Heat Transfer and Loss," *ASME J. Turbomachinery,* 124, pp. 461-471

[31] Reagle, C. J., Newman, A., Xue, S., Ng, W. F., Ekkad, S., Moon, H. K., Zhang, L., 2010, "A Transient Infrared Technique for Measuring Surface and Endwall heat Transfer in a Transonic Turbine Cascade," *IGTI Turbo Expo,* Glasgow, Paper GT2010-22975

[32] Bolchoz, T., Nasir, S., Reagle, C., Ng, W. F., and Moon, H. K., 2009, "An Experimental Investigation of Showerhead Film Cooling Performance In A Transonic Vane Cascade At Low and High Freestream Turbulence," *IGTI Turbo Expo,* Orlando, Paper GT2009-59796.

[33] Nasir, S., Carullo, J. S., Ng, W. F., Thole, K. A., Wu, H., Zhang, L. J., and Moon, H. K., 2007, "Effects of Large Scale High Freestream Turbulence, and Exit Reynolds Number on Turbine Vane Heat Transfer in a Transonic Cascade," *ASME J. Turbomachinery*, 131, pp.021021-1 to -11.

[34] Nasir, S., Bolchoz, T., Ng, W. F., Zhang, L. J., Moon, H. K., Anthony, R. J., 2008, "Showerhead Film Cooling Performance of a Turbine Vane in a Transonic Cascade," *ASME IMECE 2008,* Paper 66528.

[35] Doorly, J. E., Oldfield, M. L. G., 1987, "The Theory of Advanced Multi-Layer Thin Film Heat Transfer Gages," *Int. J. Heat and Mass Transfer*, 30, pp. 1159–1168.

[36] Joe, C. R., 1997, "Unsteady Heat Transfer on the Turbine Research Facility at Wright Laboratory," Ph.D. Dissertation, Syracuse University.

[37] Cress, R. D., 2006, "Turbine Blade Heat Transfer Measurements in a Transonic Flow Using Thin film Gages," Master's Thesis, Virginia Polytechnic Institute and State University.

[38] Popp, O., Smith, D. E., Bubb, J. V., Grabowski, H. C., Diller, T. E. Schetz, J. A., Ng. W. F., 2000, "An Investigation of Heat Transfer in a Film Cooled Transonic Turbine Cascade, Part II: Unsteady Heat Transfer," *IGTI Turbo Expo,* Berlin, Paper GT-2000-203.

[39] Newman, A., 2010, "Performance of a Showerhead and Shaped Hole Film Cooled Vane at High Freestream Turbulence and Transonic Conditions," Master's Thesis, Virginia Polytechnic Institute and State University.

[40] Incropera, F. P. and DeWitt, D. P., 2002, Fundamentals of Heat and Mass Transfer, 5th Ed., John Wiley and Sons, New York.

[41] Blair, M. F., 1983, “Influence of Free-Stream Turbulence on Turbulent Boundary Layer Heat Transfer and Mean Profile Development, Part I—Experimental Data,” *ASME J. Heat Transfer,* 105, pp. 33-40.

[42] Ledezma, G. A., Laskowski, G. M., Dees, J. E., Bogard, D. G., 2011, "Overall and Adiabatic Effectiveness Values on a Scaled up Simulated Gas Turbine Vane: Part II Numerical simulation", ASME GT2011-46616.

[43] Rigby, M. J., Johnson, A. B., Oldfield, M. L. G., 1990, "Gas Turbine Rotor Blade Film Cooling with and without Simulated NGV Shock Waves and Wakes", ASME 90-GT-78.

[44] Teng, S., Sohn, D. K., Han, J. C., "Unsteady Wake Effect on Film Temperature and Effectiveness Distributions for a Gas Turbine Blade",ASME Journal of Turbomachinery, 2000, Vol. 122, pp. 340-347.

[45] Mayle, R. E., 1991, “The Role of Laminar-Turbulent Transition in Gas Turbine Engines”, *ASME J. Turbomachinery*, 113, pp. 509-536.

[46] Mhetras, S., Han, J. C. and Rudolph, R., 2007, “Effect of Flow Parameter Variations on Full Coverage Film-Cooling Effectiveness for a Gas Turbine Blade”, *IGTI Turbo Expo,* May, 2007, Montreal, Canada, Paper GT2007-27071.

[47] Mehendale, A. B., Han, J. C., 1993, “Reynolds number Effect on Leading Edge Film Effectiveness and Heat Transfer Coefficient,” *Int. J. Heat and Mass Transfer*, 36, pp. 3723–3730.

[48] Lutum, E., Wolfersdorf, J. V., Semmler, K., Naik, S., Weigand, B., 2001, “Film Cooling on a Convex Surface: Influence of External Pressure Gradient and Mach Number on Film Cooling Performance,” *Heat and Mass Transfer*, 38, 7-6.

[49] Liess C., 1975, “Experimental Investigation of Fim Cooling with Ejection from a Row of Holes for the Application to Gas Turbine Blade”, J. of Eng Power 97: 21-27.

[50] Mhetras, S., Han, J. C., and Rudolph R., 2008, “Film-Cooling Effectiveness From Shaped Film Cooling Holes for a Gas Turbine Blade,” *Proceedings of ASME TURBO EXPO* 2008 Power for Land, Sea and Air, GT-2008-50916

[51] Abuaf, N., Bunker, R., Lee, C. P., 1997, “Heat Transfer and Film Cooling Effectiveness in a Linear Airfoil Cascade,” *ASME J. Turbomachinery,*119, pp. 302-309

[52] Arts, T., Bourguignon, A. E., 1990, “Behavior of a Coolant Film with Two rows of Holes along the Pressure Side of a High Pressure Nozzle Guide Vane,” *ASME J. Turbomachinery*, 112, pp. 512-520.

[53] Ekkad, S. V., Mehendale, A. B., Han, J. C., Lee, C. P., 1997, “Combined Effect of Grid Turbulence and Unsteady Wake on Film Effectiveness and Heat Transfer Coefficient of a Gas Turbine Blade with Air and CO2 Film Injection,” *ASME J. Turbomachinery*, 119, pp. 594-600.

[54] Drost, U., Bölcs, A., 1999, “Investigation of Detailed Film Cooling Effectiveness and Heat Transfer Distribution on a Gas Turbine Airfoil,” *ASME J. Turbomachinery*, 121, pp. 233-242.

Appendix A. Literature Review of Shock/Film Cooling Interaction

Film cooling scheme has been developed as a sophisticated technology. Besides optimizing the film cooling effectiveness at subsonic conditions, there has been interest focusing on the film cooling in some interesting phenomena at supersonic conditions in recent years, such as the shock/film cooling interaction. The shock/film cooling interaction is a very complicated phenomenon. Currently, the physics of shock/film cooling interaction is not fully understood, and more detailed studies are needed. According to the observation in literature, different patterns of shock/film cooling interaction induce different effects on the heat transfer and film cooling performance. A literature review on shock/film cooling interaction is presented in Appendix A.

Steady shock impingement effect on subsonic injected film cooling in turbine blade cascade

In a turbine cascade with supersonic exit flow, it is common that one leg of the fishtail shock from the adjacent upper blade trailing edge impinges the suction side of the lower blade. This kind of standing shock will influence the film cooling at and after the impingement. This pattern of shock wave/film cooling interaction has been experimentally investigated by Göttlich et al. [A-1]. The coolant was injected from a row of innovative geometry holes near the blade leading edge. They measured the adiabatic film effectiveness on the suction side of a blade in a linear cascade, and they concluded that the oblique shock impingement from the adjacent blade trailing edge does not significantly affect the leading edge film cooling effectiveness. Ochs et al. [A-2] used a contoured plate and curved surface to simulate shock impingement at turbine cascade exit. According to their observation, when the injection is far upstream, the shock effect on the adiabatic film effectiveness is secondary. However, the shock effect on heat transfer coefficient is obvious. The heat transfer coefficient decreases at the shock position, and suddenly rises up by 25%, after the flow crosses the shock. The CFD study by Luchi et al. [A-3] simulated some of the conditions in Ochs et al.'s experiment. The CFD result confirmed with the observation in the experiment, and provided detail view of the shock/film cooling interaction in the experimental study.

Upstream shock wave passing effect on film cooling

Another pattern of shock/film cooling interaction occurs near the turbine blade leading edge. The shock wave, generated at the trailing edge of the upstream NGV, will propagate through the rotor blade passage. When the shock wave passes the film cooling injection, it will have some influence on the local flow status, heat transfer, and film cooling performance. Experimentally studies on this kind of shock/film cooling interaction have been performed by Johnson et al. [A-4], Rigby et al. [A-5], Popp et al. [A-6], and smith et al. [A-7]. In these studies, the shock wave was generated by a shock tube, and pass through a linear blade cascade, to simulate the relative motion due to the blade rotation in the real engine. The general conclusion drawn in these studies is that increase of heat flux at the shock impingement is caused by the increase of recovery temperature due to shock heating, and the shockdoes not have an observable effect on the heat transfer coefficient or the adiabatic effectiveness.

Film cooling injection in the supersonic/hypersonic flow

Film cooling has been adopted to provide thermal protection for the supersonic and hypersonic vehicles. When the coolant is directly injected into the supersonic/hypersonic mainstream the film injection generates either shock wave or expansion waves, depends on the injection angle and injection velocity. May studied had been reported on this pattern of shock effect.

K. A. Juhany and M. L. Hunt in California Institute of Technology carried out an experimental study on the interaction between a tangential slot injection and a two dimensional shock [A-8]. The coolant was injected at two different Mach numbers, 1.3 and 2.2, into a mainstream of Mach number 2.4. They found that when the tangential injection Mach number is large, it adds momentum into the boundary layer, and helps to prevent the shock caused separation. When the shock is too strong, and the coolant is separated by the high reversed pressure gradient the recovery temperature decreases rapidly downstream. However, without separation, the shock seems has small effect on the recovery temperature.

T. Kanda et al. [A-9] [A-10] did similar experiment on the film cooling injection into supersonic flow. According to their observation, the weak shock, with pressure ratio of 1.2, does not impact the film cooling effectiveness. The stronger shock, with pressure ratio of 1.44, made a decrease of the film cooling effectiveness. They ascribed the film cooling effectiveness decrease

to the shock heating. They also observed a momentum transfer from the mainstream to the coolant in the interaction region.

K. Takita and G. Masuya from Tohoku University did numerical study on the tangential injection into a supersonic flow [A-11] [A-12]. A low Reynolds number k-ε turbulent model was employed to count in the eddy viscosity when the separation occurs. They concluded that the shock impingement does significantly change the thickness of the mixing layer of the coolant and the main flow. However, the turbulence kinetic energy was doubled after the shock. The decrease of film cooling effectiveness is due to the Mach number drop at the shock. The injection Mach number increase mitigates the shock compromising on the film cooling effectiveness.

In the experimental investigations by Ligrani et al. [A-13] and M. Gritsch et al. [A-14], the coolant was injection from discrete cylindrical holes into the supersonic main flow with an inclination angle of 30 degree. No shock generator was employed, and the shock wave develops in the immediate vicinity of the film-cooling holes. They observed an increased film cooling effectiveness in the near hole region. They attributed this to the pressure gradient at an oblique shock forcing a larger concentration of coolant to the surface.

K.A. Heufer, H. Olivier [A-15] tested the film cooling in hypersonic flow on a wedge model. They concluded that within a certain limit, the blowing ratio increase will improve the film cooling effectiveness. Reducing of the inclination angle increases the limit of blowing ratio.

The CFD investigation carried out by Zhang and Hassan [A-16] simulates film cooling on a supersonic air profile, which was experimentally studied by Furukawa, and Ligrani [A-17]. The coolant was injected at the location where local Mach number is close to units. It was found, when the blowing ratio is above 2.0, the oblique shock detaches from the injection hole leading edge, and the film cooling effectiveness dramatically decreases. A coolant-blockage and shaped-wedge similarity was proposed to explain their observation.

References

[A-1] Göttlich, E., Lang, H., Sanz, W., Woisetschläger, J., 2002, “Experimental Investigation of an Innovative Cooling System (ICS) for High Temperature Transonic Turbine Stages”. *ASME TURBO EXPO 2002*, Amsterdam, Netherlands, GT-2002-30341.

[A-2] Ochs, M., Schulz, A., Bauer, H., 2007, “Investigation of The Influence of Trailing Edge Shock Waves on Film Cooling Performance of Gas Turbine Airfoil”. *ASME Turbo Expo 2007*, Montreal, Canada, GT2007-27482.

[A-3] Luchi, R., Salvadori, S., Martelli, F., 2008, “Heat Transfer Prediction of Film Cooling in Supersonic Flow”. *Numerical Analysis and Applied Mathematics, International Conference 2008*.

[A-4] Johnson, A. B., Rigby, M. J., Oldfield, M. L. G., Ainsworth, R. W., Oliver, M. J., 1989, “Surface Heat Transfer Fluctuations on a Turbine Rotor Blade Due to Upstream Shock Wave Passing”. *ASME Journal of Turbomachinery*, Vol. 111, pp. 105-115.

[A-5] Rigby, M. J., Johnson, A. B., Oldfield, M. L. G., 1990, "Gas Turbine Rotor Blade Film Cooling With and Without Simulated NGV Shock Waves and Wakes". *ASME Gas Turbine and Aeroengine Congress and Exposition*, 1990, Brussels, Belgium, 90-GT-78.

[A-6] Popp, O., Smith, D. E., Bubb, J. V., Grabowski, H. C. III, Diller, T. E., Schetz, J. A., Ng, W. F., 2000, “Investigation of Heat Transfer in a Film Cooled Transonic Turbine Cascade, Part II: Unsteady Heat Transfer”. *ASME TURBOEXPO 2000*, Munich Germany, 2000-GT-203.

[A-7] Smith, A. C., Nix, A. C., Diller, T. E., Ng, W. F., 2003, “The Unsteady Effect of Passing Shock on Pressure Surface Versus Suction Surface Heat Transfer in Film-Cooled Transonic Turbine Blades”. *ASME TURBO EXPO 2003*, Atlanta, Georgia, GT2003-38530.

[A-8] Juhany, K. A. and Hunt, M. L., 1994, “Flowfield Measurements in Supersonic Film Cooling Including the Effect of Shock-Wave Interaction”. *AIAA JOURNAL*, Vol. 32, No. 3, pp 578-585.

[A-9] Takeshi, K., Fumiei, O., Masahiro T., Toshihito S. and Yoshio W., 1996, “Experimental Studies of Supersonic Film Cooling with Shock Wave Interaction”. *AIAA JOURNAL*, Vol. 34, No. 2, pp 265-271.

[A-10] Takeshi, K. and Fumiei, O., 1997, “Experimental Studies of Supersonic Film Cooling with Shock Wave Interaction (II)”. *J. THERMOPHYSICS*, VOL. 11, NO. 4, pp 590-592.

[A-11] Takita, K. and Masuya, G., 1999, “Effects of Shock Wave Impingement on Supersonic Film Cooling”. *AIAA J. SPACECRAFT*, Vol. 36, No. 4, pp 602-604.

[A-12] Takita, K. and Masuya, G., 2000, “Effects of Combustion and Shock Impingement on Supersonic Film Cooling by Hydrogen”. *AIAA JOURNAL*, Vol. 38, No. 10, pp 1899-1906.

[A-13] Ligrani, P. M., Saumweber, C., Schulz, A., Wittig, S., 2001, “Shock Wave–Film Cooling Interactions in Transonic Flows”. *ASME Journal of Turbomachinery*, Vol. 123, pp 788-797.

[A-14] Gritsch, M., Schulz, A., and Wittig, S., 1998, "Adiabatic Wall Effectiveness Measurements of Film-Cooling Holes With Expanded Exits," ASME J. Turbomach., 120, pp. 549–556.

[A-15] Heufer, K.A. and Olivier, H., 2006, "Film Cooling for Hypersonic Flow Condictions". *Proceedings 5th European Workshop on Thermal Protection Systems and Hot Structures Noordwijk*, The Netherlands, 17 - 19 May 2006.

[A-16] Zhang, C. X., and Hassan, I. G. , 2009, "Computational Study of the Effects of Shock Waves on Film Cooling Effectiveness". *ASME Turbo Expo 2009*, Orlando, Florida, GT2009-59279.

[A-17] Furukawa, T., and Ligrani, P., 2002, "Transonic Film Cooling Effectiveness From Shaped Holes on a Simulated Turbine Airfoil," J. Thermophys. Heat Transfer, 16, pp. 228–237.

Appendix B. Film Cooling System of Fan-Shaped Hole Injected Blade

The setup and operation of the film cooling system in the fan-shaped hole film cooling experiment are presented in Appendix B.

Film Cooling System Setup and Operation

The film cooling system used in the fan-shaped hole film cooling experiment is an upgrade of the one used by Nasir *et al.* [B-1] for the showerhead cooled vane. The schematic diagram of the cooling system is provided in Figure B.1. The coolant for the fan-shaped hole injection is compressed air from a storage tank. The air is first compressed by a 5-hp Ingersoll-Rand compressor located outside of the wind tunnel lab. The compressed air is then dried below four percent relative humidity, and stored in the storage tank inside the laboratory. The tank is charged to a pressure of 120 psi before the test to provide adequate pressure and coolant mass flow for the 3 rows of coolant injection. Since the tank volume is very large compared to the mass flow, the tank pressure drop due to the "blow-down" effect during a tunnel run is ignorable. After the on/off valve the pipe is split into three branches to feed one row of fan-shaped hole on the blade suction side and two rows of fan-shaped hole injections on the blade pressure side respectively. The flow rates of the three branches are regulated by three bowl valves, and are measured by three orifice meters at the downstream of the bowl valves. It has been tested, during the tunnel run, the flow rate of the three branches can be set by the bowl valves separately with ignorable correlations. After the orifice meter the air then flows through a copper coil immersed in a heat exchanger. For the ambient coolant tests, the heat exchanger is empty. For the chilled coolant tests, the heat exchanger is filled with liquid nitrogen. After passing through the heat exchanger, the air flows into the 3 plenums in the blade via fittings designed to pass air through the test section window, as shown in Figure B.2. The total and static pressure of each plenum are measured by Pitot-probes at the plenum inlet. Thermocouple probes sticks in from the other side of the test section to record the coolant temperature in the plenum. Air flows through the blade plenums and then ejects through the fan-shaped holes.

The on/off valve at the tank exit is a Solenoid valve. When the wind tunnel mainstream is blowing down, the Solenoid valve will be triggered to open, to guarantee the coolant injection and the mainstream flow start at the same moment.

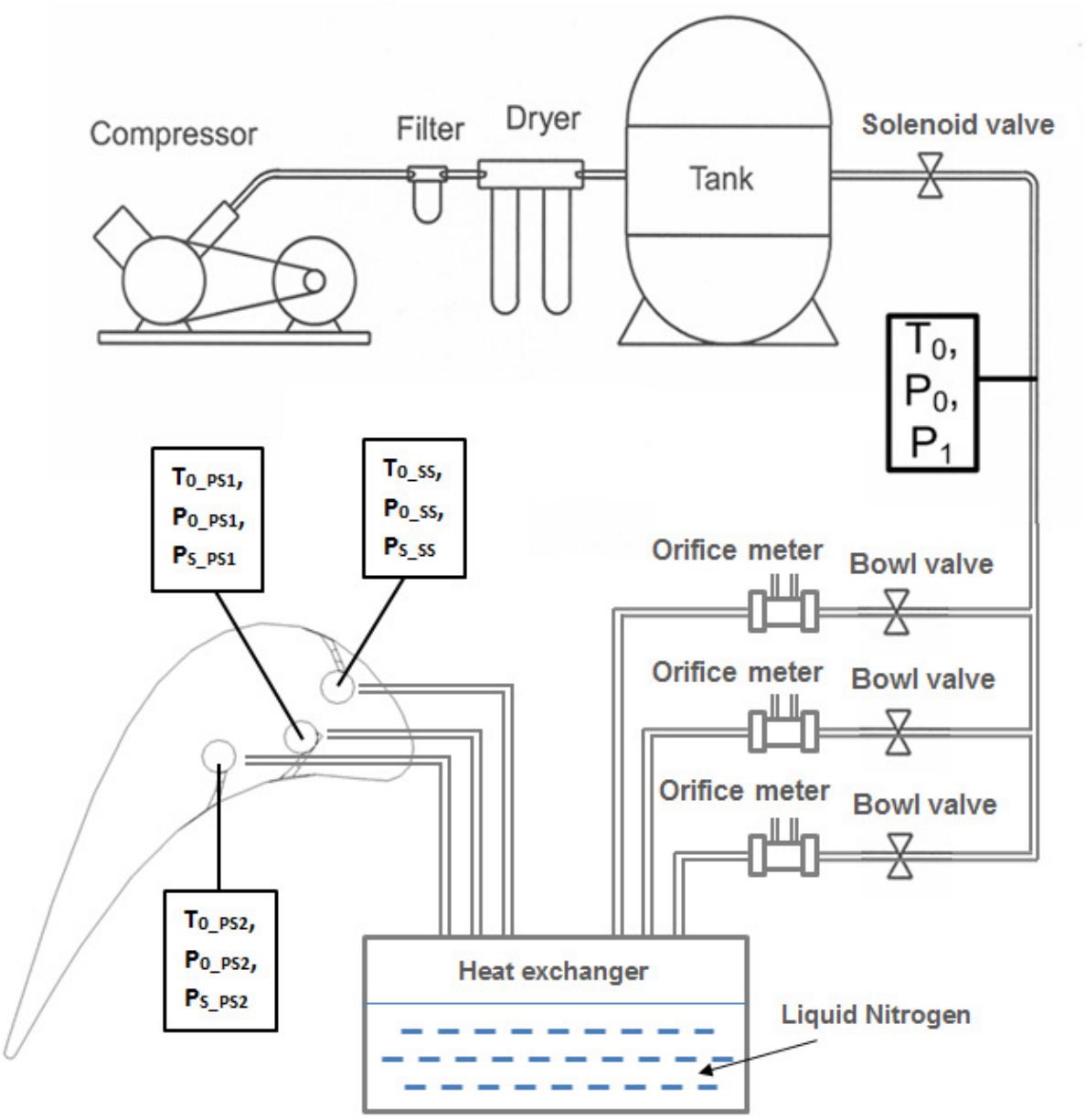

Figure B.1. Film cooling system schematic

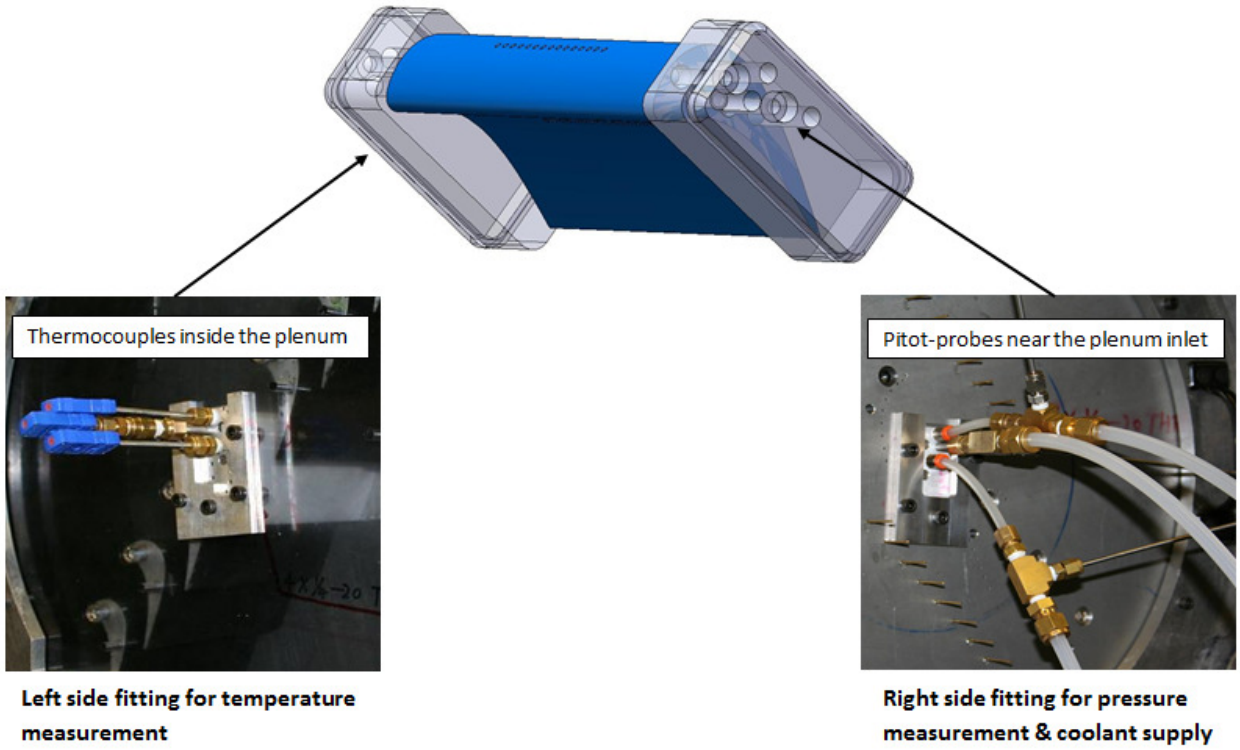

Figure B.2. Coolant supply & measurement fittings

Measurements and Calculations

In present experiment the film cooling blowing ratio is determined by the following equation:

$$BR = \frac{\rho_c U_c}{\rho_\infty U_\infty} = \frac{C_d P_{t,c}}{\rho_\infty U_\infty}\left(\frac{P_{\infty,s}}{P_{t,c}}\right)^{\frac{\gamma+1}{2\gamma}}\sqrt{\frac{2\gamma}{(\gamma-1)RT_{t,c}}\left[\left(\frac{P_{t,c}}{P_{\infty,s}}\right)^{\frac{\gamma-1}{\gamma}}-1\right]} \qquad \text{(B-1)}$$

where $\rho_\infty U_\infty$ and $P_{\infty,s}$ are the status of the mainstream in the blade cascade. Their values are calculated based on the solid blade surface pressure measurement by Carullo et al. [B-2]; C_d is the discharge coefficient tested as 0.82 for the current fan-shaped hole; $P_{t,c}$ and $T_{t,c}$ is the total pressure and total temperature of the coolant, which are measured at the plenum inlet by the Pitot-static probes and T-type thermocouples, as shown in Figure B. 2.

References

[B-1] Nasir, S., 2008, “Showerhead Film Cooling Performance of Turbine Vane at High Freestream Turbulence in a Transonic Cascade”. (Doctoral dissertation) Retrieved from ETD@VT (Accession Order etd-08072008-211337).

[B-2] Carullo, J. S., Nasir, S., Cress, R.D., Ng, W.F., Thole, K.A., Zhang, L., and Moon, H. K., 2007, "The Effects of Freestream Turbulence, Turbulence Length Scale, and Exit Reynolds Number on Turbine Blade Heat Transfer in a Transonic Cascade," IGTI Turbo Expo 2007, Montreal, GT2007-27859.

Appendix C. Instrumentation and data processing of Thin Film Gauge

Thin Film Gauge Mounting on film cooled blade

In the film cooling experimental study, the blade surface temperature was recorded by platinum Thin Film Gauges (TFG). The gages were manufactured by Air Force Research Lab using the method described by Joe [C-1], with a similar design as the Oxford gages of Doorly and Oldfield [C-2]. Each thin film gauge uses a platinum sensor approximately 2.8 mm (0.11 in.) long attached to copper leads. The electric resistance of the platinum sensor changes with temperature and provides a high frequency response with high spatial resolution between gauges. The TFGs are sputtered onto a Kapton sheet (k = 0.12 W/mK) with a 50 µm thickness, plus an approximately 20 µm thickness of the backing adhesive. During the process of instrumentation and test operation, a few gauges were damaged. There are 15 gauges provides valid data in the final result. 11 gauges was located on the SS, from s/c= 0.42 to s/c= 1.29, and 4 gauges are located on the PS, with one in between of the two rows of injection at s/c= -0.36 (negative value indicates surface distance from leading edge on PS), and the rest 3 gauges are located from s/c= -0.5 to s/c= -0.64. Figure C. 1. shows the locations of the gauges on the blade profile. Figure C. 2. shows the snapshot of the film cooled blade with TFG instrumented on its surface.

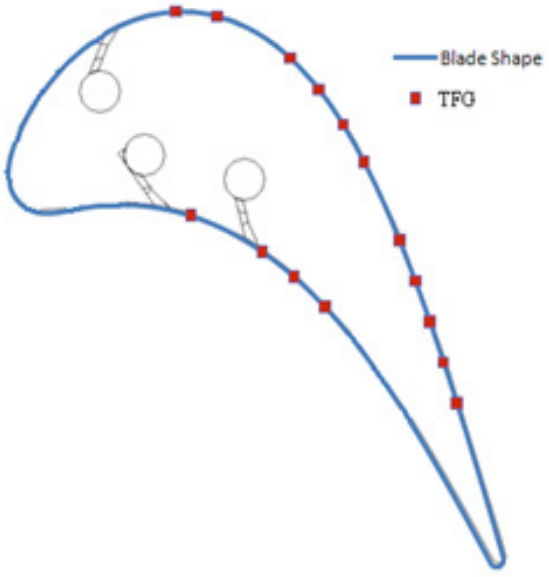

Figure C. 1. TFG location on blade profile

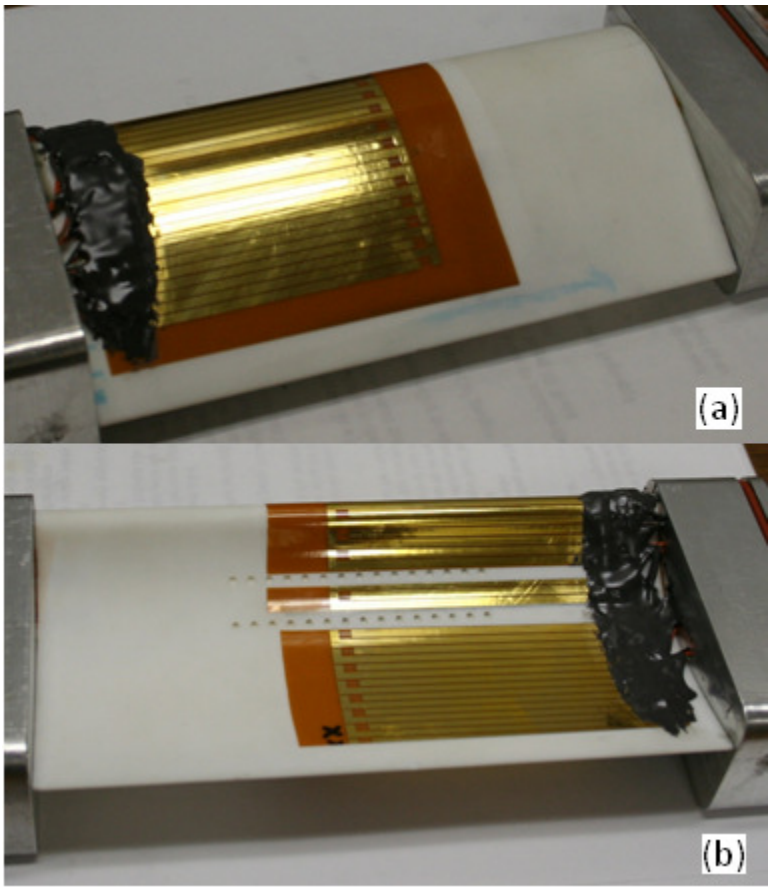

Figure C. 2. Film cooled blade with TFG instrumented on. (a) SS surface; (b) PS surface.

Thin Film Gauge Calibration

The temperature and electric resistance of the TFGs follow a linear relationship. The gages were calibrated in an incubator over the range of temperatures encountered during a tunnel test. The calibration procedure consisted of increasing the incubator temperature in five steps from ambient temperature up to ~71°C and four steps decreasing the incubator temperature back to ambient. The temperature and the resistance of each gauge were recorded at each step. Typically, it takes 2 hours before the incubator reach a steady temperature and to ensure that the blade was thermally soaked. Calibration points were recorded as the temperature increased and decreased to eliminate the effect of the gauge hysteresis. The calibration fit for one of the gauges is provided in Figure C. 3.

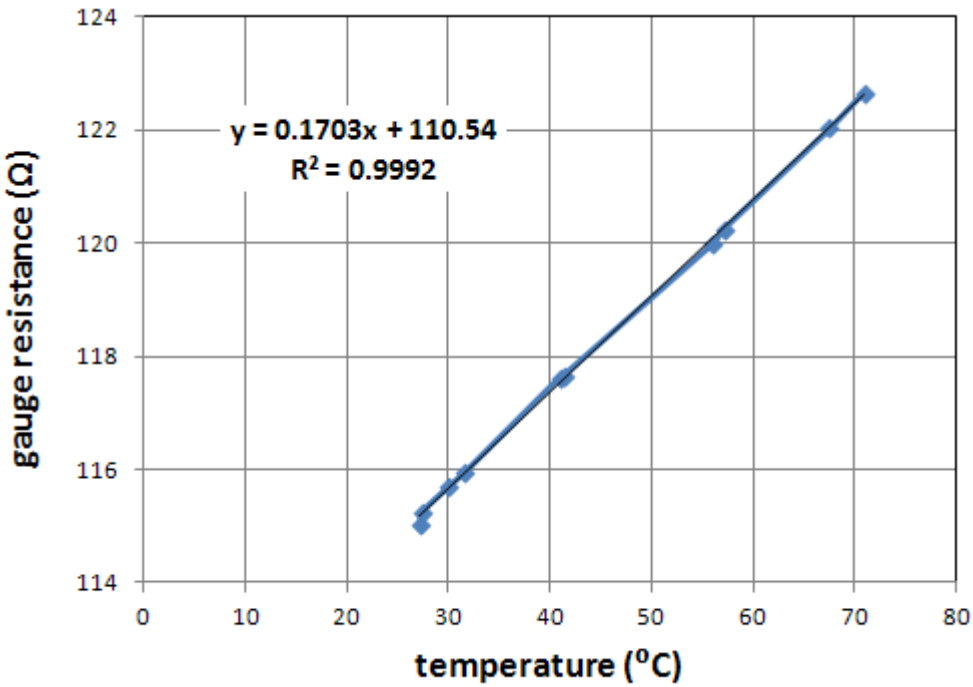

Figure C. 3. Calibration sample of the Thin Film Gauges

In the data acquisition circuit, each thin film gauge acts as one arm of an individual Wheatstone bridge. The constant current supplied by the balanced Wheatstone bridge circuit converts the resistance changes of the TFG into a voltage change that can be recorded by National Instruments (NI) data acquisition system. The surface temperature history is calculated from the time resolved voltage. Figure C. 4. provides a schematic of the Wheatstone bridge circuit of the thin film gauges.

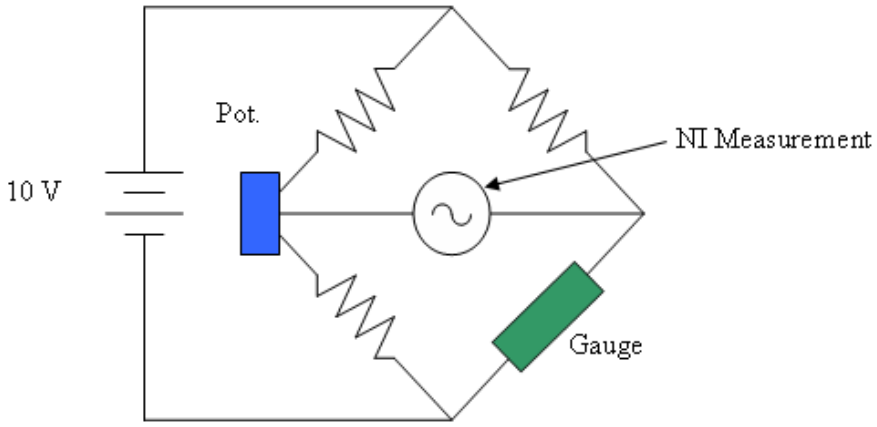

Figure C. 4. Wheatstone bridge circuit for the thin film gauges

Thin Film Gauge Single Acquisition

The thin film gauge voltages were recorded using NI SCXI-1600 data acquisition system. The voltage single from the Wheatstone bridge circuits were sampled at 1 kHz and for 30 seconds during the tunnel run. The data acquisition system consisted of a SCXI-1001 chassis and SCXI-1120 isolation amplifiers. The voltage signals below 4 Hz or above10 kHz were filtered. The amplification gain was set as 500. Each isolation amplifier was connected to the Wheatstone bridge through a SCXI-1320 terminal block.

TFG Width Effect on Adiabatic Effectiveness data

The gages were instrumented at the midspan of the blade, so that they all follow the centerline of one of the fan-shaped holes. Since the each of the TFG has a width of 2.8 mm (3.5 times of the injection hole inlet diameter), the gauge response may convey a spanwise average temperature within the TFG width, instead of the real centerline temperature. The CFD results may provide an insight of how does the lateral averaging by the width of the gauges quantitatively affect the final result of adiabatic effectiveness. Figure C. 5. shows the comparison of CFD adiabatic effectiveness between the centerline and the spanwise average within the TFG width. The lateral average value is much lower than the centerline value in the near hole region, because the kidney vortices in this region slightly lift the cooling flow away from the surface, and the cooling flow has not diffused laterally. After the near hole region, the average value then ramp back to the same level as the centerline effectiveness due to lateral diffusion of the cooling flow. The centerline and the lateral average effectiveness converge faster on the PS than that on the SS. This is because the concave surface accelerates the cooling flow diffusion, whereas the convex surface reduces the diffusion.

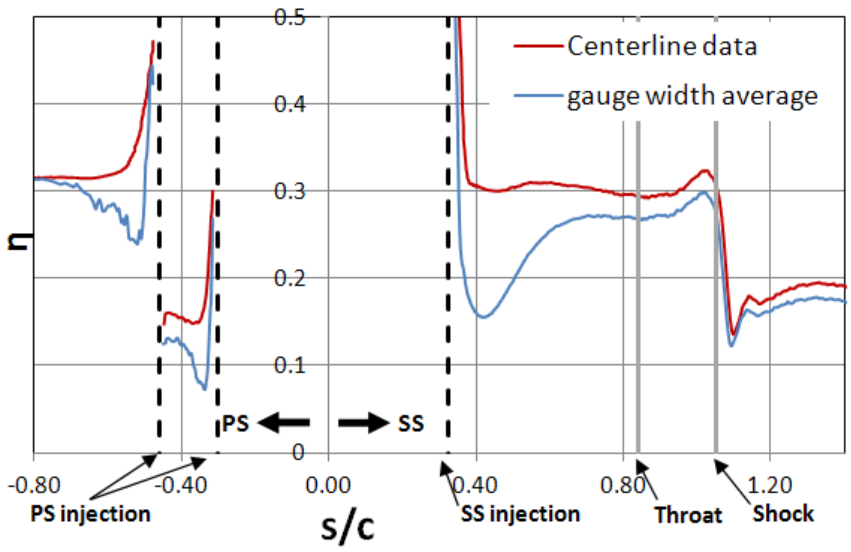

Figure C. 5. The CFD results of adiabatic effectiveness - a comparison between centerline data and the lateral average in the range of gauge width.

References

[C-1] Joe, C. R., 1997, "Unsteady Heat Transfer on the Turbine Research Facility at Wright Laboratory," Ph.D. Dissertation, Syracuse University.

[C-2] Doorly, J.E., Oldfield, M. L. G., 1987, "The Theory of Advanced Multi-Layer Thin Film Heat Transfer Gages," Int. J. Heat and Mass Transfer, 30, p. 1159–1168.

Appendix D. Data Reduction – Film Cooling Measurements

The data reduction process to estimate the heat transfer coefficient $\boldsymbol{h}$ and adiabatic effectiveness $\boldsymbol{\eta}$ for the film cooled vane and blade measurements is presented in Appendix D.

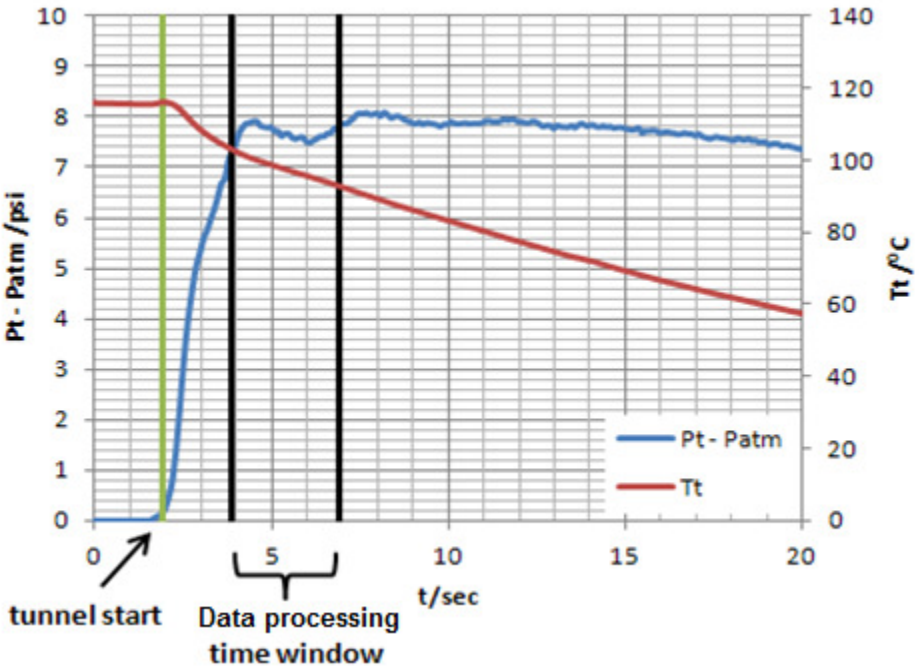

Figure D.1. Time history of upstream total pressure and total temperature

Figure D.1. shows the time history of upstream total temperature and total pressure. The thermal and aerodynamic data was recorded during the entire wind tunnel run. However, a 1-D semi-infinite model was adopted for the data reduction process. For the validity of the 1-D semi-infinite assumption, the data for the linear regression process begins at 2 seconds after the tunnel start, and lasts 3 seconds.

The test blade was made of a special ceramic glass, known as Macor ®, which has low thermal conductivity (k=1.46 W/mºC). A 1-D assumption of surface heat flux (eq. 1) is valid on the test blade during the data processing time window. A finite difference code developed by Cress [D-1] was employed to calculate heat flux from the beginning of the wind tunnel run. Figure D. 2. shows a simple of the surface temperature history, recorded by the TFG, and the surface heat flux history during a tunnel run.

$$\frac{\partial^2 T}{\partial y^2} = \frac{1}{\alpha}\frac{\partial T}{\partial t} \tag{D-1}$$

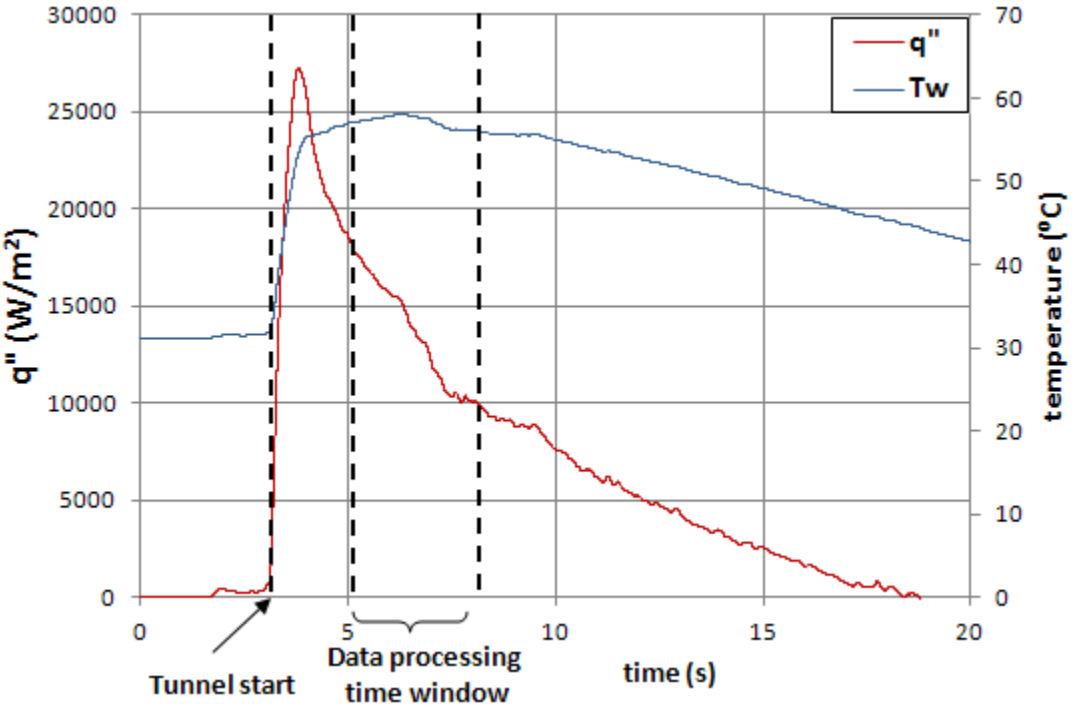

Figure D. 2. a simple of the surface temperature and heat flux time history

Method developed by Popp *et al.* [D-2] was used to determine the heat transfer coefficient and film cooling effectiveness. This method starts with the fundamental convective heat transfer equation

$$q" = h(T_{aw} - T_w) \tag{D-2}$$

The adiabatic effectiveness (non-dimensionalized adiabatic wall temperature) is defined as

$$\eta = \frac{T_{aw} - T_r}{T_c - T_r} \tag{D-3}$$

where T_r is the recovery temperature, which is determined by the assumed recovery factor ($\sqrt[3]{Pr}$) and the local Mach number.

Combining Equations D-2 and D-3 yields a linear expression of the relationship between heat flux and adiabatic effectiveness in the form of $\boldsymbol{y = mx + b}$.

$$\frac{q''}{T_r - T_c} = h\left(\frac{T_r - T_w}{T_r - T_c}\right) - h \cdot \eta \qquad \text{(D-4)}$$

To reduce the uncertainty a dual-data-regression method was employed in data reduction. For this technique, two runs are performed at identical mainstream flow conditions and blowing ratio but with different coolant temperatures. This technique reduces uncertainty by increasing the number of data points used for regression and adding points closer to the x-axis, reducing the distance the line fit is extrapolated to calculate effectiveness. Figure D. 2. shows the double linear regression technique performed on a sample data set, with heat transfer coefficient and film effectiveness highlighted.

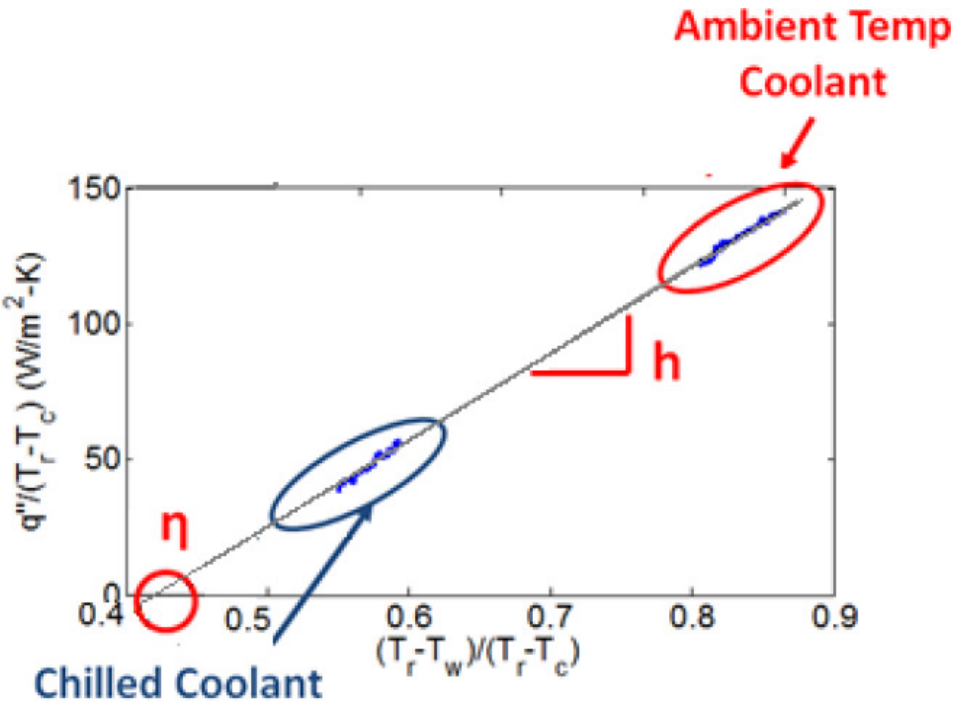

Figure D.3. Dual-data regression line fit

When using chilled coolant, the coolant to mainstream density ratio changes from the room temperature case. In general, the density ratio of chilled coolant is about 7% ~ 15% higher than that of the room temperature coolant. Ekkad et al. [D-3] have shown, for higher blowing ratios (BR>1), increasing of coolant density within a certain range showed no appreciable effect on film effectiveness distributions. Based on this information, film effectiveness distributions from the present study should not be affected by using two coolant temperatures as all cases considered are at BR>1.

The heat transfer coefficient will be non-dimensionalized as Nusselt number, defined in Equation D-5.

$$Nu = \frac{h \cdot C}{k_a} \tag{D-5}$$

Where k_a is the heat conductivity of air. C is the true chord of the blade.

References

[D-1] Cress, R.D., 2006, "Turbine Blade Heat Transfer Measurements in a Transonic Flow Using Thin film Gages," Master's Thesis, Virginia Polytechnic Institute and State University.

[D-2] Popp, O., Smith, D. E., Bubb, J. V., Grabowski, H. C., Diller, T. E. Schetz, J. A., Ng. W. F., 2000, "An Investigation of Heat Transfer in a Film Cooled Transonic Turbine Cascade, Part II: Unsteady Heat Transfer," IGTI Turbo Expo, Berlin, GT-2000-203.

[D-3] Ekkad, S. V., Han, J. C., Du, H., 1998, "Detailed Film Cooling Measurements on a Cylindrical Leading Edge Model: Effect of Free-Stream Turbulence and Coolant Density," ASME J. Turbomachinery, 120, pp. 799-807.

Appendix E. Uncertainty Analysis – Film Cooling Measurements

The methods used to estimate the uncertainty in heat transfer coefficient $\boldsymbol{h}$ and adiabatic effectiveness $\boldsymbol{\eta}$ for the film cooled vane and blade measurements are present in Appendix E.

Overview of the uncertainty propagation in the film cooling measurement

Figure E.1. shows the propagation of the major uncertainties in the film cooling measurement. The uncertainty of surface temperature $\boldsymbol{T_W}$ first comes from the calibration and the TFG resistance reading. The uncertainty of $\boldsymbol{T_W}$ propagates to the surface heat flux $\boldsymbol{q_W}$ through the calculation by the finite difference code. The uncertainty of the $\boldsymbol{x}$ and $\boldsymbol{y}$ coordinates used in the linear regression process come from the uncertainty of heat flux $\boldsymbol{q_W}$, recovery temperature $\boldsymbol{T_r}$, surface temperature $\boldsymbol{T_W}$, and coolant temperature $\boldsymbol{T_c}$. Then, the errors in $\boldsymbol{x}$ and $\boldsymbol{y}$ coordinates propagate to the heat transfer coefficient $\boldsymbol{h}$ and adiabatic effectiveness $\boldsymbol{\eta}$ through the dual-data linear regression process, and the extra uncertainty in this process comes from the blowing ratio error.

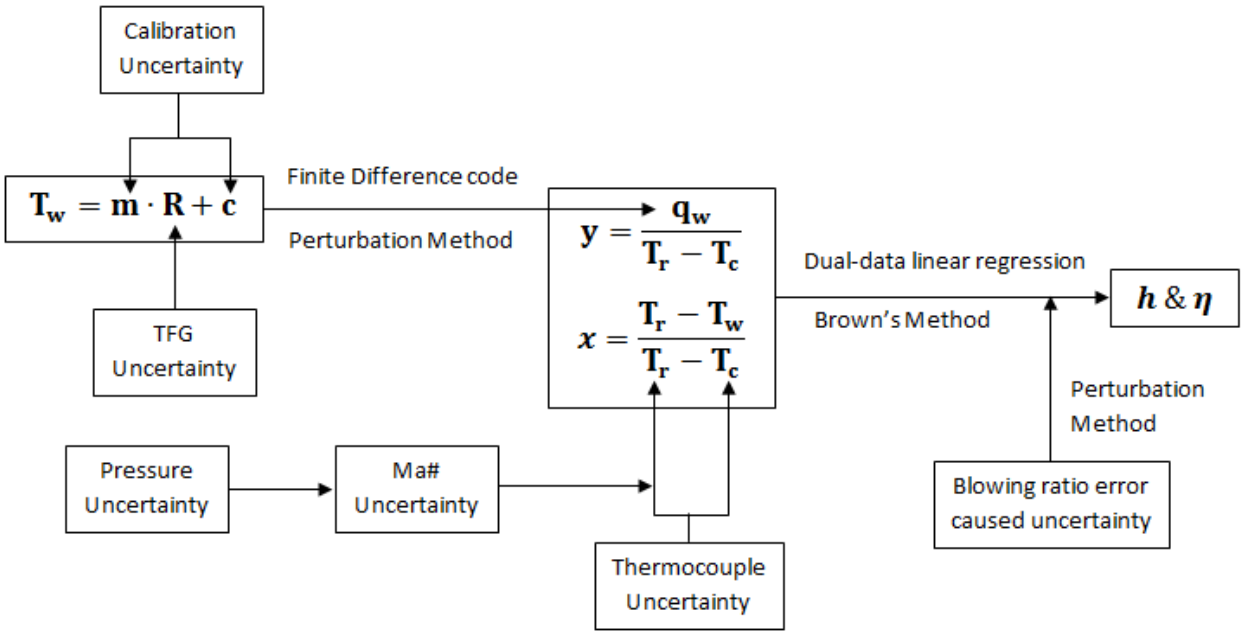

Figure E.1. Scheme of uncertainty propagation in film cooling measurement

Uncertainty propagation in the linear regression method

As discussed in appendix D, $\boldsymbol{h}$ and $\boldsymbol{\eta}$ were determined thought the dual-data linear regression method. In this method the ambient and chill cooling tests data was plot together, as

shown in Figure D.2. $\boldsymbol{h}$ and $\boldsymbol{\eta}$ were determined as the slope and x-intercept of the least-squares line fit of the x and y coordinates. Both *x* and *y* coordinates of each data point have precision and bias uncertainty. The precision uncertainty is a limit of the repeatability precision, which is caused by random errors, unsteadiness, and inability to reset the experimental conditions exactly. The bias uncertainty is the constant error for the setup of measurements, which is due to the calibration error, material properties error, and errors in the data acquisition process. Since the surface heat flux was computed through a 1-D finite difference code, there is no explicit equation to bridges the row temperature data and the *x* and *y* coordinates. The bias uncertainties for the *x* and *y* coordinate were determined through the perturbation method described by Moffat [E-1]. In the perturbation method, first, the uncertainty of each input parameters of the finite different code was collected. Then, to track the uncertainty propagation in the 1-D finite difference code, the inputs are adjusted by adding the uncertainty (±) to the original value of ach parameter. By running the finite difference code with the adjusted inputs once at a time, and leave the rest of the parameters as original, the errors on *x* and *y* coordinate from the uncertainty of each input parameter can be determined. The final result of the *x* and *y* coordinate uncertainty can be estimated by combining the errors caused by each of the inputs' uncertainties through the root-sum-square calculation.

Once the uncertainty in *x* and *y* coordinates are determined, the Brown *et al.*'s [E-2] method can be used to determine the uncertainty that propagates in the linear regression. According to Brown *et al.* [E-2], ignoring the correlation between the input parameters, the form of the expression for the uncertainty in the slope of line, *m*, is:

$$U_m^2 = \sum_{i=1}^{N}\left(\frac{\partial m}{\partial Y_i}\right)^2 P_{Y_i}^2 + \sum_{i=1}^{N}\left(\frac{\partial m}{\partial X_i}\right)^2 P_{X_i}^2 + \sum_{i=1}^{N}\left(\frac{\partial m}{\partial Y_i}\right)^2 B_{Y_i}^2 + \sum_{i=1}^{N}\left(\frac{\partial m}{\partial X_i}\right)^2 B_{X_i}^2 \tag{E-1}$$

Similar for the uncertainty in the y-intercept, *c*, is

$$U_c^2 = \sum_{i=1}^{N}\left(\frac{\partial c}{\partial Y_i}\right)^2 P_{Y_i}^2 + \sum_{i=1}^{N}\left(\frac{\partial c}{\partial X_i}\right)^2 P_{X_i}^2 + \sum_{i=1}^{N}\left(\frac{\partial c}{\partial Y_i}\right)^2 B_{Y_i}^2 + \sum_{i=1}^{N}\left(\frac{\partial c}{\partial X_i}\right)^2 B_{X_i}^2 \tag{E-2}$$

The partial derivatives are

$$\frac{\partial m}{\partial Y_i} = \frac{NX_i - \sum_{i=1}^{N} X_i}{N\sum_{i=1}^{N}\left(X_i^2\right) - \left(\sum_{i=1}^{N} X_i\right)^2} \tag{E-3}$$

$$\frac{\partial c}{\partial Y_i} = \frac{\sum_{i=1}^{N}\left(X_i^2\right) - X_i\sum_{i=1}^{N} X_i}{N\sum_{i=1}^{N}\left(X_i^2\right) - \left(\sum_{i=1}^{N} X_i\right)^2} \tag{E-4}$$

$$\frac{\partial m}{\partial X_i} = \frac{NY_i - \sum_{i=1}^{N} Y_i}{N\sum_{i=1}^{N}\left(X_i^2\right) - \left(\sum_{i=1}^{N} X_i\right)^2} - \frac{\left(N\sum_{i=1}^{N} X_iY_i - \sum_{i=1}^{N} X_i\sum_{i=1}^{N} Y_i\right)\left(2NX_i - 2\sum_{i=1}^{N} X_i\right)}{\left(N\sum_{i=1}^{N}\left(X_i^2\right) - \left(\sum_{i=1}^{N} X_i\right)^2\right)^2} \tag{E-5}$$

and

$$\frac{\partial c}{\partial X_i} = \frac{2X_i\sum_{i=1}^{N} Y_i - \sum_{i=1}^{N} X_iY_i - Y_i\sum_{i=1}^{N} X_i}{N\sum_{i=1}^{N}\left(X_i^2\right) - \left(\sum_{i=1}^{N} X_i\right)^2} - \frac{\left(\sum_{i=1}^{N}(X_i)^2\sum_{i=1}^{N} Y_i - \sum_{i=1}^{N} X_i\sum_{i=1}^{N} X_iY_i\right)\left(2NX_i - 2\sum_{i=1}^{N} X_i\right)}{\left(N\sum_{i=1}^{N}\left(X_i^2\right) - \left(\sum_{i=1}^{N} X_i\right)^2\right)^2} \tag{E-6}$$

where

B = bias limit

B_{ik} = covariance estimator

c = y-intercept of line

m = slope of line (h)

N = number of data points

P = precision limit

U = uncertainty interval

X = independent variable

Y = dependent variable

The uncertainty interval for the x-intercept (η) is

$$U_{\eta}^{2} = U_{m}^{2} + U_{c}^{2} \tag{E-7}$$

Uncertainty in heat transfer coefficient and film cooling effectiveness are represented by the uncertainty in the linear regression's slope and x-intercept respectively.

A Sample of the uncertainty analysis result

Uncertainties in the exit Mach number (M_{ex}), density ratio (DR), and blowing ratio (BR) were determined within the 95% confidence interval. The overall average uncertainty values for final results are shown in Table E. 1. The overall average uncertainty of $\boldsymbol{h}$ was determined to be ± 8%, and the overall average uncertainty in $\boldsymbol{\eta}$ is ± 0.08. A sample of data recorded on the film cooled blade at exit Mach number 0.84 with low blowing ratio are plotted with the uncertainty band for heat transfer coefficient in terms of Nusselt number in Figures E. 2, and adiabatic effectiveness in Figure E. 3.

Table E. 1. Uncertainty values

Value	Average Uncertainty
q''	±7.6%
T_r	±3°C
h	±8.0%
η	±0.08
M_{ex}	±1.3%
DR	±0.8%
BR	±2.8%

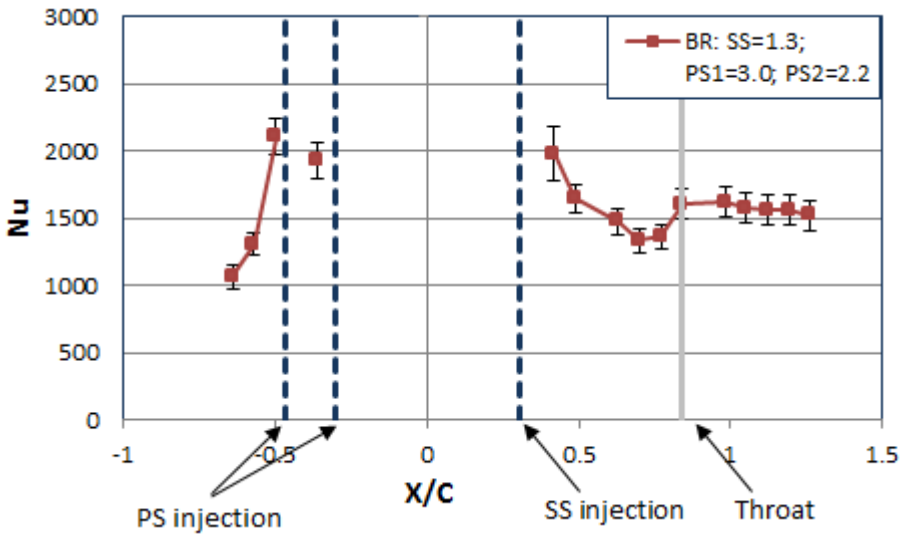

Figure E.2. Film cooled blade surface Nusselt number distribution with uncertainty band. (Exit Mach number 0.84, Low Blowing Ratio)

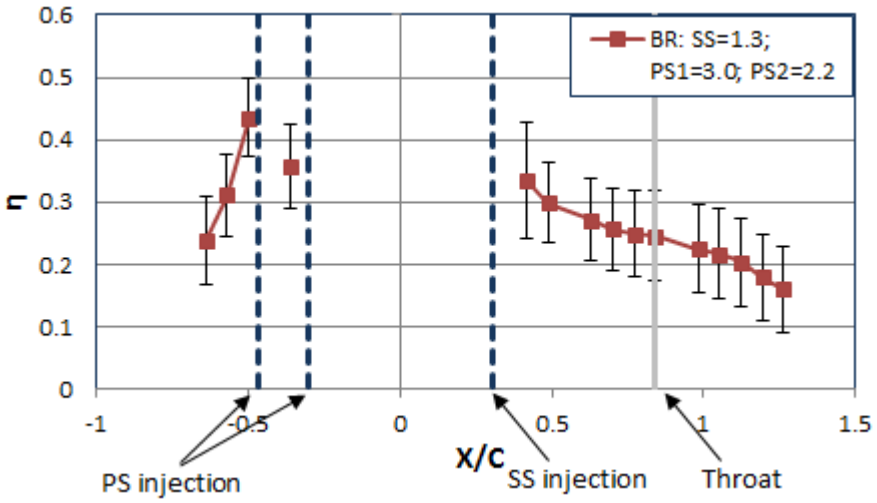

Figure E.3. Film cooled blade surface adiabatic effectiveness distribution with uncertainty band. (Exit Mach number 0.84, Low Blowing Ratio)

References

[E-1] Moffat, R. J., 1988, "Describing Uncertainties in Experimental Results," *Exp. Thermal and Fluid Science*, 1, pp. 3-17.

[E-2] Brown, K. H., Coleman, H. W., and Steele, W. G., 1995, “Estimating Uncertainty Intervals for Linear Regression,” AIAA-1995-0796.

Appendix F. Tabulated Result – Fans-Shaped Hole Cooled Blade

The entire set of tabulated result of the fan-shaped hole film cooled blade experiment is present in Appendix F.

Table F. 1. Matrix of test conditions

Inlet Tu	Exit Ma#	Exit Re#	Nominal BR	BR_SS	BR_PS1	BR_PS2
12%	0.67	$8.1X10^5$	High BR	1.6	4.0	3.1
			Low BR	1.1	2.7	2.2
	0.84	$1.08\ X10^6$	High BR	1.6	3.7	2.8
			Low BR	1.3	3.0	2.2
	1.01	$1.42X10^6$	High BR	1.5	3.8	2.9
			Low BR	1.2	2.9	2.4

Table F. 2. Data set of film cooing test at Ma#0.67

Ma# 0.67	x/c	x/D	Low BR			High BR		
			HTC	Nu#	eta	HTC	Nu#	eta
Trailing edge								
↑ SS	1.265	112.2	566	1318	0.165	529	1232	0.176
	1.195	106.0	569	1325	0.172	543	1265	0.194
	1.124	99.7	573	1335	0.180	551	1283	0.207
	1.053	93.5	577	1344	0.191	557	1298	0.223
	0.983	87.2	589	1372	0.202	569	1326	0.238
	0.842	74.7	589	1370	0.225	570	1327	0.269
	0.771	68.4	510	1188	0.227	498	1160	0.279
	0.700	62.1	454	1058	0.236	440	1024	0.292
	0.630	55.9	485	1130	0.261	463	1077	0.313
	0.489	43.4	553	1287	0.295	530	1234	0.337
	0.418	37.1	660	1536	0.329	645	1502	0.363
	SS cooling holes at x/c = 0.304							
Leading edge								
PS ↓	PS1 cooling holes at x/c = -0.30							
	-0.358	-31.8	589	1372	0.354	731	1703	0.384
	PS2 cooling holes at x/c = -0.46							
	-0.500	-44.3	638	1486	0.412	825	1921	0.437
	-0.570	-50.6	441	1028	0.298	505	1175	0.331
	-0.641	-56.8	396	922	0.241	434	1010	0.289
Trailing edge								

Table F. 3. Data set of film cooing test at Ma#0.84

Ma# 0.84	x/c	x/D	Low BR			High BR		
			HTC	Nu#	eta	HTC	Nu#	eta
Trailing edge								
SS ↑	1.265	112.2	652	1518	0.160	628	1462	0.208
	1.195	106.0	670	1560	0.179	644	1499	0.228
	1.124	99.7	670	1559	0.203	648	1509	0.245
	1.053	93.5	676	1573	0.217	654	1523	0.258
	0.983	87.2	694	1617	0.225	671	1562	0.270
	0.842	74.7	689	1604	0.246	687	1600	0.294
	0.771	68.4	585	1361	0.249	575	1340	0.306
	0.700	62.1	571	1329	0.256	554	1290	0.314
	0.630	55.9	633	1474	0.272	630	1467	0.327
	0.489	43.4	706	1644	0.299	742	1728	0.343
	0.418	37.1	848	1974	0.334	903	2102	0.365
	SS cooling holes at x/c = 0.304							
Leading edge								
PS ↓	PS1 cooling holes at x/c = -0.30							
	-0.358	-31.8	825	1921	0.356	837	1949	0.376
	PS2 cooling holes at x/c = -0.46							
	-0.500	-44.3	903	2102	0.436	1069	2488	0.454
	-0.570	-50.6	560	1305	0.311	629	1465	0.348
	-0.641	-56.8	457	1064	0.237	603	1404	0.322
Trailing edge								

Table F. 4. Data set of film cooing test at Ma#1.01

Ma# 1.01	x/c	x/D	Low BR			High BR		
			HTC	Nu#	eta	HTC	Nu#	eta
Trailing edge								
SS ↑	1.265	112.2	688	1601	0.182	771	1795	0.169
	1.195	106.0	631	1470	0.213	652	1519	0.224
	1.124	99.7	624	1453	0.214	658	1532	0.234
	1.053	93.5	494	1150	0.261	477	1110	0.269
	0.983	87.2	607	1412	0.264	676	1574	0.283
	0.842	74.7	782	1820	0.264	836	1946	0.287
	0.771	68.4	765	1781	0.272	820	1910	0.298
	0.700	62.1	779	1814	0.268	825	1922	0.296
	0.630	55.9	846	1971	0.279	900	2095	0.308
	0.489	43.4	894	2082	0.299	923	2150	0.323
	0.418	37.1	1061	2471	0.331	1141	2656	0.357
	SS cooling holes at x/c = 0.304							
Leading edge								
PS ↓	PS1 cooling holes at x/c = -0.30							
	-0.358	-31.8	899	2094	0.314	957	2228	0.328
	PS2 cooling holes at x/c = -0.46							
	-0.500	-44.3	1009	2350	0.402	1202	2799	0.402
	-0.570	-50.6	660	1536	0.271	753	1753	0.311
	-0.641	-56.8	529	1232	0.147	682	1588	0.241
Trailing edge								

Appendix G. Additional information on CFD study

Mesh generation and grid resolution

In the present study, the unstructured mesh was generated by the ANSYS mesh Generator. The total mesh element number is about 7.46×10^7. For the k-ω turbulence model, the first cell thickness is set as 1.27×10^{-3}d to give a better prediction of the boundary layer flow. To capture the details of the flow physics of the shock/film cooling interaction, the grid on SS is refined with the mesh resolution of about 1.27×10^{-2}d. Figure G. 1. shows the local grid on the SS surface. The mesh resolution on PS, after the near hole region, is about 1.0d, as shown in Figure G. 2.

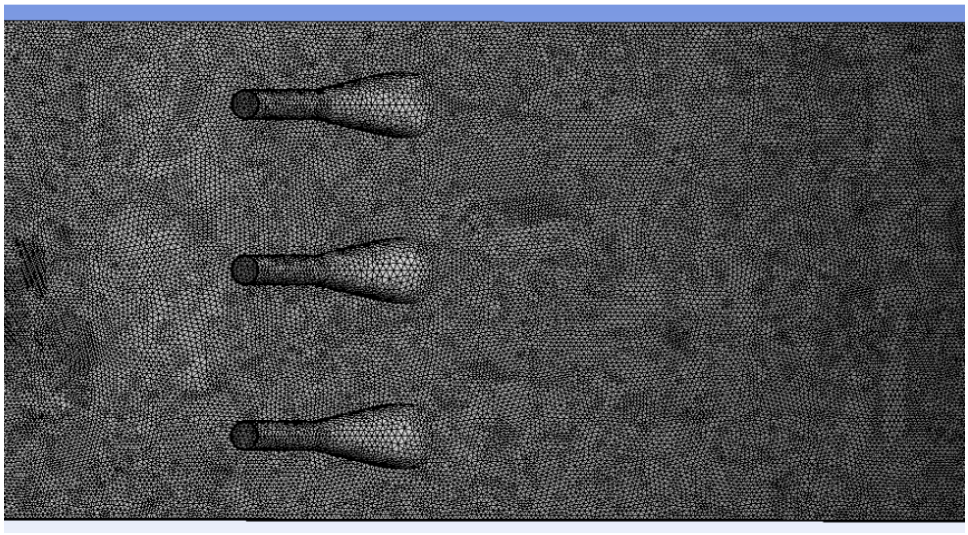

Figure G. 1. Local view of the SS mesh

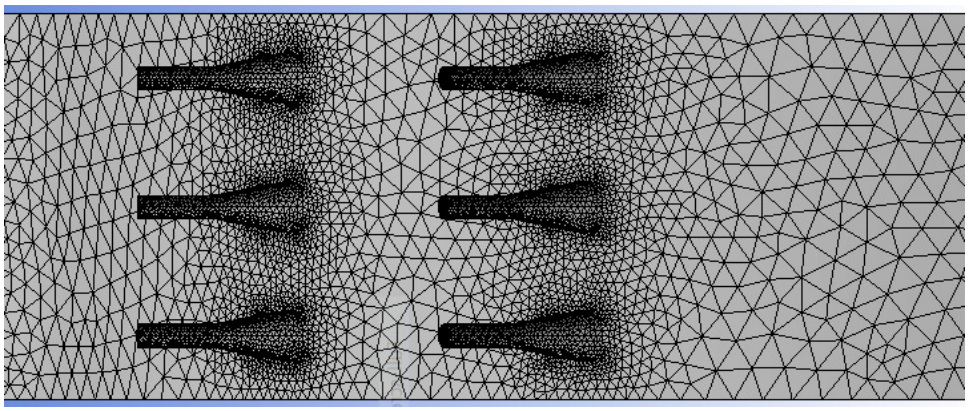

Figure G. 2. Local view of the PS mesh

Injection flow conditions CFD vs experiment

In the CFD study, the pressure ratios are set to match the test conditions in the experiment. The ratio between the exit static pressure and the inlet total pressure was set as 0.49. The pressure ratios of the film cooling injection are $PR_{SS} = 1.16$, $PR_{PS1} = 1.12$, and $PR_{PS2} = 1.10$. The blowing ratios in CFD are slightly larger than what were recorded in the experiment. This is probably because, in CFD, a full turbulence model was employed. However, in the experiment, there is an entrance velocity profile in the injection hole. Therefore, the CFD overestimates the mass flow rate. Another reason of the flow condition differences between the experiment and CFD results, may be the simplification of the geometry in the computational model. In the CFD study, the coolant plenum was ignored to reduce the computational cost, and the coolant total pressure is directly imposed on each of the injection hole inlet. Table G. 1. lists the blowing ratios (BR), density ratios (DR), and momentum ratio (IR) in the experimental and CFD studies.

Table G. 1. Cooling flow conditions comparison between CFD and experiment

	CFD			Experiment		
injections	SS	PS1	PS2	SS	PS1	PS2
BR	1.30	3.04	2.52	1.2	2.9	2.4
DR	1.16	1.24	1.23	1.23	1.36	1.33
IR	1.44	7.51	5.13	1.17	6.18	4.33

2-D contour map of adiabatic effectiveness

Figure G. 3. shows the 2-D contour map of the adiabatic effectiveness on the SS surface. Figure G. 4. shows the 2-D contour map of the adiabatic effectiveness on the PS surface. Comparing to the SS the cooling flow diffuses much faster on the PS. This is because the convex surface of SS stabilizes the boundary flow, and reduced the diffusion of the cooling flow. On the PS, the concave curvature accelerates the mixing and diffusion of the cooling flow.

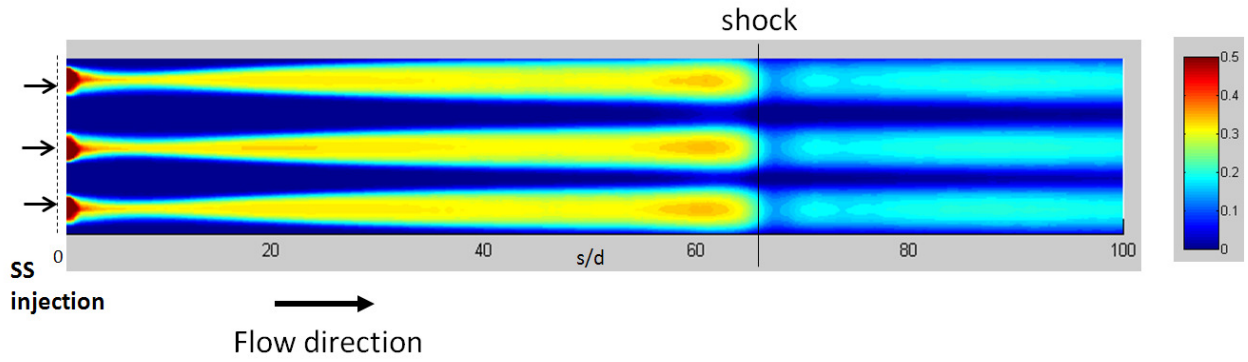

Figure G. 3. 2-D contour map of adiabatic effectiveness on the SS

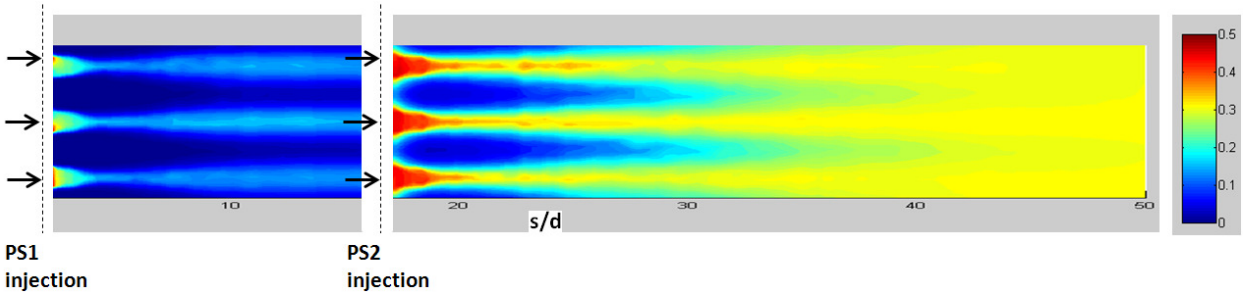

Figure G. 4. 2-D contour map of adiabatic effectiveness on the PS

Turbulence model comparison

In the present study k-ε turbulence model is also attempted. The scalable wall function was used for k-ε model, with the non-dimensional thickness of the first layer of the grid, y+, ranges from 21.7 to 46.5. Figure G. 6. compares the results of k-ε model and k-ω model with the experimental data. In general, the result of k-ε model flows a similar trend as the result of k-ω model, but at a lower level. The CFD result indicates that, compared to the k-ω model, the k-ε model predicts stronger kidney vortices in the near hole region, which is probably the reason that the k-ε predicts a lower adiabatic effectiveness.

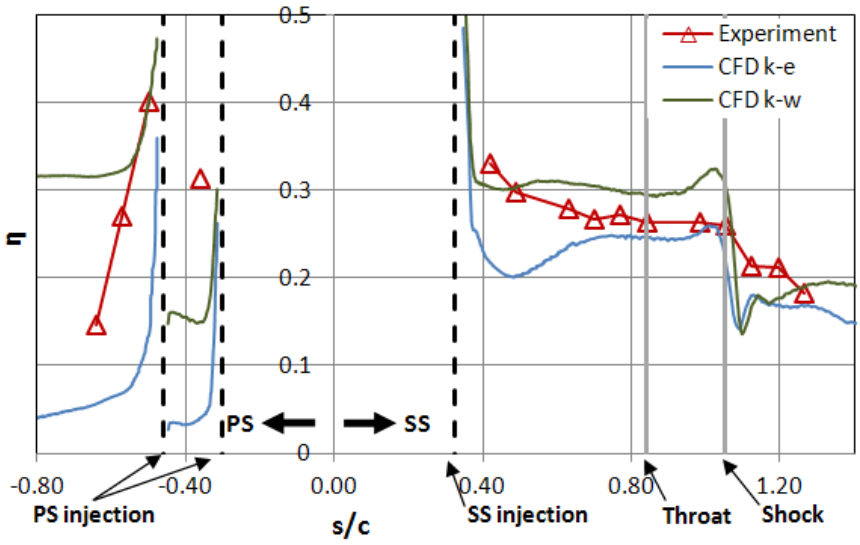

Figure G. 6. Adiabatic effectiveness – comparison between different turbulence models

Grid dependence of the CFD result

In the present study, the result form k-ω turbulence model computation with a fine mesh is used for the analysis. The total element of the fine mesh is about 74.6 million, with the fist layer thickness of the grid on the SS and PS surface is $10X^{-6}$ m. The y+ ranges from 0.04 to 1.6. To check the grid dependence of the CFD result, the same computation was performed with a coarse mesh. The total element of the coarse mesh is 8.9 million, and the fist layer thickness of the grid on the SS and PS surface is set as $10X^{-5}$ m, so that the y+ ranges from 0.17 to 10.75. Figure G. 7. compares the results of the centerline adiabatic effectiveness between the coarse mesh and the fine mesh. The coarse mesh predicts similar trend of shock effect on the SS. However, compared to the fine mesh result, the coarse mesh provides a higher adiabatic effectiveness on both SS and PS, which may indicate the coarse mesh under predicted the mixing and the diffusion of the cooling flow.

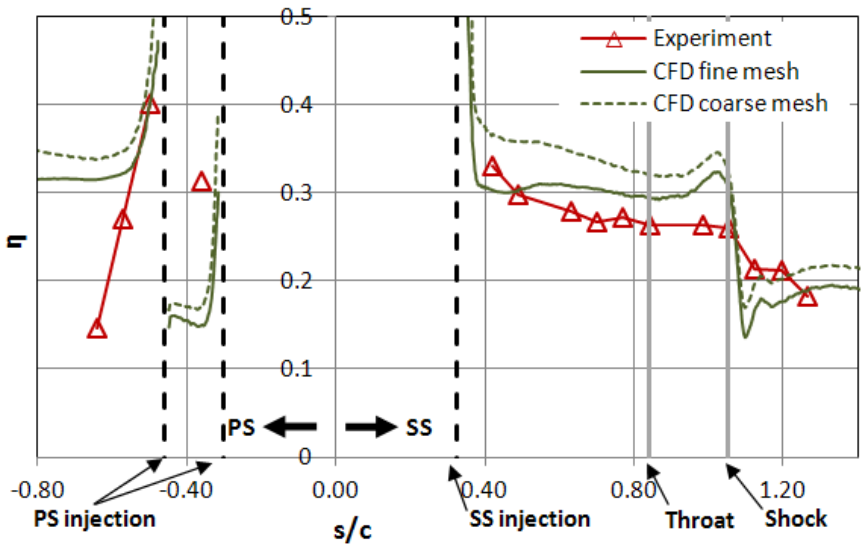

Figure G. 7. Adiabatic effectiveness – comparison between different grids